Bringing Redox Flow Batteries to the Grid: Techno-economic Modeling for Chemistry-Informed Design of Redox Flow Batteries

by

Kara E. Rodby

Master of Science in Chemical Engineering Practice, Massachusetts Institute of Technology, 2019
Bachelor of Science in Environmental Engineering, Northwestern University, 2017

Submitted to the Department of Chemical Engineering
in partial fulfillment of the requirements for the degree of

Doctor of Philosophy in Chemical Engineering

at the

MASSACHUSETTS INSTITUTE OF TECHNOLOGY

May 2022

Author .....
Department of Chemical Engineering
May 6th, 2022

Certified by .....
Fikile R. Brushett
Cecil and Ida Green Career Development Chair
Thesis Supervisor

Accepted by .....
Patrick S. Doyle
Robert T. Haslam Professor of Chemical Engineering
Singapore Research Professor
Chairman, Committee for Graduate Students

Bringing Redox Flow Batteries to the Grid: Techno-economic Modeling for Chemistry-Informed Design of Redox Flow Batteries

by

Kara E. Rodby

Submitted to the Department of Chemical Engineering on 06 May 2022, in partial fulfillment of the requirements for the degree of
Doctor of Philosophy in Chemical Engineering

Abstract:

Energy storage solutions will be crucial to decarbonizing the power sector by offsetting renewable intermittency while providing additional resiliency, flexibility, and value. With the grid comprising an array of services that vary in their technical attributes and value propositions, a portfolio of storage solutions is needed to support the many functionalities.

The redox flow battery (RFB) is one electrochemical storage technology that is particularly competitive, on a capital cost basis, at longer durations (> 4 hours) due to its unique decoupling of energy and power facilitated by an open architecture. This architecture also enables long-term cost savings by allowing for targeted component maintenance. RFBs can host a vast range of chemistries, whose choice affects the upfront and long-term cost and performance of the system, providing a wide design space. Clever chemistry design can enable efficient use of targeted maintenance; for example, the state-of-the-art RFB chemistry is the vanadium RFB uses a symmetric chemistry that allows for efficient, continuous recovery of crossover losses (often the fastest form of capacity decay in RFBs).

Despite these techno-economic benefits and decades of research, RFBs have seen minimal adoption; even within the subset of battery deployment specifically, RFBs are dwarfed by lithium-ion batteries. Limitations to RFB deployment include: a lack of demand for long duration storage, perceived risk of financing such large-scale systems of a relatively nascent technology, and high upfront costs. With little time left to develop cost-effective solutions to combat climate change, and without the high-value beachhead markets lithium-ion leveraged to drive down costs and risk while improving performance, RFBs will benefit from deeper upfront due diligence – via means like techno-economic modeling – to inform efficient research and development toward cost-competitive systems.

In this thesis, I utilize capital and levelized cost models to explore the design space of RFB chemistries. By considering chemistry-specific cost and performance attributes, particularly incorporating capacity loss and recovery over time, these models help set techno-economic benchmarks for grid viability. Supply chain studies also probe other relevant considerations regarding the scalability of these chemistries. Finally, I exemplify how such studies can drive research efforts via experimental studies.

Thesis Supervisor: Fikile R. Brushett
Title: Cecil and Ida Green Career Development Chair, Associate Professor of Chemical Engineering

Acknowledgements:

There are so many people to thank who have helped me get to this point. I surely cannot name every individual person, but I will try my best to capture all the groups of people who supported me during these five years.

First, I'd like to thank my advisor, Professor Fikile Brushett. Fik gave me a chance to join his lab, and despite being at my lowest point of academic self-confidence, he never made me feel lesser than anyone else. As someone who had previously felt helpless in addressing climate change, I deeply appreciate how the research in Fik's lab is so focused on solving very tangible, real-world problems. Further, I was allowed ample academic freedom to explore the topics I was interested in: none of the work in the four chapters of this thesis were performed with grant money for any specific projects. Rather, these were topics I came up with based on my own reading and interests and was given the support to pursue them.

I'd also like to thank the other two members of my thesis committee, Professor Alan T. Hatton and Professor Audun Botterud. Both have shown me kindness and support throughout this journey. I must acknowledge the MIT Energy Initiative (MITEI), as well, for the funding and mentorship they have provided throughout my PhD.

I am extremely grateful for the support of the other members of the Brushett group, who have been kind and supportive both in and out of the lab. While there are so many individuals I'd love to mention specifically, for the sake of brevity I will only acknowledge my original mentor, John Barton, who gave me so much of his time and attention answering countless questions that allowed me to build the foundation that this work is built off and re-build my academic self-esteem.

I have to thank my family, particularly my mom and dad for always supporting me in every way possible. Both of my parents have endured my stress with me and done everything they can to help make my life easier so I could focus on getting to this point. I love my parents very much and am so grateful for all they've done for me and the love they give me. This thesis is dedicated to my mom, who is the most remarkable, selfless, and strong person I know. She has taught me to be kind, generous, and confident, and to be the change you want to see in the world.

Finally, I want to thank my friends. In particular, I have to highlight the amazing people I've gotten to meet through the MIT Graduate Student Union. I had a hard time during this PhD, much of which was caused by what I feel are systemic exploitations and vulnerabilities of graduate student workers in academia (particularly for students of underrepresented identities). Connecting with a group of students who understood what I was feeling, empowered me to make change, and led by example was so pivotal in allowing me to feel my time spent here was worth something for myself and for others. Winning our union right before I depart from MIT was the best gift ever, and I am so immensely proud of us all. I strongly believe we can do better in academia, and I am inspired by the student-driven changes I've seen during my time at MIT that show me such a vision can and will be achieved because we have the power to demand it. I hope anyone reading this understands their power and obligation to help facilitate such changes, because we need everyone to buy in and take action if we want such changes to be lasting and meaningful.

Table of Contents:

I. Introduction

High levels of renewable energy penetration in the grid (>60%) are likely to be impractical without the development of complementary strategies to combat intermittency and meet demand, such as integration of energy storage [1,2]. No single technology can economically perform the vast array of grid services that, among other factors, vary in response and discharge timescales as well as total capacity requirements, necessitating a diverse portfolio of solutions [3,4]. In particular, one of the main characteristics of an energy storage system (and a term that will be used throughout this thesis) is the duration – defined as the ratio of the energy capacity over power rating (in units of time) – and this metric is used in determining what applications a battery technology is suited for. While much attention has been given to lithium(Li)-ion batteries (LIBs) due to their relatively advanced development, it may not be a cost-competitive solution for all grid services, particularly emerging longer-duration applications, presenting a growing need to advance new electrochemical technologies for these purposes.

Among the various energy storage technologies under development, redox flow batteries (RFBs) are an emerging solution for long duration (*i.e.*, > 4 hours), stationary applications as their system architecture offers a number of unique advantages [3,5]. The RFB is one type of electrochemical storage device, which generally utilize the potential difference between two reduction/oxidation (or "redox") reactions to drive chemical reactions, thus converting electrical energy to and from chemical energy. In the RFB architecture in particular, electrolyte (*i.e.*, the charge-storing capacity, usually in the liquid phase) is stored in tanks and pumped through the reactor where electrochemical reactions occur. This open architecture (*i.e.*, the physical separation of the electrolyte and the reactor components) decouples energy and power: one can scale the energy capacity (*e.g.*, by increasing the tank size) independently of the power rating (*e.g.*, the reactor size can stay fixed), or vice versa, meaning that RFBs can be designed for virtually any duration. This process of scaling the electrolyte tanks to meet longer durations, while keeping all else fixed, is depicted pictorially in Figure I-1 below. This decoupling is a unique and distinct feature from many conventional battery technologies (*e.g.*, LIBs) that facilitates a number of unique economic benefits, including the decrease of capital costs on a per unit energy basis at increasing durations

[6,7] and long-term cost savings through component-specific maintenance to extend the battery lifetime and remediate decay [8].

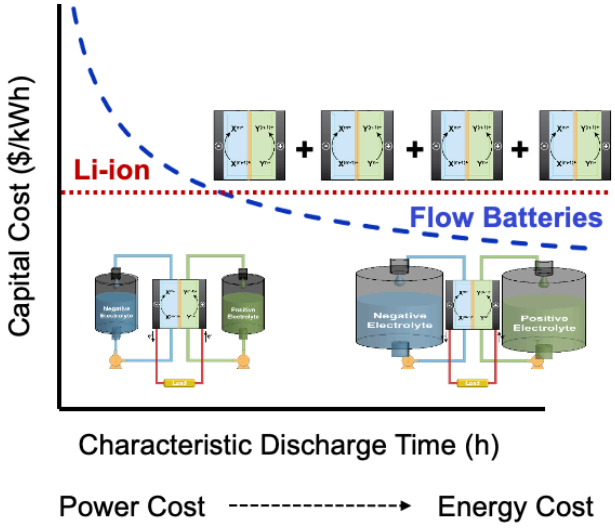

Figure I-1 – A representative schematic of capital cost as a function of characteristic discharge time (or duration) for RFBs and LIBs. As duration increases, the capital cost of decoupled battery architectures (*e.g.*, the RFB) shifts to be dominated less by power costs and more by energy costs (per Equation I-1 below).

Capital cost is a very important metric for evaluating the economic feasibility of batteries, the most cited being the Department of Energy's (DOE's) target for viable grid storage of ≤150 \$ kWh^{-1} (note: the exact target varies by office within the DOE, and is often even below 100 \$ kWh^{-1}) [9,10]. This is because the capital cost is the primary barrier to adoption: grid-scale storage systems are large capital investments, so high capital costs hinder the ability to finance and install such systems. The capital cost ($C_{capital}$) of a battery is generally defined as the sum of the energy costs (C_{energy}) and the power costs (C_{power}), the latter of which is divided by the duration to give consistent units of dollars per unit energy:

$$C_{\text{capital}}\left(\frac{\$}{\text{kWh}}\right) = C_{\text{energy}}\left(\frac{\$}{\text{kWh}}\right) + \frac{C_{\text{power}}\left(\frac{\$}{\text{kW}}\right)}{duration\ (h)} \qquad \textbf{(I-1)}$$

For RFBs, the energy costs consist of the electrolyte (comprised of the active species, solvent, and supporting electrolyte) and tank, while the power costs encompass the stack (primarily the reactor, the most important components of which are the membrane and electrodes). Other balance-of-

plant costs (*e.g.*, pumps, grid connections, etc.) and additional costs (*e.g.*, labor, installation, profit margins, etc.) may or may not be included in these calculations, depending on the study, but are usually represented as power-based costs (*i.e.*, they have units of dollars per kW and thus are also divided by the battery duration if summed and included in capital cost calculations). Equation I-1 implies that energy and power costs can be decoupled, which is how the capital cost is reduced as a function of duration. As discussed, this is true for RFBs, which is why RFBs are particularly attractive for longer duration applications, but this is not actually the case for many conventional technologies: for example, in LIBs the electrode is part of determining both the power output (its electrochemical properties determine the rate of the electrochemical reactions) as well as the energy capacity (its morphology dictates how many ions can intercalate into it for storage). Thus, there is little room to modulate the ratio of the energy or power ratings, as these are based on physical materials limitations. Rather, increasing duration must be achieved by adding entire modules (as shown pictorially in Figure I-1), meaning the total capital cost is approximately fixed (on a per unit energy basis), even with varying duration.

While the capital cost savings at longer durations is a key selling point of RFBs over other battery technologies, there is still minimal deployment of RFBs on the grid. Despite the large body of literature on RFBs (~4,500 publications, with >600 publications per year at the time of writing, via scopus.com), RFBs only account for a couple percentage points of the energy storage systems that have been contracted, announced, or are under construction globally [11]. The low deployment rate is a result of the nascency of the technology, which creates a "chicken and the egg" problem: no one wants to finance a seemingly risky project, but we also cannot de-risk a technology without financing initial demonstrations. The LIB industry avoided this situation via higher revenue beachhead markets: by the time it was ever considered for the grid, Li-ion had already demonstrated improved performance (its roundtrip efficiency is now remarkably high, usually ≥ 90%, compared to RFBs which are generally 80% or lower, depending on the chemistry) and lower costs from development and deployment in the relatively large industries of electronics and electric vehicles. RFBs, on the other hand, are really only attractive for the medium to long duration grid applications, for which the demand is still low. Thus, they are struggling to compete on a cost basis at such low production volumes. While the focus of this thesis is RFBs, this situation is representative of a number of other nascent storage technologies (*e.g.*, metal air batteries). With a need to decarbonize the power sector rapidly to meet targets for 2030, 2050, and beyond, and an

understanding that many of these nascent technologies will play a vital role in supporting the array of grid services that exist and necessitate a portfolio of solutions, this is an important issue to address. One crucial avenue needed to solve this problem is to develop new techno-economic models and arguments to motivate the development and, especially, deployment of these more nascent technologies. For example, as mentioned previously, RFBs offer a lot of long-term operational benefits that save costs, and these are not covered in capital cost calculations.

While the capital cost benefits to RFBs are well-described in the open literature, there are further economic benefits in operation due to ease of maintenance of open systems (*e.g.*, "tune-ups", component replacement) that are often not captured in techno-economic discussions. For example, crossover – defined as undesirable active species transport through the semi-permeable membrane that separates the positive and negative electrolytes in the reactor – is usually the most dominant form of capacity fade in RFBs and may halve the accessible capacity within 100-200 cycles [12]. While this is relatively fast fade as compared to that typically experienced by LIBs, the open architecture of RFBs allows for targeted, cost-efficient maintenance: in an RFB, one can access the electrolyte (the component affected by crossover) to repair or replace it directly, without altering the still-viable reactor. This is unlike conventional closed systems like LIBs that require "augmentation" (*i.e.*, replacement or addition of entire new modules), which wastes undecayed reactor components. The costs necessary to maintain performance over time impact the battery's economic viability, but are not captured in the conventional capital cost estimations that are commonly used to compare and benchmark different technologies [9]. This is especially true for the vanadium RFB (VRFB), which is by far the most researched and deployed RFB chemistry. This chemistry is particularly favored for its strong performance and resiliency in dealing with electrolyte degradation [13], which is facilitated by its design as a "symmetric" chemistry, where all active species are based on a single parent compound [14]. The benefit of this chemical configuration is that the inevitable crossover of active species becomes much less detrimental, as it will not lead to cross-contamination and these losses can be recovered via "rebalancing": the transfer and recharging of partial or full volumes of electrolyte between the two reservoirs to balance the concentrations of active species [14,15]. Rebalancing allows for indefinite crossover remediation and, thus, lifetime utilization of the same, original electrolyte (assuming other forms electrolyte degradation are managed) [16]. Not many chemistries can be configured in a symmetric

configuration, and while a handful of chemistries have been demonstrated symmetrically, vanadium remains the most promising and explored of them all.

The long-term cost benefits just detailed are primary motivators of RFB development, yet they are not captured in the vast majority of prior techno-economic modeling literature (which has primarily focused on articulating upfront capital costs [17–23]). This motivates the development of techno-economic models that consider the variable operating principles of different battery formats and chemistries. To this end, the central thread of my thesis is a levelized cost of storage (LCOS) model that I developed to model lifetime RFB costs that incorporates capacity fade and recovery. A combination of the capital cost and the LCOS allows for a better comparison across the range of energy storage technologies with different performance attributes, which can be used to assess and develop economically viable RFB systems. In **Chapter II** of this thesis, the LCOS model is described and applied to the VRFB system, where it is used to identify opportunities for cost reduction through operating strategies (*e.g.*, rebalancing schedule), performance improvements (*e.g.*, reducing fade rates), design decisions (*e.g.*, battery sizing), and investment approaches (*e.g.*, electrolyte leasing).

While the VRFB system benefits from reduced maintenance costs, it suffers from a high upfront cost, due, in part, to the price of the active species [24,25]. The magnitude and uncertainty of vanadium prices are considered key impediments to broad deployment, which have motivated research into alternative chemistries based on lower-cost and widely-available materials [26–28]. Thus, recognizing the need for RFBs with low capital costs, I extend the LCOS model to explore the methods and associated costs for capacity-loss remediation of low-cost, high-abundance chemistries in **Chapter III**. While in recent years there has been a surge in the published literature of such chemistries, there has been little consideration about the practical operation and maintenance needs of these systems. As many of these systems utilize asymmetric chemistries (unlike the VRFB, meaning active species crossover results in cross-contamination), and some even experience other forms of electrolyte degradation (*e.g.*, active species decay), their capacity-loss remediation is expected to be a more challenging and chemistry-dependent problem. In **Chapter III** I compare these systems to the VRFB system, the incumbent solution (*i.e.*, an RFB with higher capital costs and the ability to recover capacity at low costs) to determine the conditions under which the reduced upfront cost of less expensive, asymmetric chemistries offsets

the more complex and, in some cases, more expensive maintenance required to recover capacity losses.

Another practical techno-economic consideration that has become central to next-generation design for other, more developed electrochemical storage technologies (*e.g.*, LIBs) is materials availability and supply chains [29]. Understanding how and where critical active species elements are mined, manufactured, produced, etc. can provide crucial insights into the scalability of a particular chemistry. Such studies are virtually absent from the RFB field, understandably due to its nascency. However – just like practical operating considerations such as capacity fade remediation – supply chain analyses can act as another crucial consideration in navigating the vast design space of chemistries that can be employed in the versatile RFB platform. In this vein, **Chapter IV** is comprised of a study into the vanadium supply chain. Recognizing that we must decarbonize the grid to greater extents relatively quickly to limit the effects of climate change and that the technology readiness level (TRL) of the VRFB system is the highest of all RFB chemistries, I explore the materials availability and supply chain of vanadium to determine the causes of its high and volatile price as well as any limits to the magnitude and rate of possible VRFB deployment. I focus on the production scale and growth rates needed to deploy various amounts of VRFB storage by 2030 and 2050, while also examining opportunities to develop and stabilize the supply chain via rapid growth to the magnitude and distribution of vanadium production and other economic hedging strategies.

So far, I have discussed how techno-economic analyses can inform the design of economical RFBs from a theoretical, modeling-based perspective. However, another portion of my thesis exemplifies how such analyses can be translated into lab-based research as well. One chemistry that showed potential for economic broadscale deployment throughout my techno-economic analyses is iron-chromium (Fe-Cr, see **Chapter III**) because of its use of low-cost and high-abundance materials. Further, the chemistry has already been shown to successfully utilize techniques for cheaply and practically remediating crossover losses for the entire operational lifetime. The promise the chemistry showed from a modeling standpoint piqued my interest in demonstrating it experimentally. One of the lingering issues with this system that I noticed immediately upon trying to run it in the lab is its high rate of side reactions (*i.e.*, hydrogen evolution, another form of electrolyte degradation) that causes rapid capacity fade. **Chapter IV** is thus an experimental study

seeking to mitigate the rate of this degradation, specifically through use of electrochemical purification of the electrolyte to remove common metal impurities that catalyze the side reaction. This study brings the Fe-Cr chemistry one step closer to being commercially viable.

In summary, the goal of my thesis is to help close the gap between the existing, predominantly lab-based understanding of RFBs and the understanding needed for successful, long-term, and competitive grid-scale implementation of RFBs. Greater demand for grid-scale RFBs is being held back by concerns around their high prices and perceived risk. While many researchers working on RFBs are exploring exciting new materials, chemistries, architectures, etc., some concerted effort to increase the RFB's TRL, such that it can be reliably deployed, would go a long way to boost its appeal to investors. Unlike the more-developed, incumbent lithium-ion technology, the RFB field neither has the time – as deadlines to decarbonize the grid to prevent irreversible climate change are rapidly approaching – nor the alternative beachhead markets to slowly develop a commercially viable RFB solution that can economically compete on the grid. The RFB industry will strongly benefit from more upfront due diligence, via methods like techno-economic modeling, to solve practical questions and design technically and economically feasible systems. My research has developed new techno-economic models that better describe RFB costs, performance, degradation, and maintenance, and further used these models to determine paths for new research and development that provide the best economic returns and, in turn, drive RFB deployment.

II. Assessing the levelized cost of vanadium redox flow batteries with capacity fade and rebalancing

1. Introduction

Undesirable active species transport through the semi-permeable membranes separating the positive and negative electrolytes is a common mode of capacity fade in redox flow batteries (RFBs). In an ideal membrane, only supporting ions will exchange between the two electrolytes to maintain charge neutrality and balance the redox reactions in each electrolyte. Imperfect selectivity results in the passage of active species and solvent through the membrane. The crossover of active species is driven by a combination of concentration, potential, and pressure gradients between the two half-cells, which ultimately results in a concentration imbalance of charge storage materials in the negative and positive electrolytes and, consequently, a net decrease in the accessible capacity. Crossover can also lead to other chemistry-specific cross-contamination issues, such as precipitation, membrane fouling, or component degradation, which limits the combinations of half-reactions that can be used in tandem. To mitigate this effect, RFB membranes are typically designed with charge- or size-exclusion pores to impart the desired permselectivity without sacrificing conductivity. To this end, several groups are investigating new membrane materials and cell designs that minimize crossover [30–33], while others are developing models that enable a deeper understanding of thermodynamic, kinetic, and transport processes that define membrane-electrolyte interactions with RFB systems [34–37]. While significant progress has been made, crossover remains a significant issue and requires creative solutions to limit its impact on RFB performance, longevity, and, ultimately, commercial viability.

The vanadium redox flow battery (VRFB) is arguably the most well-studied and widely deployed RFB system. At the time of writing, there are approximately 330 MW of VRFBs currently installed around the world with many more systems announced or under development, including a 200 MW/800 MWh plant in Dalian, China [18,38]. This system leverages a single element, vanadium, with four stable oxidation states (II, III, IV, and V) accessible within the electrochemical stability window of acidic aqueous electrolytes on carbon electrodes. The charging half-cell reactions for the VRFB are shown in Equations II-1 and II-2 below (note: reversing their direction gives the discharge reaction).

$$V^{3+} + e^- \xrightarrow{charge} V^{2+}\ (negative) \quad \textbf{(II-1)}$$

$$VO^{2+} + H_2O \xrightarrow{charge} VO_2^+ + e^- + 2H^+\ (positive) \quad \textbf{(II-2)}$$

Because all redox species are based on the same parent compound, crossover does not lead to permanent capacity fade and can be recovered via electrolyte maintenance. This unique feature differentiates VRFBs from other RFBs that rely on asymmetric chemistries as it can significantly reduce maintenance costs throughout the operational lifetime. These cost savings can potentially negate the relatively high upfront cost of vanadium, as compared to other possible charge-storage compounds [39].

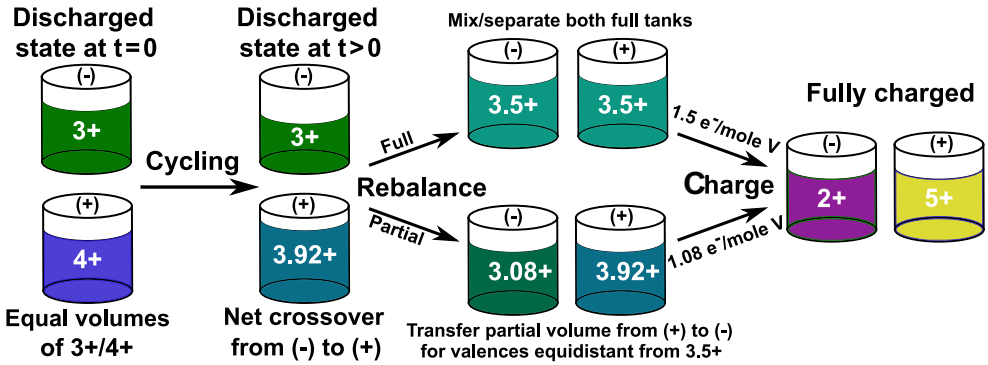

Figure II-1 – Schematic representation of the full and partial rebalancing techniques.

The primary method for recovering the lost capacity in VRFBs is termed rebalancing, where the negative and positive electrolytes are mixed to equilibrate the concentration of vanadium ions in each electrolyte. Rebalancing is generally performed once the accessible capacity drops to a predefined level that is determined by application requirements. In general, electrolyte aliquots are transferred from the positive half-cell to the negative half-cell, as concentration accumulation generally occurs on the positive side of the battery due to the cumulative transport effects of the various active species ions and the properties of conventional polymeric membranes [12,40,41]. An average 3.5+ oxidation state is expected after rebalancing if charge has been maintained amongst the active species; the battery starts with all 3+ on the negative side and all 4+ on the positive side prior to any cycling and crossover. This operation can be performed in a full or partial manner, as shown in Figure II-1. Full rebalancing consists of mixing, re-separating, and re-

charging the entire volumes of the two tanks [12,42,43], whereas partial rebalancing consists of transferring small electrolyte volumes between the positive and negative electrolytes to balance vanadium concentrations [44,45]. Full rebalancing requires charging 1.5 moles of electrons per mole of vanadium for the entire tank volume, while partial rebalancing only requires recharging the ions from the partial volume mixing. In addition, partial rebalancing prevents exhausting the full state-of-charge (SOC) window within the electrolyte, avoiding the kinetically slow V(III)/V(IV) redox couple to a great degree [46]. Accordingly, partial rebalancing is a more energy-efficient and time-effective method [8] and, in all subsequent analyses, we only consider this method of rebalancing. However, from a practical perspective, it should be noted that determination of the true SOC of the two electrolytes and thus accurate prediction of the volume required to obtain the desired SOC after re-mixing is challenging without direct analytical measurements [47]. Also, although less widely reported, other capacity recovery techniques reported in the literature include continuous rebalancing, sometimes referred to as hydraulic shunting or overflow [48–51], and hydraulic pressure rebalancing [44,52].

Rebalancing recovers losses from crossover, but should the average oxidation state drift from 3.5+, rebalancing will not restore the full capacity. Side reactions in the VRFB, primarily hydrogen evolution on the negative electrode, will cause the oxidation state of the rebalanced electrolyte to deviate from this expected average value and thus requires additional maintenance. Here, we distinguish between these two fade mechanisms by considering capacity fade due to vanadium crossover to be a “reversible” decay that can be recovered by electrolyte rebalancing and by considering oxidation state drift an “irreversible” decay, as it requires external intervention (the addition of new materials) to recover performance. These mechanisms are expanded upon in the Methods section (*infra vide*).

Despite the aforementioned advantages of rebalancing, most prior techno-economic modeling literature has focused on articulating upfront capital costs of VRFBs [17–23]. Capital cost is an important metric as it is both tangible and determines the loans that must be taken and thus the payback risk of the likely sizable investment. Indeed, several offices in the US Department of Energy use capital cost targets of 100-150 $/kWh as benchmarks for viable energy storage systems and assume constant performance over the project lifetime [9,10]. However, practical embodiments experience decay during operation and the exclusion of these recurring costs in

engineering economic assessments results in a failure to capture the value of VRFB recoverability and resilience. For example, lithium (Li)-ion batteries, arguably the leading electrochemical technology for grid energy storage, irreversibly degrade during operation and may require periodic augmentation, or the purchase and installation of new batteries to replace lost capacity [53]. In contrast, VRFBs can be rebalanced to restore lost capacity without additional capital expenditure. Thus, while VRFBs have significantly higher capacity fade rates than state-of-the art Li-ion batteries, the resilience of the VRFB electrolyte may lead to cost savings over the project lifetime. This motivates an expansion of techno-economic analyses, beyond capital cost estimations, to quantify the savings associated with regular electrolyte rebalancing and maintenance. To this end, we develop a levelized cost of storage (LCOS) model that incorporates capacity fade and recovery in a VRFB. By considering both the operating costs and the fluctuating capacity over time, the LCOS is a more appropriate method for estimating the cost of operating VRFBs over the long-term. A combination of the capital cost and the LCOS allows for a better comparison across the range of energy storage technologies with different performance attributes.

In this work, we describe a modeling framework to incorporate and systematically evaluate the impact of electrolyte rebalancing on the LCOS of a VRFB. We perform sensitivity analyses on key technical and economic parameters to determine which research and development efforts may have the greatest impact on LCOS. We also assess the impact of practical operational decisions such as rebalancing schedules and capacity sizing to meet a nominal rating. Finally, we explore the role that vanadium electrolyte leasing may have on reducing VRFB costs.

2. Methods

2.1 Model of levelized cost of storage

The levelized cost of storage is the ratio of the discounted costs to the discounted energy stored over a project lifetime, which is a useful metric for comparing different energy storage systems. The standard method for calculating the LCOS ($ kWh^{-1}) is shown by Equation II-3:

$$\mathrm{LCOS} = \frac{\text{Sum of costs over lifetime}}{\text{Sum of energy stored over lifetime}} = \frac{\sum_{t=0}^{n} \frac{I_t + L_t + T_t}{(1+r_y)^t} + \sum_{t=0}^{k} \frac{OM_t + C_t}{(1+r_d)^t}}{\sum_{t=0}^{k} \frac{E_t}{(1+r_d)^t}} \quad \textbf{(II-3)}$$

The cost variables with their respective definitions are shown in Table II-1, while the descriptions and baseline values for any parameters used are provided in Table II-2. LCOS models can use a variety of terms based on the system of interest and the desired complexity [54–58]. The base model is inspired by prior LCOS models published by Lazard in their annual levelized cost of storage studies, which serve as both a point of reference and comparison for this analysis [55,59]. Accordingly, the model includes necessary terms for upfront capital cost (I_t), charging cost (or cost of electricity, C_t), operating and maintenance cost (OM_t), and energy stored (E_t). We also elect to include loan (L_t) and tax (T_t) terms on the capital investments and to exclude a capital recovery factor, though this factor is sometimes included in other models [57]. Costs are either tracked yearly, where $t \in \{\mathbb{Z}^+ \cup [1,n]\}$ and n is the number of years of battery operation, or daily where $t \in \{\mathbb{Z}^+ \cup [1,\mathrm{k}]\}$ and $k=365n$ is the number of days of operation. As the capacity is tracked daily, any function of capacity must also depreciate on a daily schedule. Once tabulated across time, the costs are discounted with a periodic rate, r, which, again, is either yearly or daily, depending on the cost period.

Table II-1 – Descriptions/equations of the terms in Equation II-3. See Table II-2 for parameter names and values. b_s is the battery size (kWh), though note that this terms cancels out in Equation II-3 and thus LCOS is independent of b_s in this model.

Symbol	Name	Details	Equation
I_t	Investment expenditures	Capital costs, only applicable at year 0	$\begin{cases} C_{cap}\ (\$\ kWh^{-1})\ \cdot b_s\ (kWh), t = 0 \\ \$0,\ t > 0 \end{cases}$
L_t	Loan payments	Annual loan payment due to the fraction (f_d) of the capital cost that was financed by debt	$\begin{cases} C_{cap}\ (\$\ kWh^{-1}) \cdot b_s\ (kWh) \cdot f_d \cdot \dfrac{(1+d_r)^n - 1}{d_r \cdot (1+d_r)^n}, \mathrm{t} > 0 \\ \$0,\ t = 0 \end{cases}$
OM_t	Operating and Maintenance costs	Costs to have service provider center the average oxidation state via addition of reductants	$\begin{cases} b_s\ (kWh) \cdot \left[O\left(\frac{\$}{kWh - visit}\right) + \frac{n_{ox}\left(\frac{mol\ ox.}{kWh}\right) \cdot MW_{ox}\left(\frac{g}{mol\ ox.}\right) \cdot C_{ox}\left(\frac{\$}{g}\right)}{w_{ox}} \right], cap_{max} \le cap_{lim} \\ \$0,\ cap_{max} > cap_{lim} \end{cases}$ $where\ n_{ox}\left(\frac{mol\ ox.}{kWh}\right) = \left(U\ (V) \cdot \mathrm{F}\left(\frac{C}{mol\ e^-}\right) \cdot \frac{1\ mol\ e^-}{1\ mol\ V}\right)^{-1} \cdot \frac{1\ mol\ ox.}{1\ mol\ V} \cdot \frac{3{,}600{,}000\ Ws}{kWh}$
E_t	Energy stored	Varies with dynamic accessed capacity	$\begin{cases} b_s\ (kWh) \cdot \text{cycles per day} \cdot f_{cap}, t > 0 \\ 0\ (kWh),\ t = 0 \end{cases}$
C_t	Charging costs	Costs to charge battery considering state of charge and inflation rate (r_i)	$E_t\ (kWh) \cdot CF \cdot p_e\ (\$\ kWh^{-1}) \cdot (1 + r_i)^{t-2} \cdot (2\text{-}\varepsilon_E)$
T_t	Taxes	Paid on I_t	$I_t\ (kWh) \cdot T$

Table II-2 – Symbols, names, descriptions, values, and sources for model parameters. Values with asterisks (*) are baselines for each variable but are subsequently varied in sensitivity analyses. Note: the SI mentioned refers to that of the published version of this chapter [60].

Symbol	Name	Description	Value and Source	
O	Operational cost rate	Labor cost to service system (via additives)	10 \$ kWh^{-1} per visit	[6]
r_y / r_d	Discount rate	-	• 0.12 (annually) • $(1.12)^{1/365}$-1 (daily)	[59]
d_r	Debt interest rate	Interest rate on loan payments	8%	[59]
f_d	Debt finance ratio	Fraction of capital costs financed by debt	20%	[59]
ε_E	Roundtrip system cycle energy efficiency	Net energy efficiency of the entire system	85%	[61]
CF	Charging factor	Scaling factor of the charge cost, representing the # of electrons that must be transferred per vanadium ion to fully charge the battery	• 1 under normal circumstances • Between 1 and 1.5 during partial rebalancing (see SI – S2)	
p_e	Electricity price	--	10.98 ¢ kWh^{-1}	[62]
r_i	Electricity inflation rate	Projected inflation on market rate	• 0.01 (yearly) • $(1.01)^{1/365}$-1 (daily)	[63]
T	Combined tax rate	Combined USA federal and state tax rate on investment expenditures	39%	[59]
n	Operational period	Years of simulated operation or lifetime	20 years	[59]
R_{fade}	Fade rate	Linear overall capacity fade rate	* 0.44% capacity fade per cycle	[44]
r_{ED}	Electrolyte decay rate	Linear capacity fade rate that is due to drift in average electrolyte oxidation state and is not recovered upon electrolyte rebalancing (a fraction of R_{fade})	* 0.055% (see SI – S3)	
U	Open circuit voltage	--	1.4 V	[61]
F	Faraday's constant	--	96,485.33 C per mol e^-	
MW_{ox}	Molecular weight of oxalic acid	--	90.03 g mol^{-1}	
w_{ox}	Oxalic acid purity	By weight	0.996	[64]
C_{ox}	Cost of oxalic acid	--	1.10 \$ kg^{-1}	[65]

2.2 Model of dynamic capacity fade and rebalance

Whereas prior models assumed fixed performance over time, here, we include a dynamic physical model of the battery to track the capacity and energy stored (E_t) over time, which allows for the incorporation of capacity fade and recovery via rebalancing. We assume linear capacity fade over extended cycling, as this behavior has been implied in prior work [24,33], and validate this assumption with a survey of the recent peer-reviewed literature as shown in Figure II-2 [12,25,31,32,44,48,52,66,67]. It is important to note the limited amount of long-term VRFB cycling data in the open literature as compared to shorter-term cell tests (*i.e.*, cyclic voltammograms, IV polarizations, etc.), likely because cycling analyses are both more time-consuming and experimentally challenging. While the data in Figure II-2 was not collected under identical conditions (see Table S1 in the Supporting Information, SI, of the published version of this chapter for full operating conditions of each data set [60]), all were based on cycling of a single redox flow cell in an academic laboratory. Almost all sources used comparable Nafion membranes and heat-treated carbon electrodes; had similar electrolyte compositions of 1-2 M V in 2-5 M H_2SO_4 and volumes of 50-80 mL per reservoir; and were cycled at current densities between 50-80 mA/cm^2. The active areas ranged from 5 to 103 cm^2, though the volumetric flow rates generally correlated to the active area. There are many other potentially-relevant conditions that are not reported but could significantly impact performance including cell temperature, use of humidified nitrogen purging, reservoir seal, and cell compression. Finally, we note that the use of a plot digitizer adds a small source of error to the values extrapolated from the data (≤0.5% per data point) [68].

As illustrated in Figure II-2, significant variations among the capacity fade rates can be seen in the data. The outlier [52] was the only data set that used a porous Daramic separator rather than an ion-selective Nafion membrane. Additionally, this data set had the longest theoretical duration of 8.6 h, while the duration of most other data sets was less than 2 h. These two observations explain the notably higher fade rate. We assume the apparent performance increase at the beginning of life for some data sets is due to cell conditioning or imbalanced electrolytes. We include two additional data points obtained from a recent review on VRFB component degradation by Yuan *et al.* [8,69,70], which cites two experimental values for the rate of capacity decay as 1.3% and 0.067% per cycle (not shown in Figure II-2 because cycling data was not provided). If considered along

with the data plotted in Figure II-2, these final fade rates effectively represent lower and upper bounds. The average of the 11 fade rates – 0.442% capacity loss per cycle – was used as a baseline, though we perform sensitivity analyses to probe a range of possible fade rates.

Note that here we assume single cell data is representative of stack performance, though the time scales of operation are different and stacks experience other losses such as those due to shunt currents. Single-cell cycling data is limited, but stack-level cycling data is even more scarce. As we assume capacity fade rates and all other performance metrics are independent of battery size (b_s) or duration, these variables do not affect the LCOS in the current model. Rather, the fade rates are on a per cycle basis and do not take into account varying durations that would have a marked effect on fade rate since crossover under galvanostatic conditions is largely time-dependent rather than cycle-dependent. Additionally, the data shown in Figure II-2 is from cells cycled repetitively between upper and lower voltage limits at a constant current. This may not be realistic for or representative of practical applications, which are anticipated to operate under variable and potentially intermittent power loads, and, consequently, may result in different fade rates. Incorporation of operationally-dependent fade rates are beyond the scope of this initial study but will be contemplated in the future work.

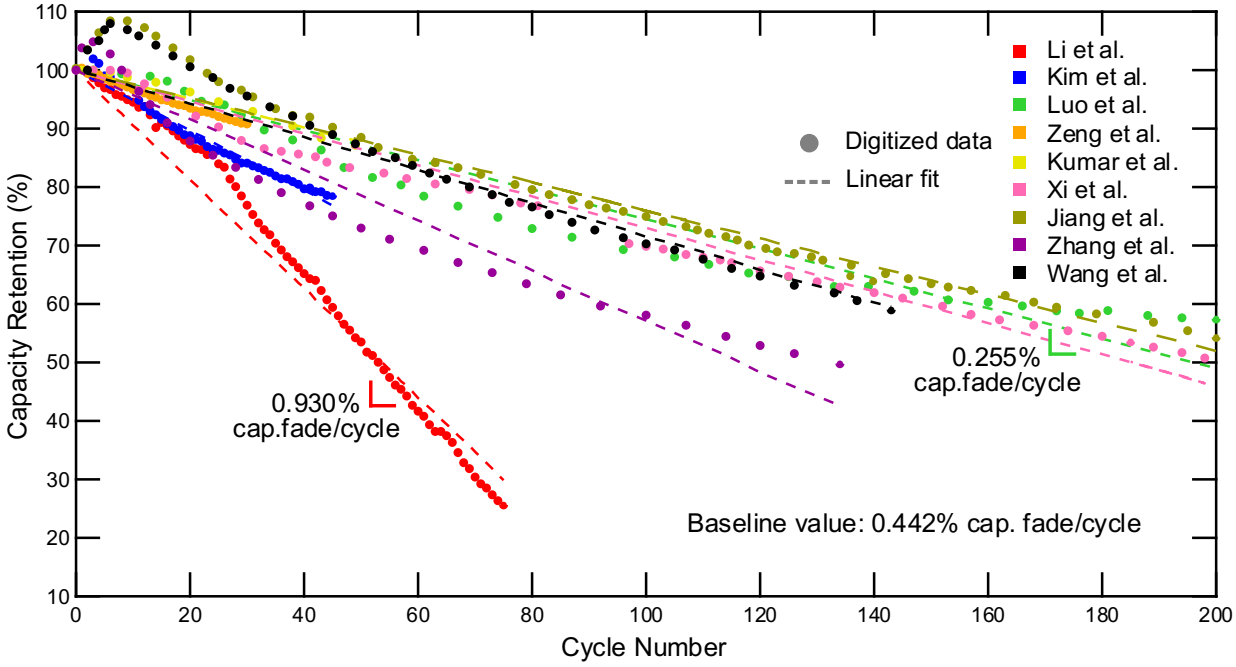

Figure II-2 – Literature review of capacity fade as a function of cycle number, adapted from: [12,25,31,32,44,48,52,66,67]. Dots represent the data and dashed lines represent the linear fit for each set. Note: the y-intercept of each fit was fixed at 100%.

The sources of capacity fade in VRFBs can be broadly divided into reversible decay due to vanadium crossover that is assumed to be fully recoverable via electrolyte rebalancing, and irreversible materials decay that requires component replacement for performance recovery. Regarding the latter, we assume the tanks, pipes, and pump linings are composed of plastic [20,22,71], and the performance decay of wetted reactor components including electrodes and membranes is minor in a well-engineered system as these processes have been reported slow under typical operating conditions [6,19]. This is further supported by the reported lifetimes of commercial VRFB systems, 25,000 cycles or 20 years with stable energy efficiency [72–74]. We acknowledge the potential of other failure modes, such as capacity loss due to leaks and system degradation due to control strategy faults, but elect to ignore these effects as we were unable to find reports in the peer-reviewed literature that articulate the likelihood of such failures or the magnitude of their effects. Inclusion of such considerations would simply have a scalar effect on the overall fade rate or maintenance costs, which could be easily modified by the user, though we do provide a sensitivity analysis on fade rate to address part of this consideration (Figure II-5). This leaves electrolyte decay resulting from species precipitation due to heat or air exposure and/or side reactions that shift the average valence away from 3.5+. We assume precipitated active species can be recovered via simple maintenance operations such as reversing the cell polarity or partial mixing of the reservoirs to electrochemically dissolve V(V) solids [8]. Thus, in this model we only consider the shift in average oxidation state over time that is caused by coulombic inefficiencies (*i.e.*, side reactions) and accounts for *ca.* 12.5% of the overall fade (see section S3 of the SI of the published version of this chapter for further details [60]). Specifically, we consider the parasitic hydrogen evolution reaction that occurs at the negative half-cell during charging in place of the desired reduction of V(III) to V(II), which is often cited as the most common and prominent cause of VRFB electrolyte decay [8,45,75]. Hydrogen evolution leaves an imbalance at the end of charging as there is all V(V) in the positive electrolyte but some amount of V(III) remaining in the negative electrolyte, and this results in a capacity loss that cannot be recovered via rebalancing. There are methods for reversing this imbalance, such as the addition of chemical reducing agents that will reduce V(V) to V(IV) and thus balance the positive electrolyte based on the composition of the negative electrolyte [76]. A common reductant is oxalic acid ($C_2H_2O_4$), which reduces V(V) via the reaction shown in Equation II-4. Note, we assume the electrolyte dilution from the

formation of water has a negligible effect on the capacity. Here, we referred to such electrolyte maintenance as battery servicing.

$$VO_2^+ + C_2H_2O_4 \rightarrow VO^{2+} + 2CO_2 + H_2O \quad \textbf{(II-4)}$$

Thus, we have an overall linear fade rate (R_{fade}, in units of % capacity loss per cycle), which encompasses fade from electrolyte decay (r_{ED}, also in units of % capacity loss per cycle) and fade from crossover (R_{fade}-r_{ED}), both of which are also assumed linear. The product of f_{cap}, the fraction of original capacity accessed at any given time, and b_s, the nominal battery size, determines the capacity accessed in a given cycle. The fraction of original capacity accessed is a function of R_{fade}, as calculated in Equation II-5:

$$f_{cap} = cap_{max}(t = R) - R_{fade} \bullet n_{cyc}^{R} \quad \textbf{(II-5)}$$

where n_{cyc}^{R} is the number of cycles passed since the last rebalancing event (*i.e.*, $t = R$), and cap_{max} is the maximum accessible capacity. The cap_{max} decreases as the average oxidation state drifts with each cycle as a function of r_{ED}. The cap_{max} can be defined by Equation II-6:

$$cap_{max}(t) = 100\% - r_{ED} \bullet n_{cyc}^{S}(t) \quad \textbf{(II-6)}$$

where n_{cyc}^{S} is the number of cycles passed since the last servicing event (at which point cap_{max} = 100%, by definition). These cycle counters are defined in Equation set II-7:

$$n_{cyc}^{R/S}(t) = \begin{cases} 0, & t = 0 \text{ or upon rebalancing (R) or servicing (S)} \\ n_{cyc}^{R/S}(t-1) + 1, & t > 0 \text{ and not rebalancing (R) or servicing (S)} \end{cases} \quad \textbf{(II-7)}$$

The following assumptions have been used within the modeling framework:

1. At the beginning of the battery life, the capacity is 100%. For simplicity, the nominal capacity is defined as the product of the power rating and duration of the battery. In actuality, the accessible capacity of a battery is dependent on many factors including current density [77], the depth of discharge [78], and average oxidation state [79], so impacts of this assumption should be explored in future work.
2. Capacity fades linearly at a specified rate (R_{fade}) according to Equation II-5. It is assumed that the battery undergoes one charge/discharge cycle per day during the expected lifetime.
3. Rebalancing occurs when the capacity fades to a predefined lower limit (cap_{lim}). The charging cost is scaled by the number of electrons required per vanadium ion to charge the battery to a

2+ and 5+ state on the negative and positive sides, respectively, as a result of rebalancing. This charging factor will be between 1-1.5 for partial rebalancing and 1.5 for full rebalancing. A description of how the charging factor is determined based on the capacity fade can be found in section S2 of the SI .

4. As a result of rebalancing, capacity is recovered to the new cap_{max}, which is equal to the maximum achievable capacity at the last rebalancing event less the fade from side reactions that have shifted the average oxidation state since (according to Equation II-6).
5. This process repeats until the cap_{max} itself decreases to the cap_{lim}. At this point, servicing occurs where a technician doses an amount of oxalic acid sufficient to return the average valence to 3.5+. The total cost of servicing is based on the labor cost (cost per nameplate kWh per visit) and the cost of the oxalic acid. Capacity is then assumed to return to 100% of the original capacity.
6. These steps repeat throughout the specified operational period.

This iterative process is illustrated in Figure II-3, which shows an annotated example simulation of the battery capacity as a function of time. We note that the physical separation of power and energy components in the RFB system and the use of vanadium redox chemistry enables open-ended operation provided suitable control strategies and periodic maintenance schedules are employed. As such, we do not include end-of-life valuation or recycling of the various components (particularly the electrolyte), though future work should more carefully consider these assumptions.

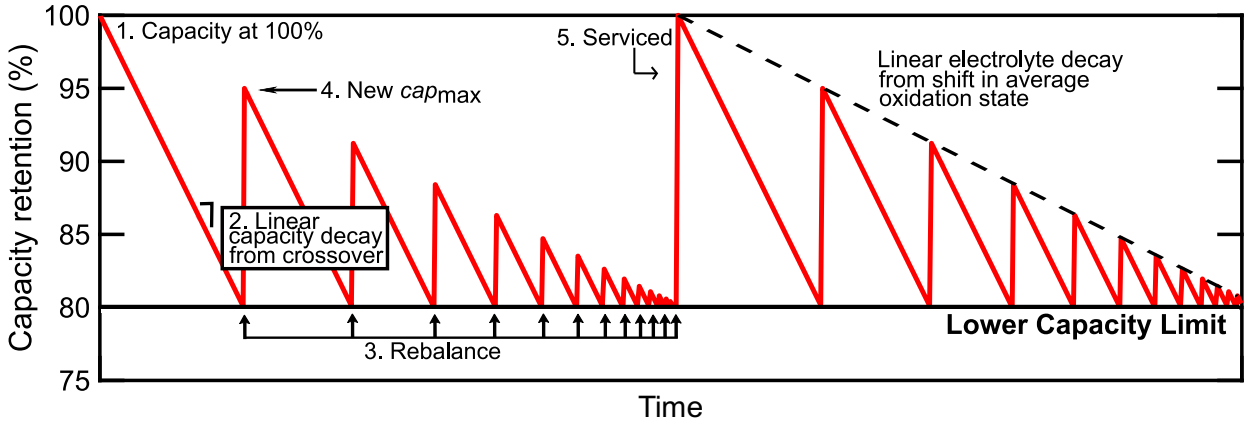

Figure II-3 – Example of the simulated VRFB capacity retention as a function of time annotated with the respective model steps (for illustrative purposes).

The discrete nature of the model presents some limitations for data analysis purposes. Particularly, under certain conditions, the model can produce seemingly discontinuous curves, because it is discrete on the scale of days, which can result in a mismatching of the fade experienced in a day versus where the capacity limit lies. For example, if fade rates differ by a small amount (say, 0.01% per day), they may result in the same number of rebalancing and servicing events and thus ultimately the same LCOS. However, eventually, that small increase in fade rate will lead to the addition of a rebalancing and/or servicing event, which will change the LCOS. Thus, curves can appear piecewise or even oscillate if the variable at hand changes the capacity and the costs simultaneously (*i.e.*, the sizing discussion in section 3.2). Because of this, polynomial fits are used in place of the raw output for some of the subsequent plots to more cleanly present trends (which are not altered by this representation).

2.3 Model validation

To validate our model outputs, we compare our base case to other LCOS models of VRFBs in the open literature. Lazard's annual levelized cost of storage analysis is a useful source for costs of various energy storage systems, and, in 2018, reported levelized VRFB costs in the range of 293-467 \$ MWh^{-1} (for mid-scale systems ~10 MWh) [55]. Running the partial rebalancing model with a capital cost of 410 \$ kWh^{-1} (the mean value given by Lazard for VRFBs of this size) and all other baseline values, the LCOS for the baseline VRFB system determined by this model is 420 \$ MWh^{-1}. Using the lowest capital cost considered in this work (300 \$ kWh^{-1}) gives a LCOS of 350 \$ MWh^{-1}. Both values are within Lazard's range of VRFB LCOS values. Other studies that calculate the LCOS of VRFBs and other RFBs report a wide range of values, though many of the more relevant scenarios, with respect to discount rate, size, etc., fall between 200 and 600 \$ MWh^{-1} [6,56,80].

3. Results and discussion

Leveraging this LCOS model, we begin our study with a sensitivity analyses of input technical and economic parameters and then explore practical operating and design considerations such as rebalancing frequency and battery oversizing. In these analyses we examine the LCOS tradeoffs

between increases in upfront costs for flexibility in lifetime operating costs. Recognizing the separate financial considerations related to capital cost that are not captured in LCOS calculations, we conclude with an examination of the emerging vanadium leasing market, which aims to reduce the upfront cost burden. Unless otherwise noted, all analyses use the baseline values from Table II-2.

3.1 Sensitivity analyses on fade rates and lower capacity limit to optimize rebalancing frequency

The sensitivity of the model predictions to capital cost, overall fade rate, electrolyte decay rate, and lower capacity limit are of relevance, as these parameters contribute substantially to the LCOS and, in some cases, reported values can vary substantially across the literature (*e.g.*, fade rates shown in Figure II-2) or are not publicly available (*e.g.*, electrolyte decay rates). We first perform a sensitivity analysis on the effect of lower capacity limit (cap_{lim}) on LCOS. Unlike capital cost or fade rate, this is an operational, and thus optimizable, parameter that does not require technology or market development. Indeed, the lower capacity limit can be changed at any time and thus can be dynamically optimized to achieve the best LCOS possible. Figure II-4 shows, in general, how the choice of cap_{lim} impacts LCOS: setting the limit too high leads to a steep increase in LCOS as the costs of frequent rebalancing and servicing grow, but, conversely, setting the limit too low also causes an increase in LCOS as the battery is often storing much less energy.

We select three capital cost (C_{cap}) values, 300, 400, and 500 \$ kWh^{-1}, which fall within present or near future cost projections per multiple sources, to assess model sensitivity [18–20,23,55,61,73,81]. Figure II-4 shows there is an optimal cap_{lim} value, around 83% for the baseline case, and this optimal point is independent of C_{cap}. Increasing C_{cap} linearly increases LCOS as it represents a one-time, upfront cost, while we observe a nonlinear dependence of LCOS on cap_{lim}. The stronger dependence of LCOS on the cap_{lim} than on the C_{cap} is apparent from the convergence of the three C_{cap} curves at high cap_{lim} values.

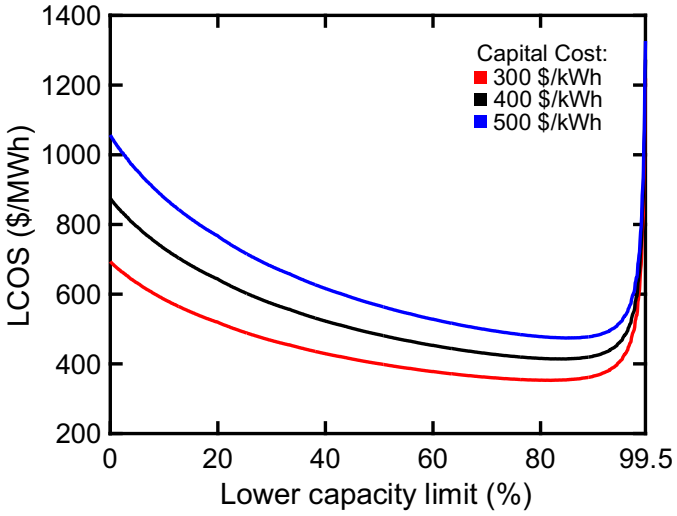

Figure II-4 – Levelized cost as a function of lower capacity limit (cap_{lim}) for three capital costs. For plotting purposes, the upper limit of x-axis set to 99.5%, as the LCOS value goes to infinity as cap_{lim} approaches 100%.

Next, we perform sensitivity analyses of the two fade rates, the overall fade (R_{fade}) and electrolyte decay rate (r_{ED}), on LCOS at the three different C_{cap} values. Since cap_{lim} is an adjustable set point, at each fade rate we optimize the cap_{lim} to give the minimum LCOS, which is then plotted in Figure II-5 for R_{fade} (Figure II-5a) and r_{ED} (Figure II-5b). In each case we hold the non-varied fade rate at its baseline value (0.442 and 0.055 % capacity loss per cycle for the overall and electrolyte decay rates, respectively). Note that in the case of R_{fade}, while improvements may be expected (*i.e.*, decreased R_{fade} values) in the near future through advances in membrane and cell design, we are also interested in the impact of increased R_{fade} values that could occur if less expensive or less resistive membranes are necessary to enable C_{cap} reductions that promote market penetration. Such reductions in membrane price and resistivity would likely occur from a loss of selectivity and reduction of membrane thickness, respectively, both of which would increase crossover rates.

It is perhaps intuitive that lower fade rates would correspond with lower LCOS values, as less rebalancing or servicing events are required. In addition, we expect systems with lower fade rates to have higher optimal cap_{lim} values, as the balance of the two trends can result in no change in the number of rebalancing and servicing events (*i.e.*, approximately the same maintenance costs), with the added benefit of higher energy stored and thus lower LCOS. Put differently, the optimal cap_{lim} decreases with increasing fade rates as it becomes more favorable to allow the energy stored to

decrease in return for less frequent rebalancing or servicing. We see this is the case for Figure II-5b: as the electrolyte decay rate increases, the optimal LCOS increases and the optimal lower capacity limit decreases. Interestingly, we see almost no change in the optimal LCOS as the overall fade rate increases (with the electrolyte decay rate held constant). This observation is a result of the near negligible cost of rebalancing as compared to the cost of servicing. Increasing the overall fade rate while holding the electrolyte decay rate constant is effectively increasing the crossover rate, which results in more rebalancing events. This appears to have no effect on LCOS, indicating the cost of rebalancing is minor, at least in the context of this model. This coarse finding suggests that improvements in membrane selectivity may not lead to long-term performance and cost benefits (though it impacts upfront costs, as explained earlier). While more detailed treatments of membrane performance within the environment of an operating cell as well as the effects of application-specific cycling need to be contemplated, this initial analysis suggests that reducing membrane cost rather than improving selectivity will have a greater effect on VRFB LCOS.

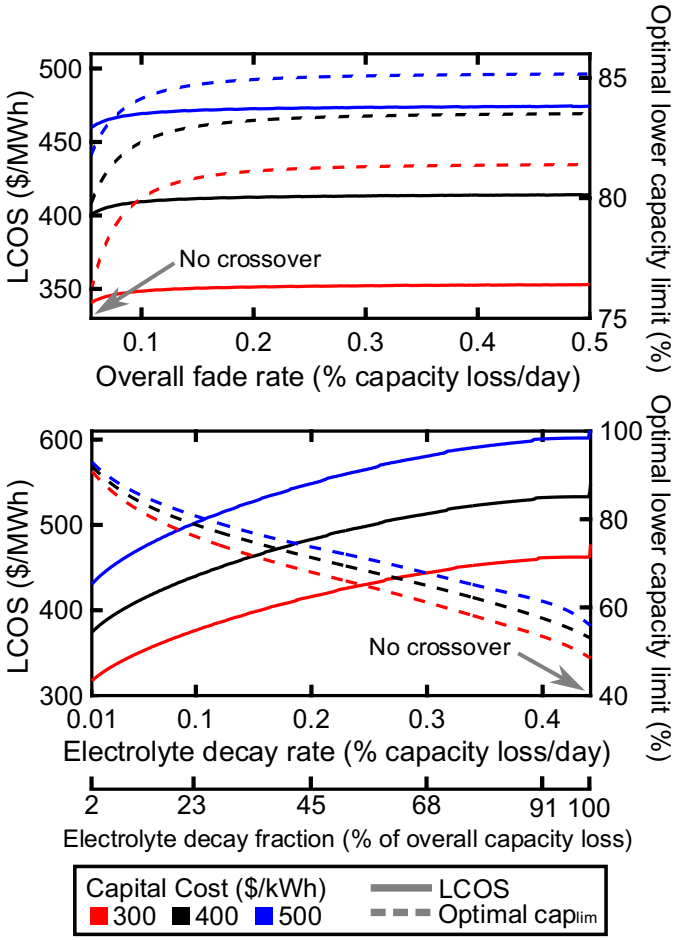

Figure II-5 – Sensitivity analysis of overall fade rate while holding electrolyte decay rate constant at its baseline value (0.055% capacity loss/cycle) (a) and sensitivity analysis of electrolyte decay rate (or electrolyte decay fraction, as a fraction of the overall fade rate) while holding overall fade rate constant at its baseline value (0.442% capacity loss/cycle) (b) on the optimal LCOS for three C_{cap} values (varying colors). The solid lines give the LCOS (left axis) and the dashed lines give the optimal lower rebalancing limit that gives rise to each LCOS point (right axis).

In these analyses the battery capacity is fading and thus the capacity available each day is changing. While a lower cap_{lim} may lead to a better LCOS in some cases, such operation may not always be feasible for commercial applications as there may not be enough capacity to meet a particular demand. This necessitates consideration of battery sizing, which will be discussed in the subsequent section.

3.2 Sizing based on fade rate and nominal capacity ratings to ensure demand load is always met

In some cases, such as when the electrolyte decay rate is very low, the optimal lower capacity limit is high (*ca.* 95%). From a practical standpoint, this is convenient for the VRFB vendor: if the optimal operating protocol allows capacity to stay within 95% of its original rating, then the seller can guarantee the battery capacity will always be within 5% of the original, nameplate rating. However, under many feasible scenarios, the optimal lower capacity limit is much lower. As battery suppliers must guarantee a certain minimum capacity rating to a buyer [82], it is informative to consider the common practice of system oversizing: while the battery may be nominally rated for 10 MWh – the capacity the user will expect – it can, in theory, provide more energy at the beginning of life. Note that this is in addition to the oversizing needed to compensate for the depth of discharge limits for a given battery. While this oversizing leads to a higher C_{cap}, it also enables less frequent rebalancing and servicing as capacity can decrease for a longer period of time, thus allowing for optimal cap_{lim} values lower than 95% based on the actual capacity while still providing at least 95% of the nominal capacity rating. Here we consider the impact of this tradeoff on LCOS.

To model capacity oversizing, we stipulate that accessible capacity must always be within 95% of the nominal capacity and then define an oversizing factor, *OF*:

$$OF = \frac{95\%}{cap_{\text{lim}}} \tag{8}$$

The *OF* enables exploration of alternative cap_{lim} values, as it scales the system capacity such that the new cap_{lim} provides the same energy as the original value of 95% for the non-oversized system, which is needed to meet user requirements. For example, should an end-user desire a 10 MWh battery, and always needs to store at least 9.5 MWh: they have the option to either purchase a 10 MWh battery and set the cap_{lim} to 95%, or alternatively to purchase a 12 MWh battery with a lower cap_{lim} of 79% (95%/79% = 1.2). In this way, the energy stored and used will always be 9.5-10 MWh, but a larger range of lower cap_{lim} values can be accessed at the expense of higher upfront costs for the additional electrolyte (a tradeoff that can potentially reduce the LCOS). Unlike prior analyses in section 3.1, here the energy stored on any day will not vary unless the actual capacity

retention of the battery drops below the nominal rating, and even then, it can only drop by an additional 5% of that rating until rebalancing must occur.

Figure II-6a shows the LCOS as a function of lower capacity limit at three different electrolyte cost fractions. A base case C_{cap} of 400 \$ kWh^{-1} was selected, and this is divided into the electrolyte cost fraction and the power cost fraction. The fraction which is due to electrolyte costs (either 15, 30, or 45% of 400 \$ kWh^{-1}) is then scaled by the *OF*. The dashed horizontal line shows the LCOS for the base case where a 95% cap_{lim} is used (and thus there is no oversizing). Figure II-6b shows the corresponding *OF* at each lower cap_{lim} value, as well as the resulting C_{cap} due to scaling from the *OF* in each electrolyte cost fraction case. We see the LCOS curves for the oversized cases in Figure II-6a resemble those shown in Figure II-4. This is reasonable, as the same variable (cap_{lim}) is changing on the x-axis, with the only difference being an addition to the C_{cap} that increases as the *OF* increases. As we begin to oversize and allow for more fade, we see a decrease in the resulting LCOS, but the returns of the greater capacity range are diminished by the escalating cost of oversizing and the LCOS eventually increases above the baseline case at very low cap_{lim} values (< 50%). Thus, an optimum for oversizing exists where LCOS is minimized. For the three electrolyte cost fractions considered, this optimum ranges from 70-80%, corresponding to moderate oversizing between 18-34%, though less aggressive oversizing still leads to LCOS savings. As the electrolyte cost fraction increases, the LCOS increases because more capital expenditure must be scaled by the *OF*.

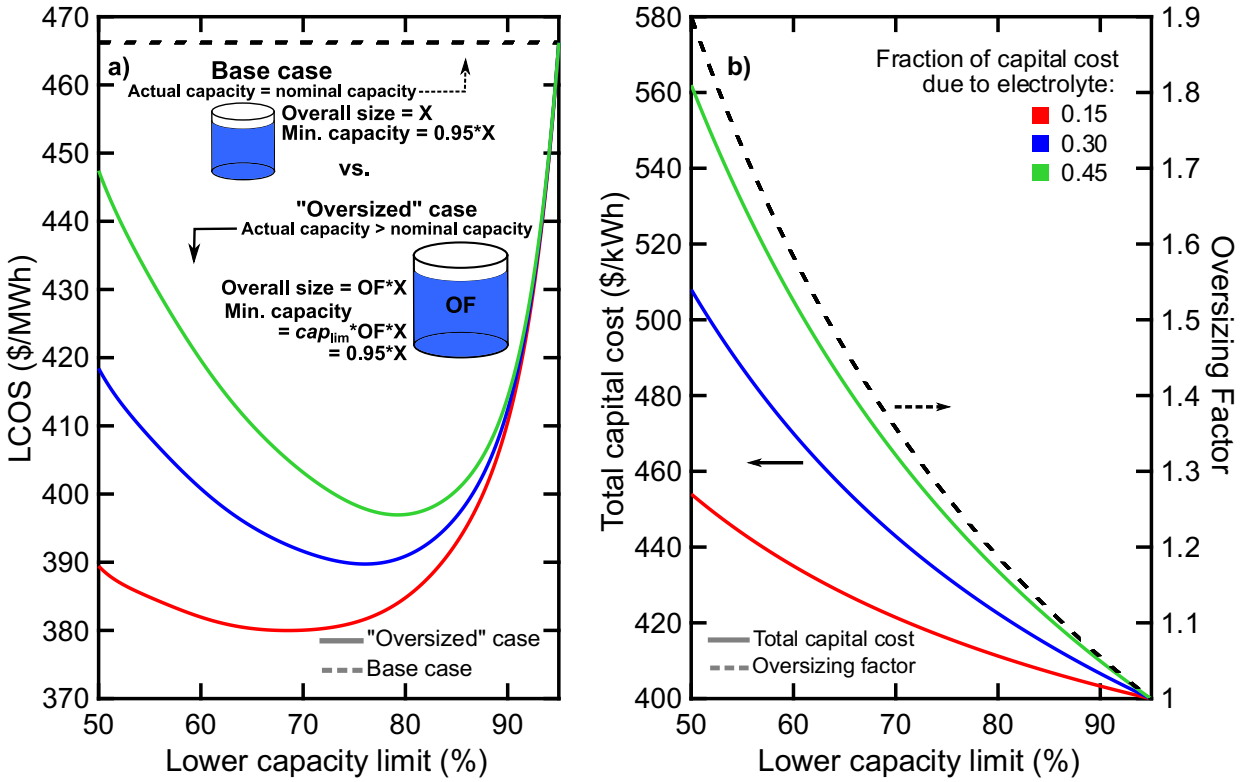

Figure II-6 – (a) LCOS (solid line) for an oversized system as a function of the lower capacity limit (cap_{lim}) for a system with a baseline capital cost (C_{cap}) of 400 \$ kWh^{-1} at three different electrolyte cost fractions (colors). The dashed line represents the base case with no oversizing. (b) The C_{cap} as a function of lower cap_{lim} (solid line, left y-axis) and the oversizing factor (OF) corresponding to each lower cap_{lim} (dashed line, right y-axis).

A key observation from Figure II-6 is that increases in C_{cap} can provide savings over the project lifetime if they correspond to sufficient improvements in operational performance. However, though these sizing considerations are necessary for any battery supplier to consider and potentially incorporate in their system engineering, it must be recognized that oversizing increases upfront cost, which may serve as a barrier to purchase for potential customers. To this end, vanadium leasing is a potential approach to reducing upfront costs, as will be discussed in the following section [83,84].

3.3 Exploring the market of vanadium electrolyte leasing

A common critique of the VRFB is the relatively high and volatile price of vanadium [24,25]. For example, in 2018, the price of vanadium pentoxide (V_2O_5), one of the most common vanadium electrolyte precursors, fluctuated greatly and nearly quadrupled before decreasing in early 2019 [39]. At this juncture, supply volatility and high prices can be attributed to the relatively small size of the vanadium market, rather than scarcity or geological constraints [84]. Vanadium use is primarily limited to a single market, the production of steel, which accounts for about 90% of demand [85], and only China, Russia, and, most recently, South Africa are major exporters [84]. In 2018, in addition to the growth of the VRFB market, demand for vanadium rose after the creation of new Chinese rebar standards for steel that mandated an increase in the vanadium content [86]. Simultaneously, supply dropped as various vendors halted or fully shut down production due to ongoing environmental inspections and project closures [86].

Vanadium leasing, whereby a third-party company leases the vanadium, usually in the form of VRFB electrolyte, to a battery vendor or end-user is a proposed solution beginning to gain market traction. While payment schemes for electrolyte leasing have yet to be fully articulated, at least in the open literature, in general, it appears to comprise of a marked reduction in upfront capital cost (*ca.* 30% [83]) coupled with the introduction of an annual leasing fee [83,84]. This option is attractive as it lowers upfront investment, however, its impact on LCOS is unclear. Thus, we model a vanadium leasing scenario to determine whether it can reduce LCOS. Unfortunately, implementing a sophisticated leasing scheme into the model is not straightforward due to the lack of information regarding how these leases are contracted. Thus, for our analyses, we define a simple leasing scheme in which the cost of the electrolyte is removed from the C_{cap} and a yearly leasing fee is imposed. To the best of our knowledge, the only reference in the published literature regarding the magnitude of leasing fees is recent work by Skyllas-Kazacos, which defined the annual fee as the "fraction of electrolyte cost per annum" and used a baseline fraction of 0.1 [38].

As the appropriate magnitude of the annual leasing fee remains unclear, we solve for the maximum annual leasing fee that makes the leasing scheme competitive with the non-leasing scheme, which can serve as an upper bound for what is profitable to the lessee. This upper bound can be determined by first calculating the non-leasing LCOS with the original model at varying electrolyte costs (optimizing for lowest LCOS over all lower cap_{lim} values) and then, subsequently,

determining the yearly leasing fee that produces an LCOS under leasing equal to that without leasing. This essentially estimates the break-even cost of the leasing scheme, and can be determined analytically without calculating any LCOS values. We also calculate the internal rate of return (IRR) for the lessor under each scenario, assuming that the lessor provides an initial investment equal to the cost of electrolyte and receives the same, fixed annual fee every year throughout the 20-year operational life. Details of these calculations are provided in section S5 of the SI of the published version of this chapter [60].

For leasing to be an attractive option as compared to upfront purchase, vanadium prices must be sufficiently high and/or annual fees must be suitably low. At the time of writing, the price of vanadium pentoxide is *ca.* 16 \$ kg^{-1} [39], which corresponds to 29 \$ kg^{-1} of vanadium. Note that, in practice, electrochemical-grade vanadyl sulfate is used, but the costs associated with materials upgrading and refinement have not been articulated in the literature [6,19,21]. While, from a materials perspective, the costs to transform a vanadium precursor to vanadyl sulfate are expected to be low, especially at scale [87], the cost of electrolyte purification is unknown and will likely depend on the impurity profile of the precursor sources. Because of this uncertainty and the ongoing debate surrounding future vanadium pentoxide prices [85,88], we elect to vary the vanadium price both above and below the baseline of 29 \$ kg^{-1}. To translate the price of vanadium into the cost of electrolyte, we employ a bottom-up capital cost model previously developed by Darling *et al*. [61], using the baseline values from that publication and a 1.2 *OF* to mimic a commercial scenario (see section S4 of the SI of the published version of this chapter [60]). The final variable that can affect the feasibility and profitability of the leasing scheme is the annual discount rate on the lessee (defined earlier for all LCOS calculations as r_y), which is varied in addition to vanadium price.

The results of the leasing analysis are shown in Figure II-7. The left plot (Figure II-7a) represents the lessee: the maximum annual fees that they could pay to break-even on their initial upfront savings through leasing is shown by the solid lines as a function of the vanadium price. The colors of each line represent different discount rates for the lessee, except for the pink lines which represent the scenario where the annual fee is 10% of the electrolyte cost (the Skyllas-Kazacos case). As the price of vanadium and thus the upfront saving from leasing increase, the maximum competitive leasing fee must also increase, which is to say leasing becomes competitive for larger annual fees. For a specified discount rate, any annual fee below the corresponding solid line

represents a scenario where the LCOS for the lessee is reduced via the leasing scheme. We note that the pink line is below all the other curves, implying that it corresponds to a lessee discount rate even lower than 4% and that, if this assumption is plausible, leasing would likely be a beneficial practice for lessees. This analysis implies that the leasing scheme not only lowers upfront cost, but, provided the fee is low enough, it can benefit battery operators by reducing the overall LCOS. It should be noted, however, that a representation of the annual fee as dynamic over time may be more realistic and would reduce the benefits to the lessee, however such an advanced treatment is beyond the scope of this initial work. Some considerations a lessor would likely take into account to develop a dynamic annual fee include inflation, predictions of future vanadium supply and demand, and the potential rise of alternative RFB chemistries that may reduce the value of the vanadium electrolyte. The dashed lines in this plot represent the IRR for the lessor under each scheme. The IRR does not vary with vanadium price in this analysis as is explained in section S5 of the SI of the published version of this chapter [60]. We can see the range of IRRs is *ca.* 8-20%. At this point in time, it is difficult to speculate what magnitude of rate of return would be acceptable to a lessor, as these values are not widely available and vary across industries. However, metals leasing is an existing industry, with developed markets for leasing platinum, palladium, silver, and gold. At least initially, we expect that vanadium leasing rates would be similar to those for platinum, palladium, or silver, as these metals are leased for industrial use and have a higher risk associated with the loan than gold, which is usually leased for investment purposes and thus is not actually used in any physical manner [89].

Figure II-7b presents similar information to Figure II-7a, leveraging the same equations and variables, but this time from the perspective of the lessor. As a lessor, one may have a target IRR and this plot can be used to determine the annual fee that should be charged to match that IRR at a specific vanadium price. The minimum annual fees needed to meet each IRR are plotted in solid lines (left y-axis), while the various line colors corresponding to different vanadium prices. As expected, the fees that must be charged increase with increasing IRR and vanadium price. The dashed lines show the corresponding discount rate to the lessee under each scenario. Note that the discount rate is the same for all vanadium prices and only varies with IRR. This observation is similar to that observed in Figure II-7a and is described in the SI (section S5) of the published version of this chapter [60]. In summary, while this analysis represents a preliminary interpretation of electrolyte leasing, it indicates that such a scheme may hold promise. However, further work is

needed to refine the economic details surrounding leasing agreements before the value proposition of this approach can be unambiguously determined.

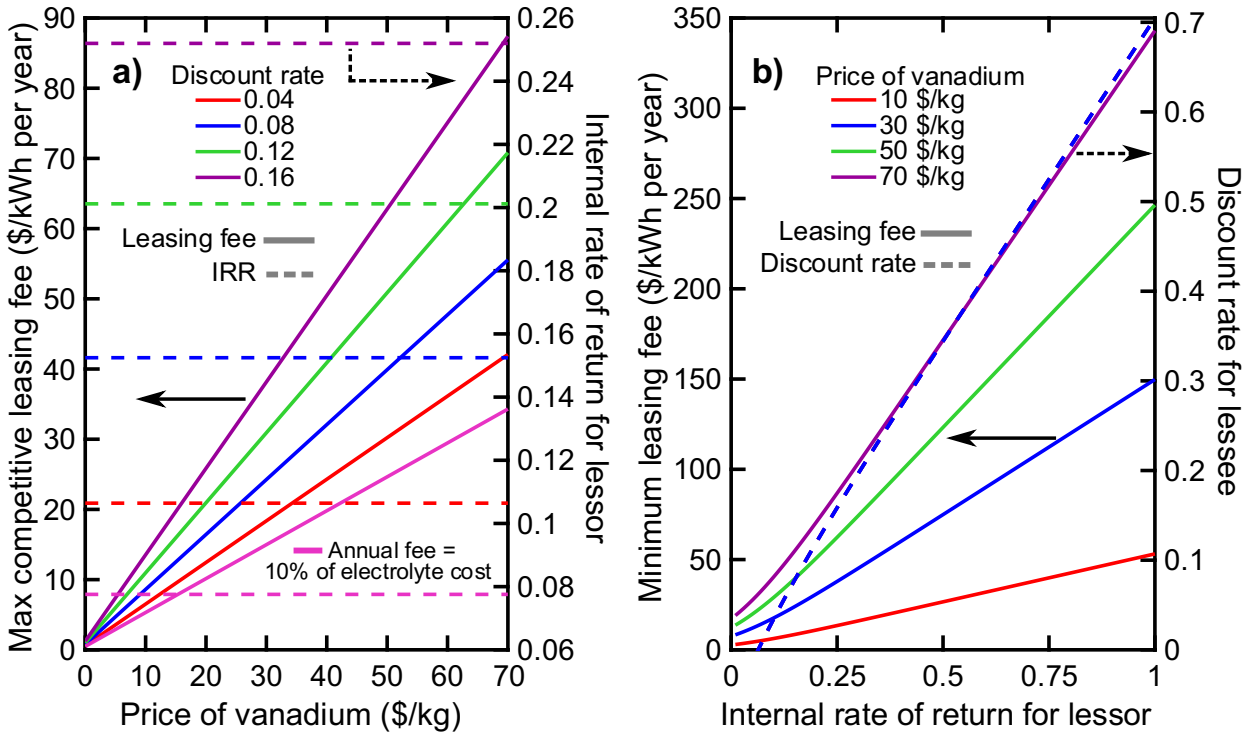

Figure II-7 – a) Maximum annual leasing fee (left y-axis, solid lines) to allow a competitive leasing scheme for the lessee, as a function of vanadium price (x-axis) at various discount rates to the lessee (red, blue, green, and purple), and the lessor's internal rate of return to the lessor under each case (right y-axis, dashed lines). The pink lines represent the case where the leasing fee is 10% of the electrolyte cost. b) Minimum annual leasing fee to be charged by the lessor (left y-axis, solid lines) as a function of the lessor's desired internal rate of return (x-axis) at various market prices of vanadium (red, blue, green, and purple), and the discount to the lessee in each case (right y-axis, dashed lines).

4. Conclusions

A defining feature of VRFBs is the ability to recover capacity via periodic rebalancing of the external electrolytes and injection of chemical reductants. However, the added value of this resilience has not yet been well-articulated in techno-economic models of VRFBs. Accordingly, we have developed a simple model to calculate the VRFB LCOS by introducing a physical model

that captures capacity fade and rebalancing over the operating lifetime. The framework offers a systematic means of assessing battery operation with rebalancing and servicing providing new insights to cost reduction strategies. Leveraging this model, we are able to draw several important conclusions. The main theme of our findings is that there is often a tradeoff between changes in capital cost and changes in lifetime performance or operating costs as they affect the LCOS. In some cases, increases in upfront capital cost can minimize repeating, long-term operational costs and overall lower the LCOS, such as the use of oversizing to help meet nominal capacity requirements rather than overly frequent rebalancing. In other cases, such increases in upfront cost that reduce operating costs did not result in overall LCOS savings, such as the purchasing of more expensive and selective membranes to reduce crossover, a result of the relatively low price of rebalancing. Alternatively, leasing schemes that decrease the upfront capital cost in exchange for yearly operating fees did indeed show potential of lowering the LCOS for battery owners. These findings highlight the need to consider metrics beyond capital cost when determining viable energy storage solutions, and for RFBs in particular.

While this study reveals several important gaps in VRFB research and development, at least in the published literature, it remains a fairly simple treatment of VRFB operation. To this end, future work should endeavor to refine aspects of this modeling framework to either further solidify conclusions described in the paragraph above or to enable assessment of other relevant technical and economic factors. With respect to the former, developing a more complete description of different fade mechanisms and their respective rates in VRFB systems as a function of electrolyte composition and cell operating conditions is of particular importance [8,90–93], especially in combination with application-informed duty cycles. Such information would enable a more refined understanding of the fade rate variability and rebalancing schedules for different use-cases. With respect to the latter, this framework can easily be extended to asymmetric chemistries which may be cheaper than vanadium but whose operation is complicated by less-recoverable crossover. Such analyses can provide further insight into membrane requirements for asymmetric chemistries and/or suitable in-situ or ex-situ techniques for separation and decontamination of electrolytes. This is the focus of the subsequent chapter.

III. Assessing capacity loss remediation methods for asymmetric redox flow battery chemistries using levelized cost of storage

1. Introduction

As discussed previously, the unique architecture of RFBs enables excellent resiliency for maintaining their energy capacities. However, crossover losses (*i.e.*, the transport of active species through the semi-permeable membranes separating the positive and negative electrodes, which are designed to allow for transport of supporting ions to maintain charge balance [94]) is crucial to minimize. If these membranes are not perfectly selective for the desired charge-carrier species, then RFBs experience capacity reductions via undesired permeation of active species, often referred to as crossover [95]. While crossover is not the sole cause of capacity decline within RFBs, it is often the largest contributor and may halve the accessible capacity within 100-200 cycles [12]. One strategy for mitigating the effects of crossover is the use of a "symmetric" redox chemistry, where all active species are based on a single parent compound [14]. In this case, crossover does not lead to cross-contamination and associated capacity losses are recoverable via periodic electrolyte rebalancing: the transfer and mixing of partial or full volumes of electrolyte between the two reservoirs to balance the concentrations of active species. Rebalancing is a powerful capacity-remediation tool, as it allows the electrolyte to be used indefinitely, assuming other non-crossover capacity losses can be managed and/or remediated as well, which significantly reduces maintenance costs [16]. A number of symmetric chemistries have been contemplated for RFBs leveraging inorganic [75], organic [96–99], and organometallic [100–102] active species, but vanadium remains the canonical example.

Vanadium RFBs (VRFBs) are the most researched and commercialized RFB technology, primarily because vanadium has four stable and soluble oxidation states accessible within the electrochemical stability window of aqueous acidic electrolytes on carbon electrodes. This, in turn, allows for a symmetric chemistry (V^{2+}/V^{3+} in the negative half-cell and V^{4+}/V^{5+} in the positive half-cell) and continual recovery of crossover capacity losses via rebalancing. While the VRFB system benefits from reduced maintenance costs, it suffers from a high upfront cost, due, in part, to the price of the active species [24,25]. Vanadium prices have been relatively volatile since the 1980's, and especially so in the last four years with a late 2018 peak of over ten-fold the price at

the start of 2016 [39]. The volatility has been attributed to: 1) the limited geographic locations of vanadium mines that leave the few countries that contain them (mainly China, Russia, and South Africa) with a strong control over the global vanadium supply [103], 2) new steel rebar standards that require increased vanadium content (already, 90% of current vanadium demand is steel [85]), and 3) decreases in supply due to mine closures [86] (discussed in more detail in **Chapter IV**). The magnitude and uncertainty of vanadium prices is considered a key impediment to broad deployment, which has motivated research into alternative chemistries based on lower-cost and widely-available materials [26–28].

In recent years, the literature has seen a surge of new, potentially-inexpensive, and usually asymmetric RFB chemistries, necessitating consideration of how one might execute asymmetric electrolyte maintenance. Since asymmetric chemistries utilize different active species in the positive and negative half-cells, active species crossover results in cross-contamination. With these chemistries, capacity-loss remediation is expected to be a more challenging and chemistry-dependent problem whose technical and economic consequences remain largely unarticulated in the open literature. A recent perspective by Perry *et al.* describes potential approaches for mitigating and remediating capacity losses due to crossover [16]. The options for crossover remediation depend on the fate of the active species upon entering the opposing half-cell; crossover can either be "destructive," where the active species are unstable in the chemical and electrochemical environment of the opposing half-cell and thus results in non-recoverable losses, or "non-destructive," where the active species remain intact in the opposing half-cell [16]. Destructive crossover remediation requires actives species replacement, but the authors note that there are no known RFB chemistries that experience destructive crossover in the published literature and thus do not explore this technique. What is more common, however, is time-dependent (*i.e.*, not crossover-dependent) active species decay in either half-cell, which would also necessitate active-species replacement [27]. In this work we divide the asymmetric chemistries and their remediation methods not by the stability of the active species upon crossover, but rather by the general stability or lifetime of the active species in their intended chemical and electrochemical environment, of which we note two classes: infinite and finite lifetime.

Finite-lifetime species experience decay and thus may require periodic replenishment or replacement. These species are generally organic compounds, which, despite uncertainty in their long-term stability, are attractive for RFBs as they are expected to be low-cost [104] and their

properties can be tuned through molecular functionalization; for example, increasing molecular size lowers crossover rates due to increased steric hindrance [105]. While organics are currently the most common finite-lifetime species used as active species in RFBs, the concept of finite-lifetime species is general and includes coordination complexes, inorganic compounds, and any other species that requires replacement during a project lifetime due to irreversible decomposition under normal operating conditions. Recent studies have shown that molecular decay rates of organics in RFB electrolytes are time-dependent and a function of the chemical, thermal, and electrochemical environment [106]. In particular, decay is generally accelerated when the molecule is in the "energized" state (for RFBs, this is the oxidized and reduced states for the positive and negative electrolytes, respectively) [24,27]. There is ongoing research into organic active species with longer lifetimes and techniques to optimize operating conditions to mitigate decay [107–109]. However, to the best of our knowledge, methodologies for removing and replacing decayed active species have not yet been systematically explored, likely due to the nascence of this particular class of chemistries. Note that the addition of active species without concomitant removal of the decay products is likely to be unsustainable in most cases, as it will lead to increases in solute concentration or total volume. Though largely chemistry-specific, removal would require targeted separation processes, which are likely to be complex, energy-intensive, and costly for concentrated multicomponent solutions, unless active species are intentionally designed to be easily separable from their decay products (*e.g.*, if decay products are gases or easily precipitable). Recovered decomposition products could potentially be regenerated or repurposed, either for fresh electrolyte or as feedstock for other chemical processes, though the technical and economic feasibility of such strategies will again depend on the underlying chemistry. These complications should be factored into techno-economic assessments; although inexpensive active species may reduce upfront capital costs, operating and maintenance costs may ultimately challenge the viability of such systems [106].

Infinite-lifetime species experience minimal degradation and primarily lose capacity via crossover, which allows for a range of capacity recovery strategies [16]. In general, these redox couples consist of inorganic materials that are ideally low-cost, abundant, and soluble in aqueous electrolytes, often in the form of redox-active salts with the cation (*e.g.*, Fe, Cr, Zn) [110,111], anion (*e.g.*, Br, I, FeCN) [112,113], or in some cases both [114], storing charge. The stability of these species usually translates to a non-destructive crossover scenario, meaning they are stable in

the chemical and electrochemical environment of both their original half-cell as well as the opposing half-cell. Thus, these chemistries can often be employed with the spectator strategy, where the electrolytes are mixed (*i.e.*, contain both active species) to make the chemistry pseudo-symmetric and enable electrolyte rebalancing [16]. However, the spectator strategy decreases energy density and increases electrolyte cost by reducing the active species solubility and adding inactive chemicals, respectively, but if employed by suitable chemistries for stationary applications, these drawbacks may not be critical. An alternative approach to preventing capacity fade due to crossover is the use of a perfectly-selective membrane, such as a non-porous single-ion conductor (*e.g.*, a ceramic). This strategy has received limited attention in the RFB field as experimental campaigns have been hampered by the cost, robustness, and increased resistance of available ceramics, as compared to polymeric membranes, all of which are anticipated to limit cell performance and system cost [115–119]. Note that both the spectator and perfect separation strategies are also viable approaches for finite-lifetime chemistries as well, but do not address active species degradation (unless the degradation primarily results from crossover), which limits their value to these systems.

Here, we use a simple levelized cost of storage (LCOS) model to evaluate the techno-economic benefits and limitations of low-cost, asymmetric chemistries with active species of finite and infinite lifetimes. Previously, we developed an LCOS model for VRFBs to assess the value of capacity recovery, and used the framework to explore practical operating considerations, such as sizing, rebalancing schedule, and electrolyte leasing [60]. While LCOS analyses consider the lifetime costs of the system for the optimal long-term solution, short-term metrics like the capital cost are also important in evaluating considerations around project investment and financing. Indeed, capital cost targets are a key metric cited when contemplating the economic viability of different energy storage solutions [9,10]. Recognizing the need for RFBs with low capital costs, we extend our LCOS model to explore the methods and associated costs for capacity-loss remediation for asymmetric chemistries using active species of finite and infinite lifetimes. For the former, we explore the logistics and costs of the active-species replacement process. For the latter, we explore the spectator strategy, using iron-chromium as a case study, as well as the use of zero-crossover membranes as capacity remediation and elimination techniques, respectively. These systems are compared to the VRFB system, the incumbent solution (*i.e.,* an RFB with higher capital costs and the ability to recover capacity at low costs) to determine the conditions under

which the reduced upfront cost of less expensive, asymmetric chemistries offsets the more complex and, in some cases, more expensive maintenance required to recover capacity losses.

2. Methods

The methodology for this work is informed by the economic and physical models developed in Rodby *et al.* to assess the LCOS of VRFBs [60], with key modifications to the operating and maintenance costs based on the chemistries considered. As such, repetitive details are omitted from the main text but can be found in the Supporting Information (SI) of the published version of this chapter [120]. In brief, we employ the following equation for LCOS ($ MWh^{-1}), defined generally as the ratio of the discounted costs to the discounted energy stored over a project lifetime:

$$\mathrm{LCOS} = \frac{\text{Discounted sum of costs over lifetime}}{\text{Discounted sum of energy stored over lifetime}} = \frac{\sum_{t=0}^{n} \frac{I_t + L_t + T_t}{(1+r_y)^t} + \sum_{t=0}^{k} \frac{OM_t + C_t}{(1+r_d)^t}}{\sum_{t=0}^{k} \frac{E_t}{(1+r_d)^t}} \qquad \textbf{(III-1)}$$

where I_t ($) is the investment expenditures, L_t ($) and T_t ($) are the loans and the taxes on those expenditures, respectively, OM_t ($) is the operating and maintenance costs, C_t ($) is the charging costs, and E_t (MWh) is the energy stored. These terms are tracked and summed across time (t), which, depending on the term, is either on a yearly ($t \in \{\mathbb{Z}^+ \cup [1,n]\}$) or daily ($t \in \{\mathbb{Z}^+ \cup [1,k]\}$) basis, where n and $k = 365n$ are the number of years and days of battery operation, respectively. The summed costs are discounted with a periodic rate, r, which is also applied yearly (r_y) or daily (r_d), depending on the cost period. Capacity loss is encompassed in the dynamic E_t term, while the costs to remediate capacity loss are captured in the OM_t and C_t terms. The full set of equations used to calculate the terms in Equation III-1, as well as the inputs used for various parameters, are provided in Section S1 of the SI of the published version of this chapter [120]. This approach for modeling LCOS has been used before to assess energy-storage technologies, and we draw input values from those published reports [54,55].

The dynamic capacity model, which incorporates fade and recovery, is similar to that used in our earlier work [60], although here it is presented in a more generalized fashion that we subsequently adapt for each chemistry. We assume linear overall capacity fade, which is the sum of a constant rate of crossover losses (r_{CO}, in units of % capacity loss per cycle), which can be remediated by

rebalancing, and a constant rate of electrolyte decay losses (r_{ED}, also in units of % capacity loss per cycle), which must be remediated using alternate servicing methods. We encompass all non-crossover losses in the electrolyte decay rate, which refers to side reactions and/or active species decay (the latter only applying to finite-lifetime chemistries). We elect to ignore any non-electrolyte losses, such as membrane fouling or electrode decay, because these components generally degrade on timescales longer than those anticipated for electrolyte crossover and decay (*i.e.*, require replacement every five to ten years [6,19]) and their degradation is assumed to be independent of the symmetry or lifetime of the chemistry, the focus of this work. The capacity accessed in a given cycle is equal to the product of the nominal battery size and f_{cap}, the fraction of original capacity accessible at that time. This fraction changes as the battery experiences electrolyte decay/crossover and subsequent remediation:

$$f_{cap} = 100\% - \left[r_{ED} * n_{cyc}^{S}(t)\right] - \left[r_{CO} * n_{cyc}^{R}(t)\right] \quad \textbf{(III-2)}$$

where $n_{\mathrm{cyc}}^{\mathrm{R}}$ and $n_{\mathrm{cyc}}^{\mathrm{S}}$ are the number of cycles passed since the last rebalancing event (*i.e.*, $t = R$) and the number of cycles passed since the last servicing event (*i.e.*, $t = S$), respectively. These counters increase each cycle and reset once rebalancing or servicing occurs and capacity is regained. These terms are further defined in Equation III-3. We note that servicing also resets the rebalancing counter, as we assume servicing achieves total capacity recovery.

$$n_{\mathrm{cyc}}^{R/S}(t) = \begin{cases} 0, \ t = 0 \text{ or upon rebalancing (R) or servicing (S)} \\ n_{\mathrm{cyc}}^{\mathrm{R/S}}(t-1) + 1, \ t > 0 \text{ and not rebalancing (R) or servicing (S)} \end{cases} \quad \textbf{(III-3)}$$

To determine when to service or rebalance the system, we define a lower capacity limit (cap_{lim}); once the accessible capacity declines to the cap_{lim}, capacity remediation is performed. In the case of symmetric and pseudo-symmetric chemistries, rebalancing will occur, which regains the capacity lost to crossover but not that lost to electrolyte decay. This process repeats until the total accessible capacity upon rebalancing has decayed to the cap_{lim} (*i.e.*, $cap_{\mathrm{lim}} \leq 100\% - r_{\mathrm{ED}} * n_{\mathrm{cyc}}^{\mathrm{S}}(t)$), at which point electrolyte servicing is performed. Where rebalancing is not feasible (*i.e.*, asymmetric chemistries), rebalancing is not employed and instead a servicing event occurs each time the accessible capacity decays to the cap_{lim}. This iterative capacity fade and recovery process is illustrated in Figure III-1, which exemplifies a simulation of the capacities of a generic symmetric and asymmetric RFB as a function of time. The nominal capacity rating is maintained

via a combination of the choice of cap_{lim} and oversizing of the capacity. Under a given scenario, the tradeoff between the increase in upfront cost to oversizing (*i.e.*, higher oversizing factor, *OF*) and the ability to remediate capacity losses less frequently (*i.e.*, lower cap_{lim}) is optimized to find the combination of cap_{lim} and *OF* that minimizes the LCOS. The optimal cap_{lim}/*OF* balance changes as the conditions or chemistries vary; Figure III-1 exemplifies how symmetric chemistries would likely have higher optimal cap_{lim} values, as compared to asymmetric systems, because their ability to regain capacity loss with low-cost maintenance makes more frequent remediation preferable (*i.e.*, results in a lower LCOS) to more significant capacity oversizing.

The costs of performing electrolyte maintenance are chemistry-specific and can be generally summarized as: (1) the cost of electricity to perform rebalancing to account for the energetic losses of crossover and self-discharge, which is only applicable to symmetric and pseudo-symmetric chemistries, and (2) the cost to perform servicing, which requires "oxidative maintenance" (*e.g.*, reductant chemicals, for VRFB, or a rebalancing cell, for iron-chromium) for infinite-lifetime asymmetric chemistries or "decay maintenance" (*i.e.*, separation and replacement or recovery of the decayed species, or total electrolyte replacement) for finite-lifetime asymmetric chemistries. The specific methods for modeling these costs are explained in greater qualitative detail in the Results & Discussion and in greater quantitative detail in Section S1 of the SI of the published version of this chapter [120]. Input values for relevant parameters that are used for the various chemistries contemplated here are summarized in Table III-1.

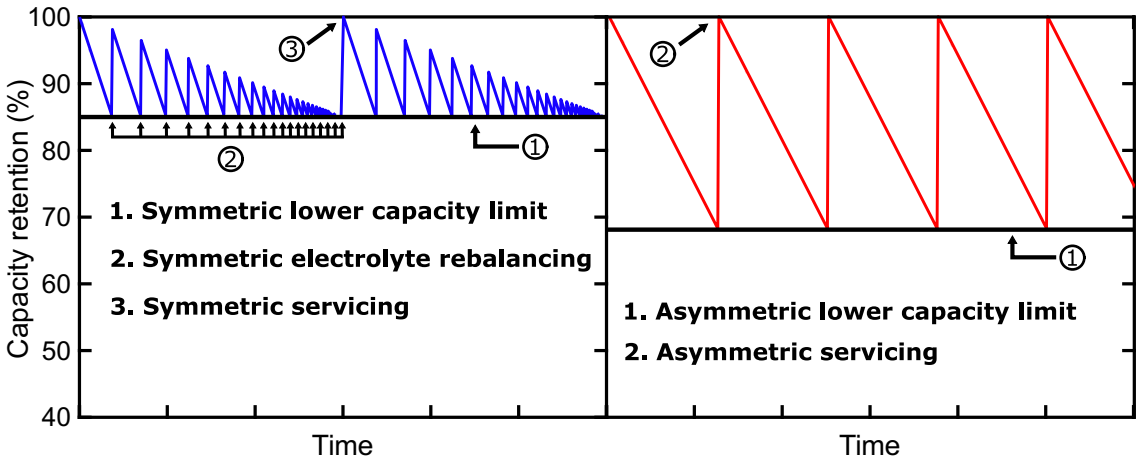

Figure III-1 – Example of the simulated capacity retention for generic symmetric (left, blue; *e.g.*, VRFB) and asymmetric (right, red) RFB chemistries (for illustrative purposes).

Table III-1 – Symbols, names, assumptions, values, and sources for the chemistry-specific model parameters. Values with asterisks (*) are baseline values but are subsequently varied in sensitivity analyses. For the "generic infinite-lifetime chemistry and/or Fe-Cr" column, the values given for each parameter apply to both cases except for the asterisked variables, of which the baseline values correspond to the Fe-Cr case but are varied for the generic case (see Figure III-3). Note: the SI mentioned refers to that of the published version of this chapter [120].

Symbol	Name	Assumptions	Values and Sources		
			VRFB	**Generic infinite-lifetime chemistry and/or Fe-Cr**	**Generic finite-lifetime chemistry**
O	Operational servicing fee	Electrolyte service fee (labor, transport, and other bulk costs; excludes electrolyte costs)	0 \$ kWh^{-1} per visit (see Section 3.1)	N.A. (see SI Section S1.2)	4-20 \$ kWh^{-1} per visit (see Section 3.1)
ε_E	Roundtrip system cycle energy efficiency	Product of voltaic, coulombic, and system efficiencies	75% [61]	75% [61]	75% [61]
r_{CO}	Crossover fade rate	Contribution of fade recovered with rebalancing	0.387% capacity loss per cycle [60]	0.3% capacity loss per cycle [25]	0% capacity loss per cycle (see Section 3.1)
r_{ED}	Electrolyte decay rate	Contribution of fade requiring servicing to remediate	0.055% capacity loss per cycle [60]	0% capacity loss per cycle (see SI Section S1.2)	* 0.1% capacity loss per cycle (see Section 3.1)
U	Open circuit voltage	At 50% SOC and relevant operating conditions	1.4 V [61]	* 0.98 V [121]	1.5 V [61]
MW_{active}	Equivalent weight of active species	-	51 g mol^{-1} (vanadium)	* 52 g mol^{-1} (chromium)	150 g mol^{-1} [61]
$conc_{active}$	Concentration of active species	Concentration near general aqueous solubility limit of 1.5 M, 1 M for spectator strategy cases	1.5 M	1 M [122]	1.5 M
c_{active}	Cost of active material	-	30.14 \$ kg^{-1} V [39] (see SI Section S2.3)	* 2.29 \$ kg^{-1} Cr [123,124]	* 3.50 \$ kg^{-1} [61,104,125]
$C_{electrolyte}$	Total cost of electrolyte	Cost per energy throughput, before oversizing (OF = 1). See SI Section S2.2	122 \$ kWh^{-1}	* 23 \$ kWh^{-1}	* 50 \$ kWh^{-1}
c_a	Areal cost of reactor	Estimated from existing RFB techno-economic analyses, see SI Section S2.2	450 \$ m^{-2}, 158 \$ kW^{-1} [19,61,126]	450 \$ m^{-2}, 323 \$ kW^{-1} [19,61,126]	* 450 \$ m^{-2} , 138 \$ kW^{-1} [19,61,126]

3. Results and discussion

We apply our LCOS model to the two asymmetric chemistry classes – those with active species of either finite or infinite lifetimes – and compare these results to a VRFB baseline to evaluate their ability to compete with the state-of-the-art. Regarding finite-lifetime chemistries, we model different options for active-species replacement and explore the feasibility of each, while also estimating the sensitivity of LCOS to electrolyte decay rate, electrolyte cost, and reactor cost for each remediation scheme. For infinite-lifetime chemistries, we consider two methods for addressing crossover losses: 1) remediation of crossover by applying the spectator strategy to make the chemistry pseudo-symmetric and allow for rebalancing, or 2) elimination of crossover altogether via use of a perfectly selective separator. In examining the spectator strategy, we focus on the ability of a chemistry to competitively employ this scheme through calculation of the electrolyte cost, and use iron-chromium as a case study. In examining the perfectly selective separator case, we determine the bounds of separator cost, cell potential, and cell resistance needed to approach viability.

3.1 Remediating capacity loss for asymmetric chemistries with active species of finite lifetime: active-species replacement

RFB chemistries with finite lifetimes inevitably require periodic active-species replacement. To our knowledge, the logistics of such processes have yet to be considered in the published literature but likely possess technical and economic challenges specific to the underlying chemistry. In these finite-lifetime systems, capacity fade is due to a combination of crossover and active species decay, although, for most embodiments to date, active species decay rates are generally one or more orders of magnitude greater than the rates of loss due to crossover [27]. We propose two potential options for capacity remediation for such systems, each employed periodically: (1) separation and removal of the "contaminants" (*i.e.*, species that have decayed or crossed over), followed by either (1a) replacement with fresh active species or (1b) recovery and reuse of the active species from these contaminants (which may require methods to reverse decay), or (2) total replacement of the electrolytes. Targeted removal of contaminants eliminates the waste of replacing non-decayed electrolyte and may even allow for reuse of the recovered species, but the selectivity, energy

requirements, and cost of chemistry-specific separation processes are unknown and may be prohibitive. Conversely, one could eliminate the need for any separation processes, at least on-site, by replacing the entire electrolyte upon reaching a capacity loss threshold (*i.e.*, cap_{lim}), but this requires the exchange of large volumes and potentially sacrifices a significant quantity of valuable material. For the first option, we model only the separate/recover/reuse scenario (1b), as the separate/replace scheme (1a) lies between the lower bound of full reuse and the upper bound of total electrolyte replacement options in terms of resources required. Again, we note that simple addition of more active species or electrolyte without concomitant removal of contaminants or contaminated electrolyte is likely to be an unsustainable solution in most cases, as it will lead to increases in solute concentration or total volume, respectively.

These two remediation schemes are modeled differently, though both are fairly simple to represent. Total electrolyte replacement cost is intuitively modeled as the product of the electrolyte cost ($C_{\mathrm{electrolyte}}$, \$ $\mathrm{kWh^{-1}}$) and the nominal capacity rating of the battery, plus an operational servicing fee. In this case, the fee should cover the labor to execute the replacement, the cost to transport electrolyte to and from the battery site, and perhaps the post-processing or disposal of the spent electrolyte. We estimate the costs for the labor and transport are ~4 \$ $\mathrm{kWh^{-1}}$, so we use this as a lower bound for the servicing fees used with the finite-lifetime cases (see SI Section S1.3 for details). Conversely, the separate/recover/reuse scenario is difficult to rigorously model, as there is chemistry-specificity regarding the exact methods and, by extension, associated costs needed to separate out decayed and crossed-over contaminants, reverse any decay, and finally reintroduce these species to their original half-cell. Accordingly, we elect to encompass all of these material and energy costs, in addition to the cost of the labor required to execute these actions, in the bulk operational servicing fee term. By varying the magnitude of the service fee (here, we show results using 4 and 20 \$ $\mathrm{kWh^{-1}}$), it is possible to estimate what additional servicing costs are allowable if the RFB chemistry is to be cost-competitive with the VRFB, on a LCOS basis. To further facilitate the modeling of these chemistries, we set the r_{CO} (the capacity fade rate that is recoverable upon rebalancing) to 0% per cycle, encompassing all fade in the r_{ED} term, as all fade experienced in these asymmetric chemistries must be recovered via servicing (*i.e.*, rebalancing to remediate crossover losses is not an option). Thus, crossover is treated as a mode of electrolyte decay, because it requires the same general remediation mechanisms as active species decay (*i.e.*, options 1 and 2, explained above). We note that crossover complicates the chemistry-specific separations

needed by adding more species to separate on top of those that have decayed, particularly because the fate of crossed-over species (*i.e.*, whether they stay intact or decay to any number of products) could be uncertain or variable [127]. Finally, as discussed in the Introduction, we assume these finite-lifetime species are organic compounds, with an average equivalent weight of 150 grams per mole, in aqueous electrolytes (we also assume that, in the case of two electron transfer, both transfer events occur at the same electrode potential) [61]. Quantitative representations of the chemistry-specific servicing costs (which includes both the servicing fee as well as other chemical costs, which are treated separately) can be found in Section S1.2 of the SI.

In addition to the operational service fee, the achievable lower bounds of electrolyte decay rate and electrolyte cost for finite-lifetime chemistries remain open questions and are the focus of active fundamental and applied research. To date, at-scale demonstrations of finite-lifetime chemistries in RFBs have been limited to a few start-up companies [128–132], and details on their specific redox chemistries, system configurations, performance abilities, and operational and maintenance approaches are not reported. Consequently, we perform sensitivity analyses on electrolyte cost and decay rate, along with reactor cost, to determine cost and performance targets. Figure III-2 below shows the LCOS sensitivity as a function of these three variables for the two remediation schemes (separate/recover/reuse in green and total electrolyte replacement in red) for an asymmetric, finite-lifetime chemistry. Values for VRFBs are provided for comparison (plotted in blue), which are treated as constant base cases because they have a relatively developed market and established body of research such that there is greater certainty around the present techno-economic parameter values. The VRFB case assumes a service fee of 0 \$ kWh^{-1}, as it must only encompass the labor of adding the chemical reductant, which was determined to be negligible (see SI Section S1.3), while two higher service fees (4 and 20 \$ kWh^{-1}) are used for the asymmetric cases. These different operational service fees are represented by varying line styles. There are two immediate insights gained from Figure III-2: (1) LCOS is highly sensitive to electrolyte decay rate and electrolyte cost, and (2) the separate/recover/reuse scheme appears more likely to be competitive with VRFBs than the total replacement scheme. Indeed, at a service fee of 4 \$ kWh^{-1}, total electrolyte replacement requires very low decay rates (≤0.02 % capacity loss per day at the baseline electrolyte cost of ~50 \$ kWh^{-1}) and/or electrolyte costs (≤13 \$ kWh^{-1} at the baseline decay rate of 0.1 % capacity loss per day), or some optimal combination between these baselines and targets for both parameters, to achieve a lower LCOS than a VRFB. Whereas, even with a higher service fee of 20

$ kWh^{-1}, the separate/recover/reuse scheme enables more lenient targets for the decay rate (≤0.06 % capacity loss per day at the baseline electrolyte cost of ~50 $ kWh^{-1}) and the electrolyte cost (≤30 $ kWh^{-1} at the baseline decay rate of 0.1 % capacity loss per day). However, these cost and performance targets are highly dependent on the service fee, particularly for the separate/recover/reuse scheme.

To contextualize these electrolyte cost targets, we can look to the limited techno-economic studies on aqueous organic electrolytes (note: all studies assume an average cell voltage of 1.5 V). Darling *et al.* estimated the electrolyte cost for an aqueous organic RFB to be ~235 $ kWh^{-1} in 2014, and between 45 and 90 $ kWh^{-1} in the "future" [61]. The 2018 work by Dieterich *et al.* modeled the production cost of AQDS (~157 grams per mole electron, assuming a two-electron transfer), a well-known finite-lifetime active species for RFBs that is relatively easy and low-cost to manufacture [24,133], and estimated the total electrolyte cost for an AQDS chemistry (assuming the cost of the negative and positive electrolytes are approximately equal) to be 50 and 65 $ kWh^{-1} at production scales ~100 and ~200 MWh of flow battery capacity deployed per year, respectively [104]. Based on their estimates of materials costs alone, it is difficult to envision reducing electrolyte costs below 30 $ kWh^{-1} while utilizing existing production methods (regardless of production scale). Furthermore, a recent study by Gregory *et al.* estimates that reducing the electrolyte price of an aqueous RFB system using AQDS on the negative side or a ferrocyanide-based positive electrolyte to our baseline electrolyte cost of 25 $ kWh^{-1} per side (*i.e.*, 50 $ kWh^{-1} overall) would require a production scale equivalent to producing 10 GWh of flow batteries per year [125]. Currently, there only ~100 MWh of RFBs deployed globally, with another ~1 GWh contracted, announced, or under construction [11]. These studies clearly demonstrate that low-cost (*i.e.*, ≤50 $ kWh^{-1}) electrolytes for finite-lifetime chemistries will require one or more of the following factors: the use of previously unstudied active molecules, development of new production pathways for existing active molecules (*e.g.*, AQDS), internal production of the active molecules by the RFB company (to minimize markups by suppliers), and/or drastic increases to production scale (either by growth of the RFB market utilizing these chemistries and/or other markets for these active species). Therefore, the more promising pathways to viable asymmetric chemistries with finite lifetimes are those that can enable low service fees or low decay rates.

With respect to electrolyte decay rates, those reported in the literature range five orders of magnitude (from as low as order 0.001 to as high as order 10, in units of % capacity loss per day),

which challenges a feasibility judgement on the decay-rate baseline of 0.1 % capacity loss per day [27,108,109]. This variability can be attributed to differences in the choices of active species, experimental apparatus, testing protocols, and other experimental conditions. Further, the protocols and the conditions used to measure these decay rates may be less aggressive than those of a deployed system, potentially making these conservative estimates. That said, several publications have reported active-species stability in the desired range of ≤0.1 % capacity loss per day [27,108,109,134,135], including many quinone-derivatives. In working to reduce these key variables, note that electrolyte price and decay rate may not be independent, as functionalization of organic molecules often improves stability [27,136] and, likely, simultaneously complicates the manufacturing process and thus adds to the chemical cost. Relative to those two variables, reactor cost has a lesser effect on LCOS, though it is important to consider as organic molecules are generally larger than their aqueous supporting salts, providing the opportunity to leverage size-exclusion membranes as opposed to more expensive ion-exchange membranes [105]. There is also the potential to employ lower-cost membranes ill-suited for VRFBs, either via the use of electrolytes with milder *pH* [108,134] or a less oxidizing active species [8].

Based on our evaluations of the feasibility of achieving the relevant targets for electrolyte cost and decay rate, the separate/recover/reuse remediation process appears capable of making asymmetric chemistries of finite lifetimes competitive with VRFBs if the service fees to employ it can be kept sufficiently low. The 20 \$ kWh^{-1} service fee already sets seemingly difficult targets; for example, an electrolyte cost of 30 \$ kWh^{-1} seems infeasible with our current solutions, even assuming the possibility of vast scale-up, as previously discussed. From these observations, we propose that the costs to separate/recover/reuse should be limited to ≤10 \$ kWh^{-1} to allow for viability at the expected lower limits for electrolyte cost and decay rate. At this juncture, it is difficult to assess the feasibility of this target, due to the absence of discussion or study of these methods in the open literature. A notable exception is the work of Goulet *et al.*, which explored decay reversibility for an aqueous chemistry with a finite-lifetime species on the negative side (*i.e.*, a quinone derivative) [107]. The authors were able to reverse 70% of the decay, which had already been mitigated to 0.14 % per day by limiting the state of charge, via aeration of the electrolyte. They estimated that the modifications to RFB operation needed to facilitate this capacity loss reduction/remediation would add ~20 \$ kWh^{-1} to the capital cost, which corresponds to an annual operating and maintenance cost of just over 2 \$ kWh^{-1} per year if calculated assuming a 20 year lifetime and 8%

discount rate [137]; while this is within our desired range, the remaining 30% of the decayed species that cannot be rejuvenated via aeration alone would eventually require separations.

Three complicating features of this system to consider regarding separations are (1) the high overall electrolyte concentrations, (2) the need to keep the main stream of electrolyte (*i.e.*, what remains after separating out the decayed species) almost entirely uncontaminated from the separations process and the further desire to recover the decayed species intact as well for reuse in the system, and (3) the likely similar characteristics of the decayed species being targeted for separations and the active species that must remain in the electrolyte. Methods for separating organics via exploitation of differences in the physical, chemical, and/or electrochemical properties exist and can even separate similar compounds (*e.g.*, isomers) [138,139]. It seems reasonable to assume that expertise in separating decay product lies within the process industry given the requirements to create products of sufficient purity. Consequently, chemical manufacturers may be uniquely positioned to design new redox active compounds with decay reversal or recovery as a key design parameter, or else offer technical solutions for separation of pristine species from decay products either on-site or at a centralized facility. Next, we consider remediation techniques for infinite-lifetime species. We note that while separations processes could be used for crossover remediation in these cases as well – and there are, in fact, relatively developed and low-cost methods for separating mono- and multi-valent ions from multi-component mixtures (*e.g.*, wastewater treatment) [140] – the other techniques available for these chemistries, discussed below, are anticipated to be economically preferable to total electrolyte replacement or complicated separations.

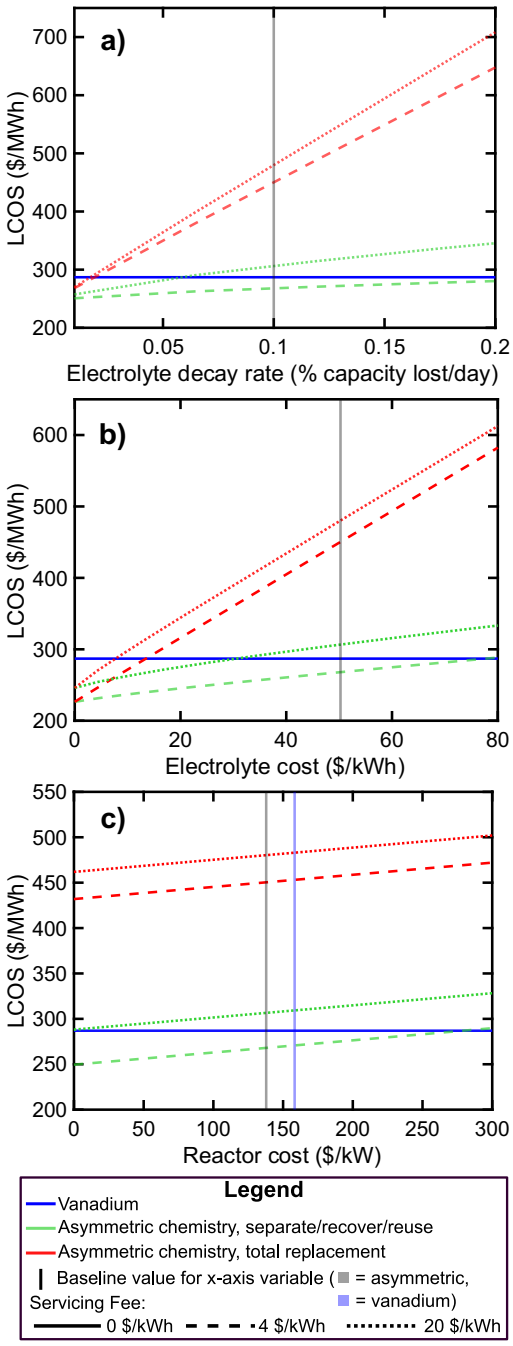

Figure III-2 – LCOS as a function of electrolyte decay rate (a, top), electrolyte cost (b, middle), and reactor cost (c, bottom) for a generic, asymmetric chemistry employing the separation/recovery/reuse remediation method (green lines) or total electrolyte replacement remediation method (red lines). These are compared against baselines for a VRFB (blue lines), which do not change with the x-axis variables. The vertical lines represent the baseline value of each x-axis variable for the asymmetric case (grey) and the vanadium case (blue) (note that vanadium does not decay and its electrolyte cost, ~122 \$ kWh^{-1}, exceeds the x-axis scale in 2b, thus the vanadium x-axis baseline is only visible in 2c). The line styles correspond to varying operational service fees.

3.2 Remediating capacity loss for asymmetric chemistries with active species of infinite lifetime: the spectator strategy

Crossover – driven by electroosmotic drag and gradients of concentration, potential, and/or pressure across the half-cells – is a primary cause of capacity loss for asymmetric RFB chemistries with active species of infinite lifetimes. However, the stability of these active species in their home and opposing cell environments enables use of the spectator strategy, where both active species are dissolved in each half-cell electrolyte. A mixed electrolyte is typically prepared with equal concentrations of active species in their discharged forms and used in both reservoirs. During operation, the active species for the positive half-cell reaction serves as the charge storage species on the positive side of the cell and as a spectator on the negative side of the cell. The opposite is true for the active species for the negative half-cell reaction. This transforms asymmetric chemistries into pseudo-symmetric chemistries and allows for utilization of the same VRFB rebalancing methods [12,42–45,60] to remediate losses due to crossover. Further, crossover is actually mitigated by the spectator methodology itself [16,25], as diffusive fluxes between the two electrolytes that drive crossover are also significantly decreased with this strategy [127].

As mentioned before, implementation of this strategy requires that both active species are chemically and electrochemically stable in the opposing half-cell, but there are also important techno-economic considerations. The spectator strategy typically decreases energy density and increases electrolyte cost, limiting the chemistries to which this approach can be applied cost-effectively. The addition of the spectator species lowers the solubility of the active species [16], limiting the energy density, as well as doubles the active material required for the same energy output, increasing electrolyte costs. Lower energy densities are arguably less concerning for stationary energy storage applications where the size and mass constraints for the battery are more lenient as compared to mobile ones, but the increased electrolyte cost could be prohibitive for grid applications where lower cost solutions (*e.g.*, fossil fuels or cheaper battery chemistries/technologies) are readily available. At the very least, the savings from employing a low-cost asymmetric material set may be lost if the spectator strategy increases the energy costs to the point they exceed that of the incumbent VRFB chemistry. Thus, we can calculate the total electrolyte cost for a spectator chemistry as a function of three key variables – active species costs, active species equivalent weight, and cell potential – to estimate the available design space for

these chemistries to be competitive the VRFB (Figure III-3). Other variables that affect electrolyte cost – such as accessible depth of discharge, cost of solvent, solubility, etc. – are generally more consistent across aqueous chemistries, as compared to these three highly chemistry-dependent variables [61]. We vary equivalent weight and cell potential within the bounds typically seen in RFB chemistries (50-150 grams per mole and 1.0-1.6 V, respectively [61]), and use a range of active species costs that would generally classify low-cost, high-abundance materials (≤20 \$ kg^{-1}). Across the range of values studied, the combination of the active species equivalent weight and chemical cost significantly impacts the final electrolyte cost and thus the economic viability, whereas cell potential has a less pronounced effect, particularly with increasing active species equivalent weight (though we note that cell potential also impacts the power costs, which is not accounted for in this simple electrolyte-cost comparison). We see the majority of the design space for these spectator strategy chemistries is competitive with the VRFB, and this space seems reasonable: many new chemistries being studied use abundant active materials, such as iron, zinc, sulfur, etc., all of which have been cited in RFB literature to cost ≤10 \$ kg^{-1} and have equivalent weights and cell voltages in the middle of these ranges [61,124]. However, using this strategy with larger active species (~150 grams per mole), such as organics or ligand-modified transition metals, requires very low costs to be competitive with VRFB (≤5 \$ kg^{-1}). Several RFB chemistries leverage the spectator strategy [141,142], with perhaps the most notable being iron-chromium (Fe-Cr).

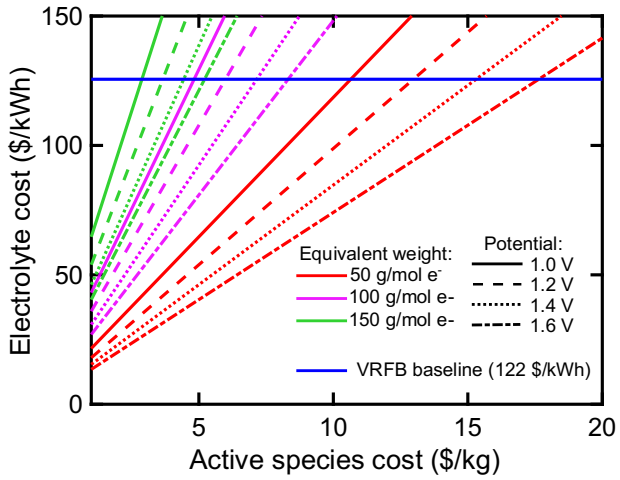

Figure III-3 – Electrolyte cost (y-axis) as a function of active species cost (x-axis), active species equivalent weight (line colors), and cell potential (line styles) for chemistries utilizing the spectator strategy. For context, the baseline electrolyte cost of the VRFB (122 $ kWh^{-1}, assuming an equivalent weight of 51 grams per mole, active species cost of ~ 30 $ kg^{-1}, and potential of 1.4 V) is plotted as a blue solid line.

The pseudo-symmetric Fe-Cr RFB offers several benefits as compared to the VRFB. Use of the spectator method for the Fe-Cr chemistry has been shown to significantly reduce net crossover rates [143], which is important as iron and chromium ions are ~20× more permeable than vanadium ions in Nafion membranes [144]. The chemistry uses charge-storage species of high crustal abundance, as iron is the most abundant element in the Earth (by mass) and there is nearly 1000× more chromium resources than vanadium [103]. These active materials are also low-cost: from late 2019 through early 2020, the price of ferrochromium was ~2 $ kg^{-1} of chromium content [123]. Further, ferrochromium contains forms of both active species, which can facilitate cost savings by minimizing waste and reducing the processing steps needed to generate to electrochemical grade electrolyte if employed in an Fe-Cr system utilizing spectator strategy [143]. However, the open circuit voltage of Fe-Cr is ~0.98 V at typical operating temperatures (*i.e.*, ~65 °C) [143] and the active species solubility in the spectator configuration are ~1 M [25,121], limiting energy and power densities. Assuming a four-hour duration, we estimate the capital cost of the Fe-Cr RFB to be lower than that of the VRFB, at ~211 and ~268 $ kWh^{-1} (including optimal oversizing to minimize LCOS, as explained previously), respectively, where the electrolyte costs of the Fe-Cr are about a fifth of the VRFB electrolyte costs (~23 and ~122 $ kWh^{-1}, respectively, not including oversizing) and the reactor costs of the Fe-Cr are about double that of the VRFB (~323 and ~158

$ kW^{-1}, respectively). These numbers align with other techno-economic assessments of these systems [6,25]. Despite also facing capacity loss due to hydrogen evolution at a rate ~20× that seen in VRFBs (~1 % vs 0.055 % of capacity loss to hydrogen evolution per cycle) [19,25,145], the Fe-Cr system also shows improvement over VRFBs in terms of LCOS. We estimate the LCOS of Fe-Cr to be ~260 $ MWh^{-1}, a moderate reduction from the LCOS of the VRFB (~290 $ MWh^{-1}). Even artificially increasing the hydrogen evolution-induced capacity fade rate in the Fe-Cr system to as much as 10% capacity loss per cycle does not raise the LCOS of the Fe-Cr system above 270 $ MWh^{-1}. Modeling details used to derive these numbers can be found throughout the SI. The techno-economic promise for Fe-Cr is evident, however, the capital cost of the system still exceeds the Department of Energy target of ≤150 $ kWh^{-1} for viable grid storage [9,10]. Reductions in the power costs (*i.e.*, beyond the chemistry choices probed in this work, perhaps by increasing the duration or using lower-cost reactor materials) are likely needed. There is, however, the potential for further cost reductions for the Fe-Cr system with any significant improvements to performance. Most of the Fe-Cr research was executed in the 1970's and 1980's when NASA first introduced this chemistry as the first true RFB while exploring energy storage solutions for deep-space missions [146]. Research into the Fe-Cr system has been limited relative to that for VRFBs, and it is likely that many of the significant improvements to the VRFB system seen over the past 5-10 years can be applied to the Fe-Cr system to increase performance and reduce costs. Some of this has already been demonstrated; for example, recent studies have shown the benefits of advanced cell engineering and optimized electrolyte composition for the Fe-Cr system [110,122].

3.3 Eliminating crossover with ceramic membranes

Membranes with perfect selectivity for the desired charge-carrier species, such as non-porous, single ion-conducting (SIC) materials, could eliminate crossover losses experienced by stable RFB chemistries, obviating the need for symmetric and pseudo-symmetric electrolytes. Research into SIC membranes, mainly ceramics and ceramic-polymer composites, for RFBs has been limited, with most studies employing them for energy dense semi-solid/hybrid redox chemistries or systems utilizing two electrolytes of different pH [115–119,147]. More extensive exploration has likely been hampered by the absence of broadly-available commercial materials, the lack of cross-disciplinary expertise between the fields, and the experimental challenges of integrating a ceramic

into a contemporary flow-cell architecture. There is an inherent tradeoff between improving (*i.e.*, increasing) selectivity and worsening (*i.e.*, increasing) resistivity, and thus high selectivity typically results in large ohmic resistance; for example, Allcorn *et al.* measured a resistance of ~90 Ω-cm^2 for their 1.1 mm thick ceramic membrane (using a symmetric ferro-/ferri-cyanide chemistry) [115]. The total area-specific resistance (ASR) of a state-of-the-art RFB cell is mostly ohmic resistances, plus some minor contributions from kinetic and transport losses. Therefore, these large resistances not only represent significant performance losses, but they also have major economic consequences since they substantially impact power density, efficiency, and ultimately the cost of the reactor (the power delivered per unit area of reactor is inversely proportional to ASR [61]). The price of these membranes is also uncertain; although there is a sizable body of literature on ceramic membranes for water-treatment applications, a subset of which focus on the development of low-cost options ranging from as low as 25 \$ m^{-2} to 500 \$ m^{-2} [148–152]. At present, it is not clear how relevant these estimates are to the material sets conducive to use in RFBs, as application-specific design criteria vary (*e.g.*, flexibility, conductivity, chemical compatibility, etc.).

While the lower bounds of the cost and ASR for SIC membranes have yet to be determined, one may use techno-economic analyses to estimate what values these parameters would need to be in order to present a competitive solution for RFBs. We estimate the LCOS as a function of ASR (Figure III-4), which, as mentioned previously, linearly scales the reactor cost. We use the inputs for the infinite-lifetime species in Table III-1, as SIC membranes are most effective for chemistries which experience losses that are dominated by crossover, and accordingly assume zero capacity fade (*i.e.*, negligible capacity loss from non-crossover sources). We then vary the SIC membrane price between 100 and 300 \$/m^2, which is within the range seen in water treatment literature and comparable to the present-day cost of Nafion [6,17]. We also vary two critical chemistry-dependent parameters: active species cost (Figure III-4a) and cell potential (Figure III-4b). We find that LCOS is not particularly sensitive to active species cost and is more sensitive to membrane price, which makes sense as the reactor cost dominates the capital cost at high ASRs such that changes to electrolyte cost have a relatively small impact on both the capital cost and the LCOS. This is also why we find a strong LCOS sensitivity to cell potential (U), which scales both reactor costs ($\propto U^{-2}$) and energy costs ($\propto U^{-1}$). Thus, higher cell potentials can, at least partially, offset elevated cell ASRs. Reducing the measured ASR to ~15 Ω-cm^2 in RFB cells employing SIC

membranes, a 6x reduction from published reports [115], may be technically achievable, but a viable implementation also requires a moderate cost for the SIC membrane (*i.e.*, ~100 \$ m^{-2}) and a high voltage redox chemistry (*i.e.*, ≥3 V). Such requirements likely necessitate the use of non-aqueous electrolytes, a subfield of RFB research that has not yet broadly demonstrated such technical capabilities [153] but is still nascent and expected to grow. Furthermore, such high ASRs create physical complications: a cell with an ASR of 15 Ω-cm^2 would require 30× the area of a conventional cell configuration with a polymeric membrane like Nafion (~0.5 Ω-cm^2, for aqueous systems) for a given power output and chemistry, which is a substantial increase to the reactor footprint that must be considered. This may be less of an issue for long-duration applications, as the energy-capacity components increasingly dominate the system configuration. While the design space presented here suggests what a successful SIC membrane might look like, further studies of SIC membranes for RFBs, with particular focus on understanding tradeoffs between resistance, cost, and mechanical stability, are needed to more completely assess the viability of this approach.

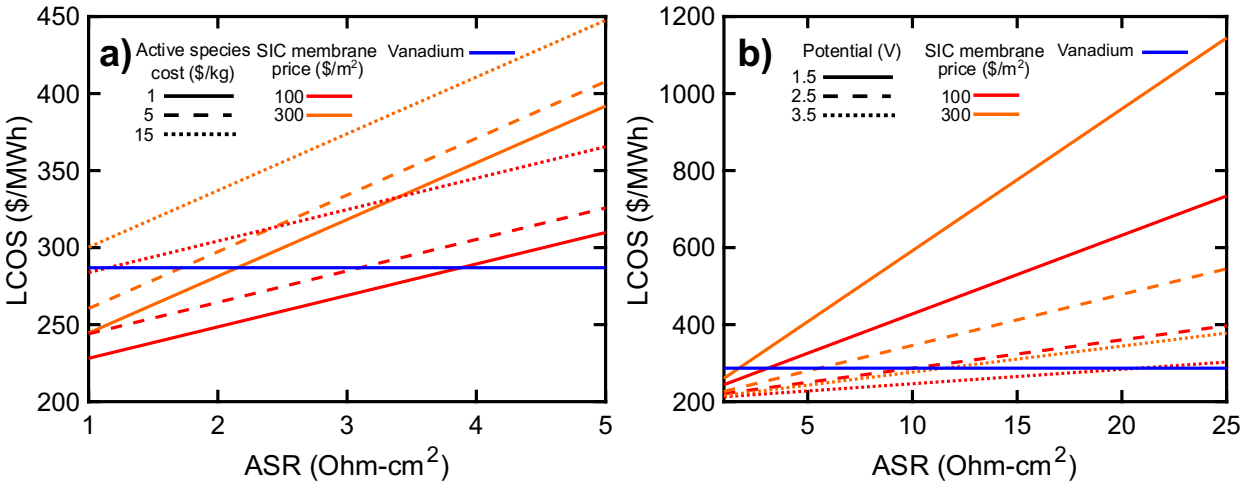

Figure III-4 – LCOS as a function of the cell ASR, with membrane price (line colors), and active species cost (a, left) or potential (b, right) (line styles) as variable parameters. The left plot assumes a cell potential of 1.5 V, and the right plot assumes an active species cost of 5 \$ kg^{-1}. The baseline LCOS of vanadium (assuming a potential of 1.4 V, ASR of 0.5 ohm-cm^2, active species cost of ~30 \$ kg^{-1}, and membrane cost of 300 \$ m^{-2}) is plotted in blue.

4. Conclusions

The desire for and research of potentially-inexpensive RFB chemistries has been growing in response to financial concerns around the cost of vanadium active species in the most mature RFB chemistry, the VRFB. However, these options present more challenges to consider beyond the alteration in cost of the electrolyte or even the kinetic, thermodynamic, and mass transport challenges of these new chemistries. As many of these new chemistries are asymmetric, the methods and associated costs of asymmetric capacity-loss remediation must be explored to determine if the complications that arise from cross-contamination outweigh the reduced capital cost relative to the more easily remediable VRFB. Accordingly, we have adapted our LCOS model, used in previous work for VRFBs, to evaluate two classes of asymmetric chemistries: those using active species of finite and infinite lifetimes. Finite-lifetime chemistries, often employing organic active species, primarily suffer capacity losses from active species decay, necessitating their periodic replacement. This can be achieved by performing total electrolyte replacement, or by selectively separating out and replacing or reusing the decayed species. We found that the separations route is substantially more economically effective, but only if such processes can be executed with low enough costs, and the LCOS of these systems is highly sensitive to the electrolyte cost and decay rate. We estimate that the cost to separate/recover/reuse should be limited to $\leq$10 \$ kWh^{-1}, and future work should explore electrolyte separation and recovery methods to better assess the feasibility of this target. This analysis has revealed an opportunity for chemical-manufacturing companies who may be uniquely positioned to design organic redox active species with decay remediation in mind as a key design criterion. Infinite-lifetime species primarily suffer capacity losses from crossover, which can be remediated by making the chemistry pseudo-symmetric via the spectator strategy or avoided altogether with the use of perfectly selective separators. The spectator strategy, which employs mixed electrolytes, is only effective if the species are stable in their opposing half-cell's environments and if the resulting decrease in energy density and the increase in required active material do not increase the electrolyte cost above that of other potential symmetric chemistries like the VRFB; this requires active species with relatively low active species costs and/or equivalent weights ($\leq$15 \$ kg^{-1} for active species ~50 grams per mole, or $\leq$5 \$ kg^{-1} for active species ~150 grams per mole). We found that the Fe-Cr system, which has not been as widely studied or improved upon as compared to VRFBs, is a promising candidate chemistry for effective use of the spectator strategy to reduce the capital cost

and the LCOS, as compared to the VRFB system. However, this case study highlights that, in order to reduce capital costs below 150 \$ kWh^{-1}, reductions in power costs (*i.e.*, beyond choice of chemistry) are likely needed. Perfectly selective separators, likely ceramic-based materials, eliminate crossover at the expense of high cell resistances and power costs. The reduction in cell resistance needed to make this solution competitive seems feasible if the separator can be produced at sufficiently low costs and employed with high potential chemistries, as cell potential counters the effect of resistance on power costs and also reduces energy costs. This approach appears to be most suitable for non-aqueous electrolytes, where cell potentials ≥3V are viable, though such high-voltage demonstrations have yet to be widely demonstrated in this still-emerging field [153].

Looking forward, this LCOS model can be used as a framework to determine cost and performance targets for evaluating the techno-economic promise of new RFB chemistries and their potential capacity-loss remediation strategies. Future work should focus on expanding our treatment of capacity fade to encompass its dynamic nature, both in its mechanisms and rates, as a function of cell operating conditions (*e.g.*, the application-informed duty cycle or temperature), cell components (*e.g.*, choice of membrane or flow field), and electrolyte composition (*e.g.*, choice of active or supporting species). This can be done by building on existing crossover and decay models to incorporate more fade mechanisms and power-dependence, and subsequently determining the inputs to these models for various chemistries. This will allow for a more accurate understanding of chemistry-dependent crossover, as well as evaluation of the efficacy of crossover remediation approaches (*e.g.*, rebalancing or the spectator strategy).

Further, while this work demonstrated the competitiveness of the VRFB from an LCOS perspective, necessitating stringent targets (*e.g.*, use of sufficiently low-cost active materials) for viable alternative chemistries, there are other potential limitations to scaling VRFB deployment that have not been explored here. In particular, there are crucial questions regarding the supply chain of vanadium that must be answered, such as: How does the supply chain facilitate (or, possibly, necessitate) such prohibitively high costs of vanadium? How rapidly can it scale to meet deployment targets? The answers to such questions may limit the scalability of the VRFB and thus further support the case for higher abundance chemistries. This topic is the focus of the subsequent chapter.

IV. Materials availability and supply chain considerations for vanadium in grid-scale redox flow batteries

1. Introduction

Throughout this thesis, I have discussed how the vanadium redox flow battery (VRFB, whose chemistry is represented in Equations II-1 and II-2 in **Chapter II**) is the state-of-the-art redox flow battery (RFB) chemistry due to its high technology-readiness level and low operational costs facilitated by a symmetric chemical configuration. I have also discussed how its deployment has been minimal (even within the sub-category of electrochemical storage, RFBs are dwarfed by lithium-ion batteries, or LIBs [11]), in part due to the high upfront cost of the system. In particular, the cost of vanadium itself is a big contributor to the overall cost; the current market price of vanadium translates to a total VRFB electrolyte cost of *ca.* 125 $/kWh [39,60], which is close to the price of some entire, state-of-the-art LIB packs (whose continual cost declines are primarily being driven by electric vehicle demand) [154]. In addition to the magnitude of the vanadium price, its volatility is cause for further concern. While historically the market price of vanadium, shown in Figure IV-1 as vanadium pentoxide (V_2O_5, a common vanadium product sold on the global market [39]), has demonstrated notable volatility, the last five years have been particularly instable with a 10× difference between the minimum and maximum [39]. While the current VRFB electrolyte price of *ca.* 125 $/kWh is challenging for competitive grid storage, it also represents a relatively low point for the last five years and may spike even higher in the future. Such uncertainty can make investments in VRFBs less attractive. However, while new chemistries are being proposed that utilize lower-cost and higher-abundance materials, many of these efforts are at earlier stages of technology readiness, as compared to the VRFB, and while the issues they face may be known, solutions have yet to be fully developed which prevents near-term deployment (as discussed in **Chapter III**). For example, recent studies show the costs to manufacture electrochemical-grade, organic or organometallic active species can be substantial [125] and have more complex decomposition processes that are difficult to remediate [27,120]. Other research into chemistries that utilize stable, inorganic materials reveals chemistry-related issues such as competing parasitic reactions and, in the case of hybrid systems with deposition/dissolution

reactions, difficulties preventing dendrite formation without severely limiting operating current densities [155,156].

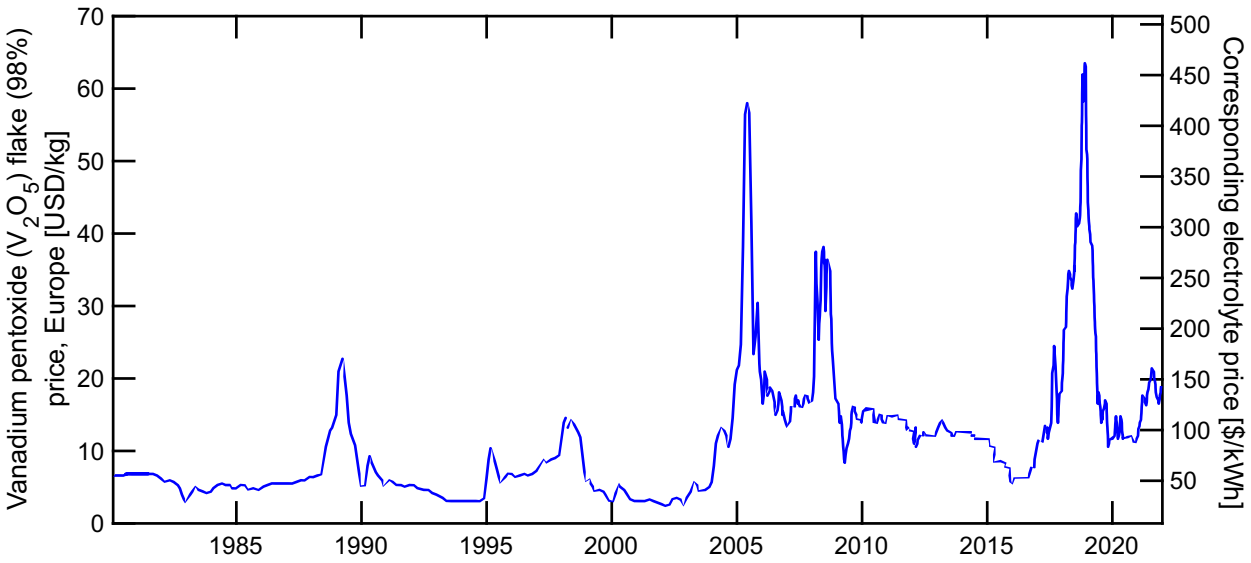

Figure IV-1 – Vanadium pentoxide (left y-axis) and corresponding VRFB electrolyte (right y-axis) prices in Europe from 1980 through 2021. Prices for ferrovanadium during this period follow nearly identical trends [34].

With growing demand for stationary energy storage, VRFBs may play an important role in near-term decarbonization efforts, making it important to consider the factors that impact their scalability. Currently, the price of vanadium (both in magnitude and stability) presents significant concerns regarding the deployment potential of VRFBs. To this end, we explore the materials availability and supply chain to understand the causes of the high and volatile vanadium price. Supply chain studies have provided useful, research-driving insights for related technologies such as LIBs (*e.g.*, concerns with the cobalt supply chain [41] have motivated research into alternative chemistries that minimize or avoid its use [42]). Such analyses have been lacking in the RFB field; while some recent studies have started to illuminate the vanadium supply chain, these have generally focused on the environmental, health, and safety considerations of vanadium production and VRFB operation [43–48]. Here, we focus on the production scale and growth rates needed to deploy sizable amounts of VRFB storage and examine opportunities to more rapidly expand and stabilize the vanadium supply chain via the development of various supply streams and

employment of economic hedging strategies. We believe these analyses can inform and drive the broader-scale deployment of RFBs.

2. Current landscape of the global vanadium supply chain

A first step in exploring the availability and supply chain of vanadium is to review data from the United States Geological Survey (USGS) on the global production and resources levels for vanadium and other elements utilized in various battery technologies (Figure IV-2) [49,50]. Here, "global resources" are defined as the amount of a geologic commodity that exists in both discovered and undiscovered deposits (*i.e.*, a "best guess"), though this value is generally an underestimation and often grows with demand and interest in a particular material (as demonstrated by the notable relationship between resources and production quantities across the minerals shown in Figure IV-2). Vanadium is considered relatively abundant and has multiple orders of magnitude greater global resources as compared to scarce materials such as platinum group metals (PGMs, common catalysts in clean energy conversion and storage technologies). The world production and resources of vanadium are similar to those for critical LIB materials (*i.e.*, lithium, cobalt, and, to a lesser extent, nickel), though these elements are one or more orders of magnitude less abundant than elements like sulfur, iron, zinc, copper, and manganese, which are the focus of many next-generation battery chemistries [40,51,52].

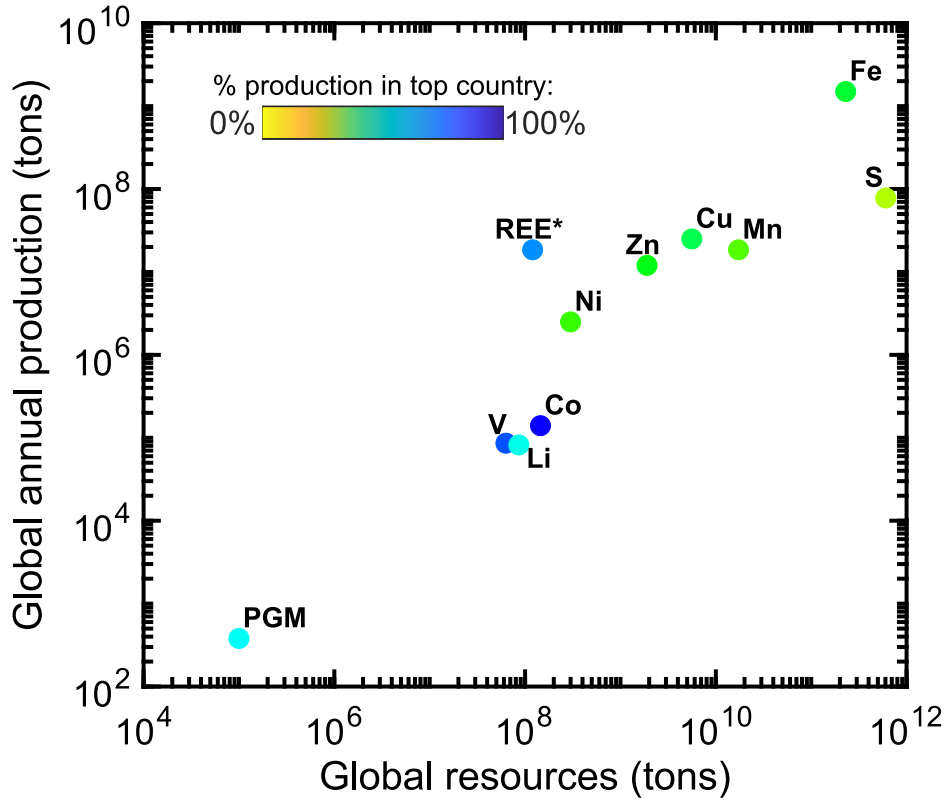

Figure IV-2 – 2020 global annual production (y-axis) versus global resources (x-axis) of vanadium, elements widely used in current Li-ion battery technologies, and minerals common to emerging energy storage technologies (in units of metric tons) [164,165]. The color of each element's market corresponds to the production concentration (*i.e.*, the percent of production coming from the top-producing country), as measured by the color bar. REE and PGM refers to rare earth elements and platinum group metals, respectively. Note: the global "reserves" (fraction of total resources that are currently economically recoverable) is used as the x-axis input for REEs, as total resources were not reported.

While vanadium resources may not be scarce, their abundance is confounded by highly concentrated production that can cause market instability and insecurity that translates into high and volatile prices. The percent of total production coming from the top-producing country is represented by the marker color of each element in Figure IV-2. Vanadium production is one of the most highly concentrated, with 62% of production originating from one country (exceeded only by cobalt at 68%), as compared to the most abundant and produced minerals like sulfur, for example, for which the leading country is only responsible for 22% of global production.

Vanadium production is concentrated in China (62%), Russia (21%), South Africa (10%), and Brazil (7%), where the parenthetical percentages represent each country's proportion of global vanadium production [53]. With so few countries dictating the supply, the global vanadium market can experience strong price volatility in response to local changes (see Figure IV-1) [47], and this uncertainty in future prices can make it difficult for these large-scale and capital-intensive VRFB systems to attract investment. Further, the geographic concentration would require most countries to outsource their vanadium, so that sizable VRFB deployments would increase dependence on global supply chains. For this reason, vanadium was declared one of 35 "critical minerals" – minerals that are deemed vital to the Nation's security and economic prosperity but are primarily imported to the US – by the US Department of the Interior in 2018 [54].

Beyond the geographic concentration, looking within those few countries that produce vanadium, there is even more severe concentration of supply as the majority of production arises from only a few facilities. Before exploring supply sources, an understanding of the current approaches to vanadium beneficiation is necessary. In general, vanadium must be extracted from vanadium-bearing compounds, of which there are two categories. The first is mined shale- and sandstone-hosted deposits, from which vanadium is currently recovered most often as vanadium titanomagnetite (VTM). The other category is vanadium-bearing waste products of carboniferous materials (*e.g.*, coal, crude oil, oil shale, and tar sands), typically residues from burning and refining oil herein referred to as "secondary sources" [48,49]. The vanadium content of these materials can vary widely: generally, minerals from the earth contain ≤ 5 wt% V_2O_5, while slags and other waste streams are often more concentrated. Because of the low grade of vanadium found in minerals, mining of vanadium is often performed indirectly as a compliment to other materials (*e.g.*, iron for steel). Thus, there are three pathways for vanadium production (Figure IV-3): 1) co-/by-product production in steel mills (75% of global production), 2) mines dedicated primarily to vanadium production (10% of global production), and 3) secondary sources (15% of global production) [45]. All three methods utilize some subset of a common repertoire of extraction and refinement techniques. In general, roasting (oxidation at high temperatures) is followed by leaching, where the vanadium is dissolved into an acidic or basic aqueous phase. The vanadium is then concentrated and recovered via solvent extraction or ion-exchange processes, after which it is precipitated as ammonium metavanadate (AMV, NH_4VO_3) or ammonium polyvanadate (APV, $[NH_4]_2V_6O_{16}$). From there, the APV or AMV precipitate is de-ammoniated and fused to produce

vanadium oxides (typically V_2O_3 or V_2O_5) or ferrovanadium (via various thermal processes that ultimately react the vanadium oxide products with some Fe-containing material, usually in the presence of lime), which are then sold to vanadium consumers [55]. For this work, we report vanadium content in terms of V_2O_5, as this is a common vanadium product sold on the global market and is typically used for such metrics, though trends and insights regarding the vanadium market broadly apply to all of these vanadium products [34]. A comprehensive review of vanadium production methods is beyond the scope of this work, but can be found in the open literature [48].

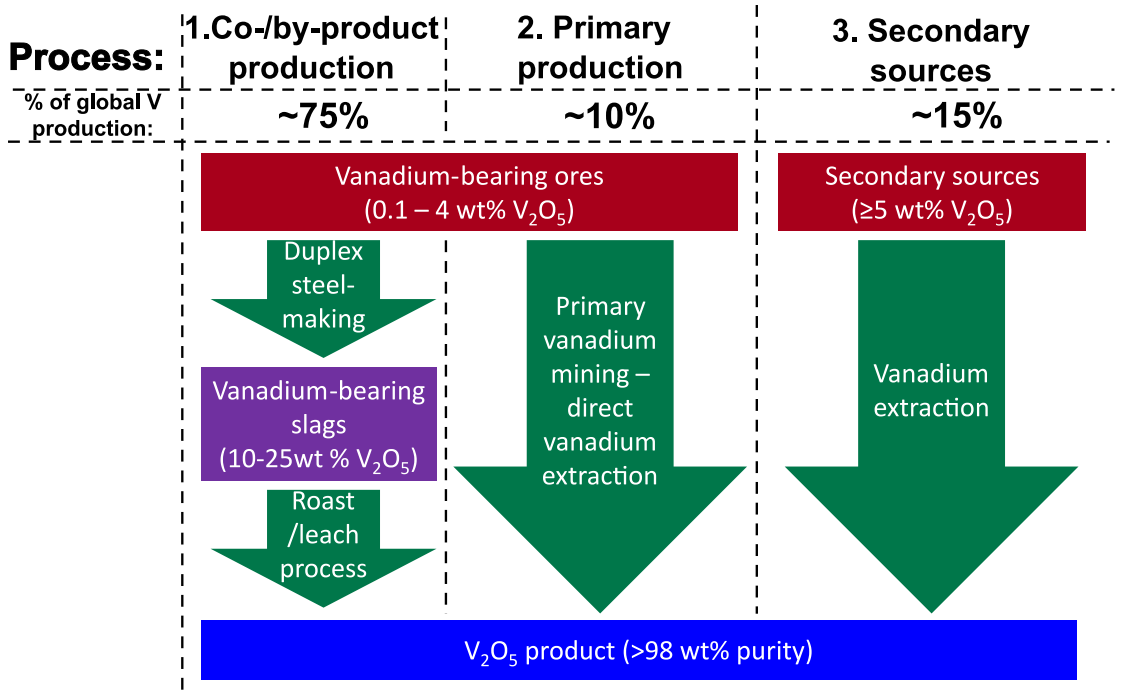

Figure IV-3 – Schematic of the three main production routes for vanadium pentoxide (V_2O_5).

Primary production (*i.e.*, mining ores for the primary purpose of extracting, refining, and selling its vanadium content) has the smallest market share (*ca.* 10%) because the low grades or concentrations of vanadium in mined precursors make vanadium recovery uneconomical in most cases [46]. Currently, primary mined vanadium mainly comes from Brazil, with the majority of operations run by Largo Incorporated, and South Africa, with the majority of operations run by Bushveld Minerals and Glencore [56,57]. Secondary sources account for a similarly small portion

(*ca.* 15%) of vanadium supply, broadly consisting of vanadium-rich slags and fly ash from burning petroleum products – a process which is often executed at power stations or at petrochemical factories – mainly heavy, "sour" crude oils found in the Caribbean (*e.g.*, Venezuela and Mexico), Canada, as well as parts of the Middle East (*e.g.*, Kuwait and Jordan) [45,58,59]. Co-/by-product production, defined as the extraction of a mineral in the process of mining and producing another mineral, represents the vast majority of the vanadium market (*ca.* 75%). The distinction between co- and by- products lies in the value of the secondary material: co-products carry similar value to the primary material(s) they are produced with, while by-products generate less revenue than the primary material(s) [60]. In the case of vanadium, it is produced as a result of iron extraction for steel-making: iron is extracted from magnetite ores for further use in steel, though those ores may also contain vanadium that can be recovered. The crux of this process is oxidation, primarily to remove the carbon from the ores. However, the execution of this oxidation is crucial to facilitating or prohibiting economic vanadium recovery: the mills that produce the ~75% of global vanadium supply utilize a "duplex process," where an additional oxidation step is imposed first to selectively oxidize vanadium, enriching it into the slag phase as oxides where is it more easily recovered [48]. This process is a sensible and profitable choice for ore precursors with notable vanadium content, as it allows for economic recovery of the vanadium. Other facilities utilize a single-step method that is currently prohibitive for viable vanadium recovery as it adds calcium (to suppress the slag's ability to solidify upon encountering the relatively cooler oxygen [61]), which creates vanadium-calcium bronze complexes that are difficult to break apart [62,63]. Indeed, conversations with industry experts revealed that slags containing vanadium-calcium compounds are sitting idly at steel-making factories because the vanadium cannot be economically extracted.

Supply chain complications arise when the majority of a material's production is as a co-/by-product [41]. In this case, the vanadium production scale depends primarily on the production scale of other resources or products (*i.e.*, iron or steel, respectively). In other words, the price or demand for a co-/by-product does not strongly affect its supply (at least in the short term). Vanadium is even more complicated than the average co-/by-product material due to the entanglement between its supply (which, as discussed, is mainly as a secondary product from steel-making) and its demand, as currently ~90% of vanadium production goes to steel manufacturing (*i.e.*, alloying to bolster the strength of steel) [64]. Further inspection of the vanadium co-/by-product supply distribution reveals more causes for concern: while co-/by-product production represents the

majority (75%) of the global vanadium supply, conversations with industry experts revealed that this stream is concentrated around ~10 steel mills, primarily in China and Russia. Such severe concentration reflects extreme precarity in the supply chain and can intensify volatility in supply and price. For example, the price spike that began in 2016 (Figure IV-1) was partially a result of the bankruptcy-induced closure of Highveld Steel & Vanadium in South Africa in 2015 [65], previously the world's largest producer of vanadium slag from steel production [66], which caused an ~11% decrease in global vanadium production [67]. This decrease in supply was compounded by other mine closures in China due to increased enforcement of environmental regulations [67,68]. Supply has remained depressed for years [67] and has only begun to rebound as of 2019 [49], likely due to increasing primary production in Brazil led by Largo Incorporated. Simultaneous to these supply constrictions were increases to demand in late 2018 due to revised Chinese "rebar" standards (regarding steel strength) that promote greater use of vanadium in high-strength steel alloys [67,69]. The combination of circumstances ultimately led to the price spike in the final months of 2018, which peaked at 10× the price relative to early 2016 [34] (Figure IV-1).

3. Quantitative analysis of vanadium supply chain scale-up needed for VRFB deployment targets

The expansion of VRFB production and deployment depends on the ability to increase the production scale of vanadium. To illustrate the required expansion of vanadium production required by a targeted level of deployment we assume, following Kavlak *et al.* [70], that the production of vanadium increases at a uniform compound annual growth rate (CAGR) year over year. In terms of the CAGR, the production in year n, p_n, is related to the present-day global production, p_0 by,

$$p_n = p_0\,(1 + CAGR)^n \qquad \textbf{(IV-3)}$$

where $p_0 = 8.6 \times 10^7$ kg(V) per annum (in 2020 [49]). Assuming only new vanadium supply is available for VRFBs, one must specify the fraction of new vanadium production going towards

VRFBs (*f*), as well as the materials intensity (*I*), which is a conversion between the amount of vanadium needed for a given amount of storage deployed:

$$I = \frac{2(MW)}{n_e F U \chi} \quad \textbf{(IV-4)}$$

The calculation of *I* depends on the molecular weight of vanadium ((*MW)*, 0.051 kg mol^{-1}), the open-circuit cell potential (*U*, 1.4 V), the depth of discharge (χ, 0.8), the number of moles of electrons transferred per mole of vanadium (n_e, 1 mol(e$^-$)/mol(V)), the Faraday constant (*F*, 96,485 C/mol(e$^-$)), as well as other necessary unit conversions [12]. Further, the factor of two in the numerator accounts for the two electrolyte tanks per system (as vanadium is used on both sides of the cell). The value of *I* is found to equal 3.4 × 10^9 kg(V) per TWh of energy storage capacity. Next, the VRFB capacity that could be deployed in a future year *n* (d_n, in units of energy/year) is calculated by scaling p_n by *f* and I^{-1}:

$$d_n = \frac{p_0 f}{I} \left((1 + CAGR)^n - 1\right) \quad \textbf{(IV-5)}$$

The subtraction of one is included to eliminate the present-day production quantity of vanadium from consideration for use toward VRFB deployment, as we assume existing supply is already accounted for. To determine the cumulative deployment in year *N* (D_N), the annual deployments (d_n) from each year beginning now through year *N* must be summed:

$$D_N = \sum_{n=0}^{N} d_n \quad \textbf{(IV-6)}$$

Using the identities $\sum_{n=0}^{N} x^n = \frac{x^{N+1}-1}{x-1}$ and $\sum_{n=0}^{N} 1 = N + 1$, we find a closed-form, analytical solution for D_N:

$$D_N = \frac{p_0 f}{I} \left(\frac{(1+CAGR)^{N+1}-1}{CAGR} - 1 - N\right) \quad \textbf{(IV-7)}$$

Equation IV-7 is used to determine the CAGRs needed to achieve varying total deployment scales in 2030 (Figure IV-3a, *N* = 10 years) and 2050 (Figure IV-3b, *N* = 20 years), relative to 2020,

under varying scenarios of fractional new vanadium supply going toward VRFB deployment. Where applicable, the resource limit (*i.e.*, the case where all the global vanadium is mined) under each fractional scenario is shown as a vertical dashed line.

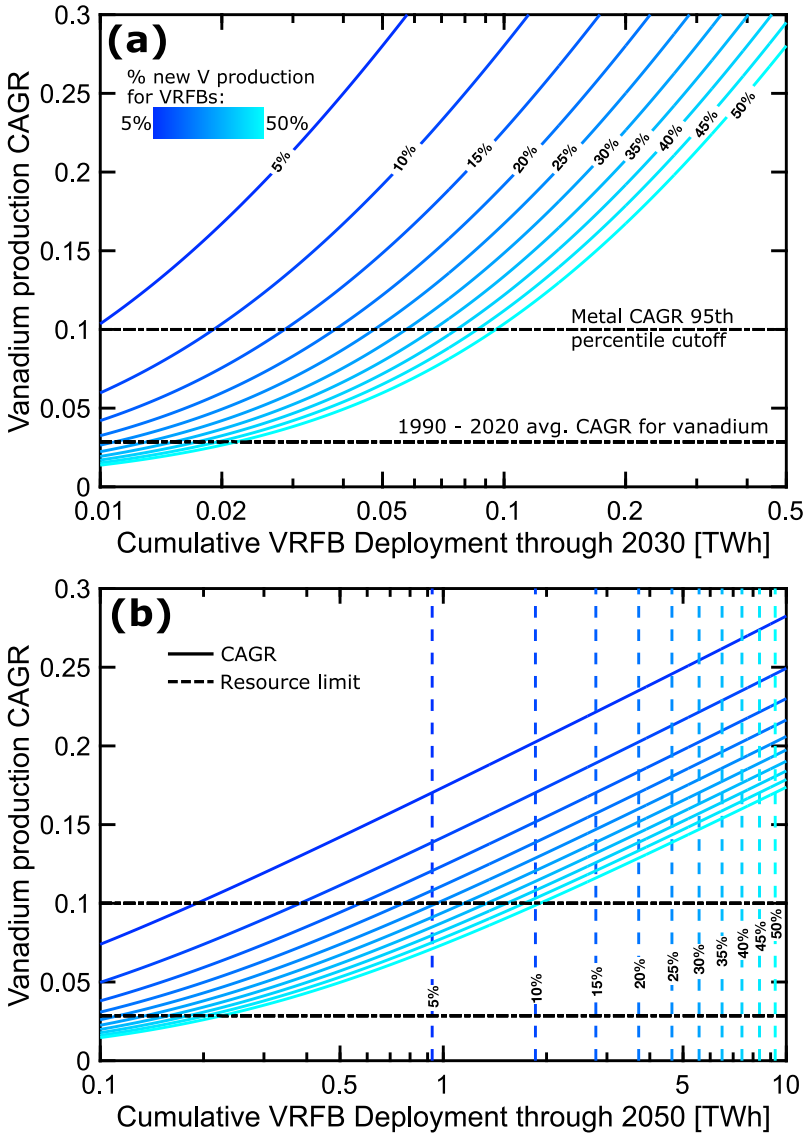

Figure IV-3 – Compound annual growth rate (CAGR) of vanadium production needed to achieve various amounts of cumulative VRFB deployment by 2030 (a) and 2050 (b), relative to 2020, based on various scenarios of new fractional production routed to VRFB production over other applications (various shades of blue). The 2050 plot also shows the resource limit under each scenario (vertical dashed lines). The black horizontal lines show relevant historic CAGRs.

When considering the growth potential of vanadium production, it is useful to reflect on historical ranges for vanadium and other metals. The blue contours represent the fraction of new production going towards VRFBs, the relevant magnitude of which depends on the competition between vanadium for steel and vanadium for VRFBs, although other use-cases may appear in the future. At present, *ca.* 90% of vanadium production goes to steel manufacturing and this demand is likely to grow in the future given continued global economic development as well as a shift towards higher-strength steel in construction to reduce total material requirements [71]. While there are opportunities to substitute vanadium with other alloying elements (*e.g.*, manganese, molybdenum, niobium/columbium, titanium, and tungsten) – indeed, some steel mills in China have switched from ferrovanadium to ferroniobium due to high vanadium prices [49] – there is no evidence such substitutions will re-route significant vanadium supply away from steel demand in the near future. Thus, a conservative (business-as-usual) estimate would assume that steel will continue to drive the demand for vanadium at historic rates and only *ca.* 10% of new vanadium production will be available for VRFBs. However, with growing energy and sustainability concerns, it is reasonable to believe that larger fractions of new vanadium production (say, as much as 50%) may be diverted to VRFBs, particularly if we are able to more rapidly scale supply (as will be discussed in the next section, though note the assumption of CAGR is somewhat coupled to the accessible fractions in this way). We can set a context for the various CAGR scenarios displayed in Figure IV-3 via the results of a study on metal production requirements by Kavlak *et al.*, which determined that only the top 5th percentile of the 32 metals analyzed by the study observed CAGRs over 10% (analyzed from 1972-2012, over 18-year periods), with none exceeding 15% [70]. Comparing vanadium production from 2020 to that of 1990, we compute an average CAGR across this 30-year period of 3.55% [49,72]. However, it should be noted that the year-to-year growth rate is generally highly variable, and vanadium is no exception: some years have seen greater than 30% or 40% growth, though the compound annual growth rate over longer time horizons averages much lower. This is an important distinction captured by the CAGR, as sustained growth of the supply chain is critical to supporting VRFB growth. Notably, the last two years of reported data (2019 and 2020) have shown sizable growth, *ca.* 20% per year, mainly due to rapid expansion of Chinese co-/by-product production to support record domestic steel manufacturing volumes as a response to stimulus measures triggered by the COVID-19 pandemic [73]. While promising, it is unclear if this growth

rate can be maintained. In light of this analysis, we can now evaluate our ability to scale up production and deploy various amounts of VRFB storage.

Looking, for example, at 10% CAGRs as an optimistic value, it appears new VRFB deployment is limited (*i.e.,* $f \leq 50\%$) to ≤ 100 GWh by 2030 and ≤ 2 TWh by 2050. At the time of writing, there are currently ~100 MWh of RFBs in operation globally [31], and projections for global grid storage demand are anticipated to be at hundreds/thousands GWh- and tens/hundreds TWh- scales by 2030 and 2050, respectively [60]. It must be noted that global demand projections are hard to anticipate, and further only a fraction of it is likely to be filled by RFBs. The bounds to production scalability may not limit VRFB deployment ambitions in the near-term (*i.e.*, 2030), particularly as relevant applications (*e.g.*, renewables support) for long duration energy storage are still nascent. Deployment at this scale (*i.e.*, 10's-100's of GWh) would represent promising scale-up for the RFB industry and could drive down manufacturing costs and, potentially, increase vanadium demand such that the vanadium market begins to resemble a traditional commodity market (*i.e.*, reducing price volatility and starting to drive some increase in supply). There is also a broader benefit to VRFB development that is a testament to the versatility of the RFB platform: RFBs represent an architecture that can house a diverse array of chemistries, and the cost reductions and technical advancements from accelerated VRFB deployment could be reasonably translated to other RFB chemistries. For example, GWh-scale deployment of the VRFB could advance general efforts in cell and stack design and optimization, as well as reactor and electrolyte maintenance. Unfortunately, the longer-term (*i.e.*, 2050) bounds – both those determined by realistic CAGRs and those imposed by the resource limits, which do not drastically different in scale – are more limiting since they differ from the global demand projections for grid storage by about an order of magnitude. However, scaling VRFB deployment in the near-term will help drive down costs and reduce the perceived investment risks of RFB systems such that other lower-cost and higher-abundance chemistries may be utilized in these more distant horizons. VRFB systems could even be modified with a new chemistry, simply by replacing the electrolyte, 10+ years into the RFB's deployment, especially if the vanadium electrolyte is leased [74]. Thus, the VRFB is a well-developed system that could be used as an entry point for larger scale RFB deployment of other chemistries. Conversely, by 2050 it may become evident that systems previously projected to be promising and "low-cost" may in fact require prohibitively expensive active materials (*e.g.*, costs

to upgrade precursors are high or degradation requires too-frequent replacement of materials) or cannot achieve necessary technical performance metrics. Many other RFB systems may ultimately struggle to compete with the high-performing VRFB system that already overcomes a lot of challenges presented by other chemistries. In this sense these "limits" could spark meaningful growth to the VRFB and, potentially, RFB markets broadly that will catalyze important reductions in cost and perceived risk, facilitating further deployment.

4. Opportunities to expand and stabilize the global vanadium supply chain

In this section, we look at opportunities to scale vanadium production more rapidly through expansion and de-concentration of the supply chain, as well as other market solutions to reduce the burden of the high and uncertain upfront cost of vanadium.

4.1 Vanadium production scale-up opportunities

To meet or exceed the limits identified for 2030 and 2050 deployment (which assume 10% CAGRs), production scale-up must dramatically accelerate relative to historic vanadium CAGRs (< 4%) [49,72]. Rapid supply chain growth relies on the expansion of existing vanadium production routes as well as economical beneficiation of new vanadium precursor sources. While vanadium is not scarce and exists in many regions of the world, it presents in low grades and thus is costly to extract. Prior to considering different routes for production expansion, it is useful to contemplate other metals that have historically shown high CAGRs and the factors that contributed to those growth rates.

Cobalt and indium are two metals produced as co-/by-products that have seen significant growth in recent decades due to drastic demand increases driven by technology adoption. The global production of cobalt, a critical component of positive electrode chemistries in advanced LIBs (*e.g.*, lithium cobalt oxide, nickel-cobalt-aluminum, nickel-manganese-cobalt), has grown by over 7.5× (*i.e.*, an average CAGR of ~8%) since the mid-1990's due to ever-expanding demand for LIBs in portable electronics, electric vehicles, and stationary energy storage [75]. Despite the increased

demand, cobalt still is mostly produced as a co- and by-product of copper and nickel, respectively [41]. Similarly, indium production has experienced a CAGR of ~10% since the 1970's due to its use in semiconductors that underpin photovoltaic devices and electronic displays [70]. Indium is also produced predominantly as a co-/by-product of zinc. While co-/by-product production generally decouples its supply and demand, supply can still be driven by demand for some limited period of time: for example, Frenzel *et al.* showed how indium production has grown ~10× faster than production of its host material, zinc [76]. Such a phenomenon often results from increased demand for the material of interest (in this case, indium) that facilitates higher utilization and recovery rates of it from the host material (*i.e.*, a higher percentage of the total amount of extractable co-/by-product is actually recovered from the host material than before, bolstering its production rate). Gao *et al.* reports that vanadium recovery from duplex steel slag is generally only ~50% (~80% recovery in each of three steps: reductive smelting, selective oxidation, and vanadium extraction), suggesting that it may be possible to increase vanadium recovery in existing production methods through process optimization [48]. However, there are other notable complications hindering the expansion and stability of these operations.

Expansion of co-/by-product production via duplex steel-making processes is perhaps the least promising avenue of supply chain growth due to their unfavorable economics. The duplex process is not the most efficient steel-making method, as it requires a multi-step oxidation of the steel to recover vanadium, thus necessitating additional capital and operating expenses while introducing more inefficiencies as compared to single-step processes [77]. Additionally, the iron content of vanadium-bearing titaniferous magnetite (VTM) ores – used for duplex steel-making as they enable vanadium recovery – is low, making VTM-based steel more expensive to produce [48]. While duplex mills may benefit financially from vanadium co-/by-product production, the primary driving force that will keep them operating is revenue from steel. Thus, duplex mills may have an inherent competitive disadvantage and single-step processes may ultimately displace these legacy technologies. These considerations have probably contributed to the low number of duplex facilities at present, could cause the closure of existing facilities (*e.g.*, Highveld Steel and Vanadium, discussed earlier), and may deter the formation of new duplex operations in the future. Contrary to these points, sustained growth of global vanadium production by ~20% in both 2019 and 2020 was primarily due to expansion of co-/by-product vanadium from steel-making in China

[73]. However, diversification of the supply chain is as important as sheer growth, so we turn our attention to other potential supply streams for the remainder of this discussion.

There are promising opportunities to expand and diversify supply via the development of alternate methods for recovering vanadium as co-/by-products of other materials. First, other potential routes for vanadium production could lie in non-duplex steel-making processes, necessitating further research efforts into this space. As discussed previously, many steel mines produce vanadium-calcium residuals that are currently unutilized due to the economic infeasibility of recovering their vanadium, though there are efforts to develop and scale-up vanadium extraction from such precursors: Neometals, an Australian company, claims to have developed a hydrometallurgical process to recover vanadium from these mono-process slags. The company recently partnered with Scandinavian mineral development company Critical Metals Ltd, which has executed a 10-year supply agreement with Swedish steel giant SSAB to access approximately 2 Mt of stockpiled high-grade vanadium-bearing slag from three operating steel mills [78]. While details on the Neometals process are not public, significant project challenges are anticipated including potentially prohibitive capital cost requirements (presuming the need for on-site smelters), as well as technical challenges in the vanadium recovery itself. Another potentially sizable input stream could come from recycling of existing products: steel is already one of the most recycled materials, meaning vanadium is already recycled to an extent [45], but vanadium extraction and recovery from steel for other uses is, at present, economically infeasible due to its dilute nature in these products [79]. Gao *et al.* also note that the low concentration of vanadium in most minerals may limit primary production opportunities for the foreseeable future, and expanding the co-/by-production of vanadium with other valuable metals beyond iron for steel (*e.g.*, chromium, titanium, or manganese) may be necessary for rapid growth [48]. While co-/by-product production presents inherent challenges, diversification and expansion of the operations contributing to this stream would at least reduce the most imminent supply concentration problems.

Perhaps the most promising avenue for near-term growth and diversification of the supply chain is through secondary-source vanadium. These precursors are attractive due to their higher vanadium content ($\geq$ 5% V_2O_5) that makes vanadium extraction more economical [58,59]. Conversations with industry experts revealed that while the precursor materials are generally

wastes from burning and refining oil, they are currently sold to vanadium producers at market-based prices and utilized in smaller batches, making the cost to produce vanadium from these materials relatively high as compared to other methods. Vertical integration of the vanadium recovery and production operations into existing oil refineries could significantly cut costs, as would expanding these facilities to process larger volumes of secondary-source precursors. While the anticipated modifications to the power generation infrastructure (*i.e.*, decarbonization and electrification) may impact the operation of the fossil fuel industry and potentially disrupt the supply of secondary-source precursors, this stream could provide a near-term bridge in supply while new technologies and methodologies for vanadium extraction from lower-grade precursors are developed (as discussed next). Without relying on techno-economic advances in vanadium recovery, this supply stream could rapidly expand and diffuse the distribution of vanadium production (note the potential magnitude of supply that this stream could provide is uncertain and is beyond the scope of this work). The US is particularly suited to expand secondary-source vanadium production, due to its arsenal of oil refining facilities that are concentrated in the south of the country [46], and development of a domestic vanadium supply chain could further advance energy independence efforts if utilized for the deployment of VRFBs.

In the longer term, the largest potential to grow and stabilize vanadium production – contingent upon crucial technological advances in vanadium extraction and recovery from low-grade sources – likely lies in primary mining, as vanadium is relatively abundant globally with major deposits in each inhabited continent [80]. While vanadium mines have been proposed for decades, many have yet to be realized due to financing issues. Generally, mines are capital-intensive and require years of operation to pay back; a 2011 report from the German Institute for Applied Ecology cites investment costs of $30,000 per ton of recovered capacity for rare earth element mines [81]. The ease or difficulty of financing the construction of a new mine is determined by a number of factors, but a critical piece is the feasibility study, which lays out the development and production schedules that are used to derive a cash flow model in order to determine the internal rate of return and payback period. The apparent inevitability of delays in announced primary vanadium mining projects across numerous locations is likely due to difficulty justifying the project economics found in these feasibility studies to investors, pointing to inherent challenges to extracting the relatively low grade of vanadium from precursor materials. However, if economic ways to recover vanadium from these mines could be found, it could create a sizable new supply stream.

Opportunities for new primary vanadium mining ventures exist in a range of locations – most notably in Australia, the US, and China – which could facilitate substantial supply capacity. Australia has substantial vanadium reserves, though no reported production in recent years, likely due to the lower vanadium concentrations present in their precursor supply: ~ 1% V_2O_5 content [82,83], as compared to ~ 2-3% in South Africa and Brazil (where the overwhelming majority of primary production currently occurs) [48]. Plans have been announced to develop three sizable vanadium mines: the "Australian Vanadium Project" in western Australia, the "Mount Peake Project" in northern Australia, and a mine at Saint Elmo in Queensland [82–84]. These projects are based on new proposed methods for vanadium extraction and recovery, though the technical details have not been publicly disclosed. While the projects are still in the planning stages, if completed, they are expected to collectively produce ~ 27,000 metric tons of V_2O_5 per year, which would represent an ~ 18% increase to the current global production of vanadium. While this represents a marked growth of the supply chain, continuous growth for at least 10-30 years would require new mines of this scale to come online annually, which appears to be challenging. Further, these mines have finite operational lifetimes of 10-50 years (*i.e.*, until resources are depleted). However, circulation of their vanadium extraction methods could facilitate the market entry of other mines to sustain growth; in particular, primary production in the US and China. The US recently announced plans for a primary vanadium mine called the Gibellini project, to be located in Nevada's Battle Mountain region. The V_2O_5 content is low (< 0.4%), and anticipated production is ~ 4,600 metric tons of V_2O_5 per year [85]. Major reserves lie in China in the form of stone coal, which is an abundant resource (~62 billion tons) that contains ~ 1.5% or less V_2O_5 content, but currently only contributes ~10% of Chinese vanadium production [48].

This new supply will take time, as mines typically require 5-10 years to come online due to the lengthy approvals process through relevant regulatory avenues, which vary based on location and can take up to 50 years in the worst cases [81]. Thus, expansion of primary production should be expected to be a longer-term endeavor, which presents new challenges and risks to financing such operations in the first place as the vanadium demand may drop (*e.g.*, if the VRFB is supplanted by another RFB chemistry or a different energy storage solution). Further, this timeline is already optimistic, as it does not account for the time needed to advance vanadium recovery technologies that make these mining approaches economically viable. Economic recovery of low-grade vanadium mainly depends on the same methodologies currently being used for vanadium

extraction, though the lower grade makes the process less profitable. In particular, transportation of precursor material can become prohibitively expensive if the grade is too low, as costs scale in $ per unit weight (hence why co-/by-product production is attractive, as it reduces the deadweight fraction). Thus, the burden of the added deadweight must be offset by higher efficiencies, recovery rates, and lower costs in processing the materials. High transportation costs may necessitate the development of processing sites that are mobile and/or co-located with the mine. This is a route many new mines are taking, though it adds significant capital requirements on top of already expensive projects.

It should be noted that, beyond the economics of vanadium recovery, there are also a multitude of environmental, health, and safety concerns to be considered in vanadium production processes (*e.g.*, production of pollutant gases in duplex recovery, ecological and geological impacts of building and operating mines, etc.). While such matters are beyond the scope of this work, future research may consider quantifying the associated risks and costs in order to more holistically determine the best paths for vanadium supply chain expansion. Further research and development efforts to mitigate these effects in existing processes are similarly critical, not only to address the direct impact of these factors but also because they, if left unmitigated, have the potential to cause the closure of existing operations as regulations become stricter (as seen recently in China [68]). We recommend works by White *et al.* and Gao *et al.* for more information on this topic [45,48].

4.2 Economic strategies to mitigate price volatility and reduce the upfront cost burden of vanadium

While supply scale-up is necessary to augment VRFB deployment and will likely help stabilize the market, there are other potential more-immediate solutions to mitigate volatility of vanadium prices. One tactic is vertical integration, where a corporation owns the vanadium mining and refining company as well as a VRFB or vanadium electrolyte company. While logistics may vary, vertical integration is expected to enable the battery vendor to reduce the impact of vanadium price volatility and plan long-term technology pricing trajectories. While vertical integration may also facilitate lower vanadium prices to the VRFB company, this is not guaranteed and depends on the outlook of the overarching corporation regarding profit allocation. Another layer of vertical integration could easily be incorporated to process and recycle the spent vanadium electrolyte at

the end of life – whether purifying for re-use or recovering and reselling the vanadium for other applications – which requires unique expertise that could be shared by a vanadium miner and refiner [86]. This approach is being pursued by two major primary vanadium producers, Largo Incorporated and Bushveld Minerals, who have created subsidiaries Largo Clean Energy (which will sell VRFB systems, a result of Largo's acquisition of VRFB company Vionx in late 2020 [87]) and Bushveld Energy (which will sell VRFB electrolyte [88]), respectively. A related method to prepare vanadium supply for future demand and therefore reduce price volatility and uncertainty to the buyer exists through hedging strategies such as futures contracts, which are agreements between suppliers and buyers to transact vanadium at a pre-determined price at some specified future time. Futures contracts are common in some commodity industries such as those for oil, precious metals (*e.g.*, gold, silver, and platinum), agricultural products (*e.g.*, corn), etc., and could potentially be employed in the vanadium industry. In fact, cobalt – a metal with a similar supply chain structure to that of vanadium, in many ways, as discussed previously – can now be bought and sold via a futures contract launched in late 2020 [89]. Even prior to this development (*i.e.*, as of 2010), cobalt became one of only two "minor metals" (along with molybdenum) traded on the London Metal Exchange, the largest global market for a range of metals. The transparency of such a market can help stabilize the supply chain, and indeed the cobalt price volatility is more than 3× lower since 2010 than between 1970 and 2010 [41]. While more comprehensive economic analysis regarding the promise of these strategies for VRFB deployment is beyond the scope of this work, it should be explored by others with cross-disciplinary expertise.

In addition to its volatility, the magnitude of vanadium prices is an issue. While efforts to expand and stabilize the supply chain may help reduce vanadium prices in the long-term, any near-term expansion of supply may only occur as a response to price increases (*e.g.*, to offset the more expensive recovery of low-grade primary production). Thus, the prohibitive price of vanadium may remain a separate issue from the supply chain challenges discussed here. One method to reduce the burden of the vanadium price does exist via a new market of electrolyte leasing, where a third-party company leases the vanadium – usually in the form of VRFB electrolyte – to a battery vendor or end-user. This reduces the upfront capital cost of the battery while increasing long-term costs (*i.e.*, a shift of capital expenses to operational expenses) by introducing some recurring fee [90,91], which is attractive as it lowers the cost and risk of the required upfront investment for VRFB customers. In some schemes, a portion of the financial burden of leasing is shifted from the

lessor to third-party investors who can buy and trade vanadium – akin to markets for other physical holdings, like gold – though it is held and maintained by the lessor, who simultaneously rents it out as electrolyte to VRFB customers [92]. These markets are new, and little has been published regarding their logistics or early-stage utilization and efficacy, though a few academic studies have demonstrated the techno-economic potential for leasing [33,93].

5. Conclusions

RFBs are a promising solution for grid-scale storage, with the VRFB being the most studied and deployed RFB chemistry due to its remarkable performance attributes and unique chemistry design. Despite these benefits, the high and volatile price of vanadium has remained a major impediment to VRFB (and, more largely, RFB) deployment. In light of this, we explored the causes behind the high and volatile price of vanadium and evaluated the outlook for growth and stabilization of the supply chain.

While vanadium is relatively abundant and found in many parts of the world, the difficulty lies in its economic extraction that currently prevents many low-grade vanadium precursors from being utilized. This issue has limited present-day supply mainly to co-/by-product production from duplex steel slag, where vanadium is extracted as a lesser-valued product along with iron for steel-making. Reliance on co-/by-product production presents inherent challenges due to a decoupling of supply and demand for vanadium, as supply is driven by demand for steel rather than demand for vanadium. What is more immediately concerning, however, is the concentration of this supply stream, as it comprises only ~10 mills (mainly in China and Russia), which together provide 75% of global production. Such concentration can create extreme volatility in supply that can lead to surges in price, such as the 10x price spike of 2018. Further, it creates geopolitical vulnerability to importing countries and thus hinders efforts toward energy independence. Other minimal vanadium supply arises from primary production (mining of vanadium directly for vanadium) and secondary production from residues and wastes used in the refinement of vanadium-containing petroleum products.

We also sought to quantify market growth needed to achieve various cumulative VRFB deployment goals by 2030 and 2050. Metal supply chains rarely see CAGRs > 10%, and vanadium

has demonstrated much more modest growth in the last 30 years (< 4%). As existing vanadium demand is accounted for (primarily by markets for high-strength steel), relatively rapid growth in supply is needed to achieve sizable future VRFB deployment. In the near-term (*i.e.*, 2030), we find vanadium production scale-up is likely feasible to meet expected demand (up to 100 GWh). Deployment to this extent would certainly represent significant growth to the RFB market broadly and would have a notable effect in reducing both the cost of chemistry-unspecific RFB components as well as the perceived risk around RFB deployment, thus accelerating further RFB commercialization efforts. However, the long-term prospects are more restrictive: the relatively modest magnitudes of both existing vanadium production and historic rates of supply chain growth for metals limit feasible future VRFB deployment to only ~2 TWh by 2050. This diagnosis itself, as well as hopes of 10's-TWh or greater deployment scales, depend on growing the vanadium production scale more rapidly than it has historically (*i.e.*, at a CAGR of ~10%), which largely relies on improving our vanadium recovery capabilities to utilize lower-grade sources of vanadium, making such efforts worthwhile recipients of more devoted research and development resources. Due to the low grades of vanadium found in natural precursors, economic vanadium production may always be dependent on co-/by-product recovery. While duplex steel co-/by-product production demonstrates poor steel-making economics that may make this supply precarious and less likely to expand, new avenues for co-/by-product production from alternate steel-making methods or with other metals can grow and diversify the vanadium supply chain. However, economical primary vanadium production is potentially within reach, with projects being announced across the world that would expand production capacity significantly. Further, production from secondary sources can help bridge supply, as development of these sources does not require major technological advancements. These primary and secondary vanadium sources have the potential to bolster US production capacities in particular; indeed, one US VRFB manufacturer has announced plans to domestically source all of their vanadium, implying the US vanadium supply chain is already growing [94]. Other economic strategies can help reduce price volatility and upfront costs of vanadium in the near-term, including vertical integration of VRFB companies, hedging supply/demand risk via futures markets for vanadium, and electrolyte leasing.

Ultimately, near-term decarbonization goals necessitate deployment of energy storage as soon as possible. The VRFB has the highest technology-readiness level of all RFB chemistries and its rapid deployment at reasonable and, per this study, feasible scales (*i.e.*, up to 100 GWh by 2030) can

help meet decarbonization goals while simultaneously promoting future, broader-scale RFB deployment by de-risking the technology and lowering costs for chemistry unspecific components. In tandem, the RFB community must also develop alternative chemistries (and operation and maintenance strategies to facilitate their viable long-term performance) based on lower-cost and more widely-available materials [38,95,96]. Ultimately, these RFB systems may prove to be more expensive or challenging to make and operate than previously thought [36], supporting the need for more expansive and rapid growth and stabilization to the vanadium supply chain.

V. Hydrogen evolution mitigation in iron-chromium redox flow batteries via electrochemical purification of the electrolyte

1. Introduction

As evidenced by **Chapter IV**, next-generation chemistries beyond vanadium are crucial for the scalability of redox flow battery (RFB) deployment in the future. Already, there are many avenues of active research looking into new RFB chemistries that utilize low-cost and high-abundance active materials including commodity-scale inorganic materials (*e.g.*, iron, sulfur) and engineered compounds enabled by molecular functionalization (*e.g.*, redox-active organic molecules, metal-centered coordination complexes). As a relatively new storage concept, most efforts have thus far focused on demonstrating the proof-of-concept and refining electrochemical and physicochemical metrics at the bench scale. While promising, these emerging materials face an array of challenges. First, most chemistries are not inherently symmetric, utilizing disparate redox species on either side of the electrochemical cell, which means cross-contamination due to active species crossover can be technically and/or financially difficult to remediate or counter [16]. Second, engineered organic molecules and coordination complexes typically exhibit finite decay rates under operating conditions that cause further capacity loss, which is similarly difficult to address [120]. Third, many proposed chemistries exhibit other unfavorable technical attributes, such as relatively low open-circuit voltages (OCVs), limited solubility in different oxidation states, and poor ionic conductivity that results in reduced energy/power densities and poor efficiencies [203].

Though not a new chemistry, the iron-chromium (Fe-Cr) RFB system appears promising as it seemingly avoids or mitigates many of these aforementioned challenges. Specifically, it utilizes active materials that are abundant, low cost, stable under RFB operating conditions, and can remediate crossover losses by utilizing a mixed electrolyte configuration (also known as the "spectator strategy") [16]. Iron is the most abundant element in the Earth (by mass), and there is almost 1,000× more terrestrial chromium than vanadium [164]. Since late 2019, the price of ferrochromium – produced in a range of locations throughout Asia, Africa, Europe and the Middle East – has remained under one dollar per pound of chromium content [123]. Additionally, this mineral precursor contains forms of both active species (*i.e.*, Fe and Cr), allowing for potential cost savings by providing both species in one mineral, which could minimize the waste and reduce

the number of separations and other process steps needed to convert the precursor to electrochemical grade electrolyte (since it is ultimately employed as a mixed electrolyte) [143,204]. As inorganic species, neither Fe nor Cr decompose, and crossover is remediable via the spectator strategy electrolyte configuration where the two electrolyte tanks contain both active species in equal concentrations, making it "pseudo-symmetric." This general operating approach is only employable if both active species are stable in the (electro)chemical environment of the opposing half-cell but, if such conditions are met and in the absence of other forms of electrolyte degradation, it enables utilization of the same or substantially similar methods pioneered for remediating crossover losses in vanadium RFB (VRFB) systems. Not only does the spectator strategy facilitate crossover remediation, but it actually lowers crossover rates: by having all active species ($Fe^{2+/3+}$ and $Cr^{3+/2+}$) present in nearly-equal concentrations on either side of the membrane, the diffusional driving force for crossover is diminished, which, in turn, significantly reduces the net crossover rate [143]. This approach is particularly important for the Fe-Cr system, as the Fe^{n+} and Cr^{n+} are ~20× more permeable than vanadium cations in Nafion™ membranes, the current state-of-the-art ion-exchange membranes for RFBs [144]. Further, the ability to utilize rebalancing can enable economically viable replacement of these more expensive membranes (*e.g.*, Nafion™) with lower-cost but less-selective options (*e.g.*, size-exclusion membranes) [25,60]. Although the chemical configuration of the spectator strategy essentially doubles the amount of active materials required and sacrifices energy density (as the solubility of true active materials is reduced due to presence of spectators) and thus increases the electrolyte cost, with sufficiently low-cost charge-storage compound this tradeoff may not be prohibitive. For the Fe-Cr system, utilizing the calculations by Rodby *et al*. (and adjusting the depth-of-discharge to reflect the data in the Fe-Cr RFB literature – 60%, shown in Table V-1 (*vide infra*)– as opposed to the 80% used in the original work), the total electrolyte cost is only ~ 31 $/kWh [120]. Thus, this RFB chemistry may represent a viable alternative to the VRFB, at least from an electrolyte cost perspective [25,120]. Further, the system shows promise from a practical standpoint; it has been successfully demonstrated with the spectator strategy in the past [143], though several technical hurdles remain that challenge the economic viability of long-term operation.

Generally considered to be the first modern RFB, the Fe-Cr system was first advanced by the National Aeronautics and Space Administration (NASA) in the 1970's and 1980's as a potential energy storage solution for deep-space missions [146]. The system uses the following two half

reactions for discharge (while the reverse direction represents the charging reactions), with all reactants in the aqueous phase:

Positive electrode: $Fe^{3+} + e^- \underset{\text{charge}}{\overset{\text{discharge}}{\rightleftharpoons}} Fe^{2+} \qquad E^0 = 0.77 \text{ V vs. SHE}$ **(V-1)**

Negative electrode: $Cr^{2+} \underset{\text{charge}}{\overset{\text{discharge}}{\rightleftharpoons}} Cr^{3+} + e^- \qquad E^0 = -0.41 \text{ V vs. SHE}$ **(V-2)**

Since it proved unsuitable for space missions, due to its low energy and power densities, the Fe-Cr RFB has seen limited research, development, and deployment efforts since the late 1980's, at least as compared to the VRFB, despite the surge of interest in RFBs in subsequent years. This may stem from the known difficulties of operating this chemistry. Elevated temperatures (≥ 50 °C) are required in order to shift the equilibrium from the inactive Cr^{3+} complex, $[Cr(H_2O)_6]^{3+}$, to its electrochemically active counterpart, $[Cr(H_2O)_5Cl]^{2+}$ [110,121,143,205]. Further, the electrode potential for the Cr redox reaction is negative enough (E^o = -0.407 V vs SHE) to lead to competition with the hydrogen evolution reaction (HER), where protons are reduced to hydrogen gas (E^o = 0 V vs SHE). This parasitic side reaction remains a strong impediment to the decadal operation expected for successful grid applications. Recent reports cite HER as the cause of ~1% of capacity loss per cycle for Fe-Cr RFBs [25], which is ~20× the estimated rate of capacity loss from HER in VRFBs [60]. The charge imbalance caused by this reaction also complicates electrolyte remediation protocols, necessitating additional system components to counter its impact [206,207]. Finally, the moderate open circuit voltage (OCV) of 1.18 V for the Fe-Cr RFB and corrosiveness of HCl are also limiting factors, though HER mitigation has historically been the research focus for the aforementioned reasons.

While there are methods to address the HER retrospectively, using various methods to reintroduce electrons back into the system to correct the charge imbalance, these can complicate the system operation. The simplest method is to add stoichiometric amounts of chemical reductants, as is often done for VRFBs [76,208]. This is part of the design and operating strategy proposed by Creek Channel (also referred to as "Tiger Creek" and "Cougar Creek"), a new Fe-Cr company [209]. However, over time this approach can become problematic, as the evolving hydrogen gas leaves the RFB system, shifting the electrolyte pH and/or diluting the active species in the electrolyte. These effects may be further compounded by the reaction between the reductant and the electrolyte. A more complicated but arguably preferable method for rebalancing the charge is to

use a secondary “recombination” cell to oxidize the generated hydrogen, (preferably using the species that was oxidized against the HER reaction originally, in this case the Fe) and return these species to their original electrolytes, as has been demonstrated in several Fe-Cr [210,211] and, more recently, all-Fe hybrid RFB systems [212]. However, this approach adds costs and complexity to the RFB system, further reducing the appeal of researching, developing, or deploying this technology. While mitigation strategies may ultimately be necessary with any appreciable amount of HER, it is still desirable to minimize the amount generated to reduce the costs of its remediation (*e.g.*, the number of secondary cells needed for a system is proportional to the percent of capacity lost per cycle to HER) and facilitate longer-term operation in the absence of remediation methods for simplified pathways to commercialization. Indeed, the technical challenges imposed by high HER rates have seemingly impeded commercialization efforts for the Fe-Cr system, in addition to the general barriers to RFB adoption, such as limited demand for long-duration energy storage. Beyond Creek Channel (*vide supra*, a relatively newer effort), two notable prior attempts include EnerVault and Imergy (formally Deeya): the former liquidated its assets in 2015 following financial struggles [213], while the latter pivoted from Fe-Cr RFBs to VRFBs before liquidating as well [214]. In sum, the Fe-Cr RFB system poses further complications in addition to already stymying challenges present in VRFBs that necessitate broadly encompassing expertise in mechanical, chemical, electrochemical, and materials science. However, as the Fe-Cr RFB and VRFB both utilize inorganic, metal-based active species in acidic supporting electrolytes and have negative redox reactions that compete with HER, many lessons learned in recent decades from the advanced development of VRFBs may be applicable to spurring progress in Fe-Cr RFBs. Accordingly, there has been a renewed interest in the Fe-Cr RFB since the mid 2010’s, much of which focuses on improving performance, including HER minimization. For the interested reader, a more comprehensive discussion of historical Fe-Cr RFB development can be found in the work by Sun and Zhang [204].

There are many potential avenues to reduce the rate of HER [203]. One approach is to minimize local overpotentials that drive HER through electrode and/or flow field design that increase the local interfacial surface area accessible to the electrolyte. Zeng *et al.* showed improved performance in an Fe-Cr RFB using thinner electrodes and serpentine flow fields, as compared to a flow-through design with much thicker electrodes, 0.8 mm and 6.0 mm, respectively (although the authors of this work mainly focus on reduced ohmic and pumping losses, rather than HER

suppression) [110]. Another approach is to improve the reaction selectivity, either by utilizing catalysts that promote the desired redox reactions or through minimizing the concentrations of potential HER catalysts. To this end, bismuth (Bi) has been particularly been well-studied in Fe-Cr RFBs and has consistently demonstrated an ability to promote the Cr redox reaction and suppress the HER, via direct nanoparticle deposition onto the negative electrode and/or as a negative electrolyte additive [215–218]. Lead and indium (In) have shown similar benefits as catalysts and additives [218,219]. Electrolyte composition is another avenue to address HER; beyond the use of additives, the concentrations of active species and supporting salt [122,220], as well as choice of supporting salt, can impact HER rates [203]. For example, the recent Fe-Cr commercialization efforts by Tiger Creek (*vide supra*) claim to be utilizing a less acidic electrolyte, which could reduce HER by diminishing local proton concentrations [209], although thermodynamically-driven metal oxide formation at higher pH may challenge the implementation of milder acidic electrolytes. It should be noted, however, that catalysts and additives – particularly those based on Bi or In – can be expensive, especially if they need to replaced over the course of the system lifetime. To this end, ligand-modified approaches focused on complexing Fe and Cr species to yield near-neutral pH and higher OCV systems have shown promise [209,221,222].

Electrolyte purification is another method to reduce HER rates by removing known catalytic precursors prior to use in a battery. Many metals are known to act as HER catalysts (*e.g.*, copper or nickel), so their presence in electrolytes, even in trace amounts can lead to their unintended electrochemical reduction (*i.e.*, electrodeposition) onto the negative electrode where they promote hydrogen evolution [76,203]. This is especially a concern in long-duration RFB systems where the ratio of electrolyte volume to electrode area is high. Purification methods include physical or chemical removal strategies [223], as well as electrochemical procedures that intentionally electroplate contaminants on a sacrificial electrode before the electrolyte is used in the actual cell of interest [224,225]. The referenced examples are focused on or applicable to VRFB and Fe-Cr RFB systems. However, they comprise mere descriptions of the methodologies in the patent literature and do not demonstrate the actual impact of purification on cell performance. To our knowledge, this simple and low-cost approach of electrochemical purification has not been extensively investigated as a HER mitigation strategy for Fe-Cr RFBs in the peer-reviewed literature. In this work, we develop a protocol for electrochemical purification of the Fe-Cr negative electrolyte (shown in Figure V-1 below) and explore its effects on the performance of an

Fe-Cr RFB cell. We observe a marked reduction in HER activity of the purified electrolyte through cyclic voltammograms. Next, we show that the purification process facilitates a notably reduced fade rate (*ca.* 5× slower) in long-term galvanostatic cycling of an Fe-Cr RFB cell, and that the effectiveness of the protocol is dependent on the relative amount of electrolyte purified. Finally, we extract performance metrics (*i.e.*, coulombic, voltaic, and energy efficiencies along with capacity decay rate) of other cycled Fe-Cr RFBs reported in the peer-reviewed literature, illuminating a correlation between coulombic efficiency and capacity decay rate. Following this trend, the performance of our cell using purified electrolyte is comparable to the performance of cells utilizing expensive catalysts and additives, thus evincing a potential cost reduction pathway as compared to other contemporary approaches.

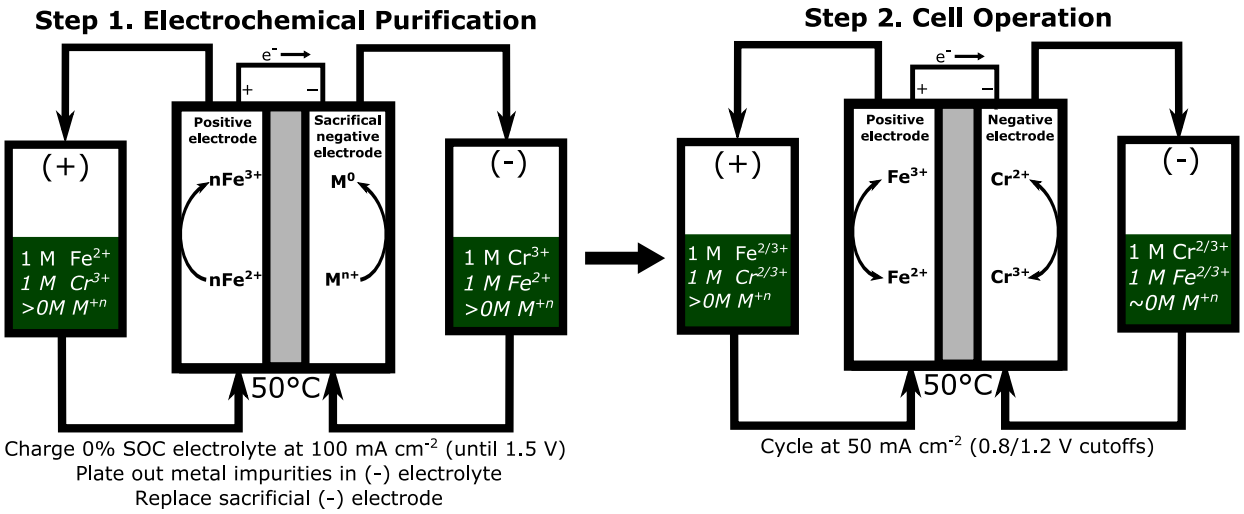

Figure V-1 - Schema of electrolyte purification and cycling procedures. In Step 1, pristine 0% SOC electrolyte (1 M Fe^{2+} and 1 M Cr^{3+} in 3 M HCl, where, in each tank, the non-italicized species denote those that are intended to be redox active and the italicized species represent spectator or impurity species) is discharged at 100 mA cm^{-2} until a 1.5 V cutoff to plate out impurities present in the negative electrolyte onto the negative electrode; the sacrificial electrodes are then replaced. In Step 2, the cell is cycled with the purified electrolyte (discharging first) at 50 mA cm^{-2} using 0.8 V and 1.2 V cutoffs for discharge and charge, respectively.

2. Methods

Cyclic voltammetry in elevated temperature – Ex situ electrochemistry was conducted in a three-electrode cell with a 3-mm diameter glassy carbon electrode (BASi), Pt coil (BASi), and Ag/AgCl in a 3 M NaCl reference electrode (BASi). The glassy carbon electrode was mirror-polished in a 0.05 μm MicroPolish alumina powder (Buehler) slurry on a microcloth disk, briefly sonicated in acetone and deionized (DI) water, rinsed in DI water, and allowed to air-dry. Chromium (III) chloride hexahydrate ($CrCl_3$•$6H_2O$, ≥99.5%, Alfa Aesar, Lot No. Q16G036), iron (II) chloride tetrahydrate ($FeCl_2$•$4H_2O$, 98%, Alfa Aesar, Lot No. S18H053), and hydrochloric acid (HCl, 37%, balance of water, Sigma Aldrich) were dissolved in DI water (Milli-Q Millipore, 18.2 MΩ cm). The electrolyte was 1.0 M $FeCl_2$ / 1.0 M $CrCl_3$ in 3.0 M HCl. A temperature of *ca.* 50 ± 5 °C was maintained by submerging a sealed vessel containing the electrodes and electrolyte into an oil bath heated by a VWR® Professional Hot Plate Stirrer with a temperature probe (VWR). Cyclic voltammograms were measured at a scan rate of 50 mV s^{-1}, starting from open circuit potential, scanning in the positive direction to a voltage bound of 1.2 V vs Ag/AgCl, scanning in the negative direction to -1.0 V vs Ag/AgCl, and returning to the starting potential. Full *i*R-correction (100%) was employed during data acquisition by a Bio-Logic VSP potentiostat (Bio-Logic).

Heat-treatment of electrodes – Sigracet (SGL) 39AA (Fuel Cell Store) electrodes were thermally oxidized in a muffle furnace (Barnstead Thermolyne Type 47900), ramping at a rate of 20 °C min^{-1} from room temperature to 500 °C, holding for 5 h, and cooling down to ambient conditions without further intervention. The electrodes were subsequently stored under air in plastic containers (McMaster-Carr).

Full cell RFB operation – Single-cell RFB cycling was performed in a subscale cell with a 5 cm × 5 cm (25 cm^2) active electrode area. 3× thermally-treated SGL 39AA were used for both positive and negative electrodes. The thickness of PTFE gaskets were selected such that the electrode stack was compressed by *ca.* 20%. Interdigitated flow fields, milled from Tokai G347B resin-impregnated graphite plates of 3.18 mm thickness (Tokai Carbon Co.), were also employed, along with a Nafion™ 117 membrane presoaked in 3.0 M HCl for ≥ 24 h. The starting solution for each

electrolyte (posolyte and negolyte) was 50 mL of 1.0 M $FeCl_2$ / 1.0 M $CrCl_3$ in 3.0 M HCl. Humidified nitrogen gas (Airgas, 99.999%) was bubbled through the electrolytes for > 1 h to purge residual oxygen prior to the electrochemical measurements. A flow rate of *ca.* 93 mL min^{-1} was maintained with a MasterFlex™ pump set at 100 rpm and circulated using LS/16 Norprene™ tubing (Cole-Parmer). The cell temperature was maintained at *ca.* 50 ± 5 °C using silicone adhesive-mount heating pads with a 10 W in^{-2} heating density (McMaster-Carr) connected to a benchtop PID controller (Platinum Series, CS8DPT, OMEGA Engineering), calibrated to the internal temperature of the cell components using a thermocouple probe (McMaster-Carr). The cell was cycled at a constant current density of 50 mA cm^{-2} between upper and lower cell voltage cutoffs of 1.2 V and 0.8 V, respectively, using an Arbin battery tester (FBTS-8).

Purification Protocol – To purify the negative electrolyte, the subscale cell was charged starting from 0% state-of-charge (SOC) at 50 °C at 100 mA cm^{-2} until a cutoff voltage of 1.5 V was reached. A potential beyond the cycling voltage cutoff of 1.2 V was set to favorably drive cathodic plating reactions on the negative electrode, thus maximizing reduction of contaminants out of solution and onto the electrode without over-oxidizing the positive electrode. Following the galvanostatic precharge, the electrolytes were recirculated into their respective reservoirs, the cell was disassembled, the used electrodes on both sides were removed and fresh electrodes were inserted into the cell. To avoid air ingress and self-discharge, the reservoirs remained sealed throughout the entire process of replacing the electrode. The purified electrolyte was subsequently discharged in the reassembled cell, thus initiating the cycling protocol.

Scanning Electron Microscopy (SEM) / Energy Dispersive X-ray Spectroscopy (EDS) – SEM was performed using a Zeiss Merlin High-Resolution SEM. A 10 keV electron energy and 9.2 mm working distance with an in-lens secondary electron detector were used. Using the same acquisition parameters, energy dispersive spectroscopy (EDS) was used for elemental mapping of post-purified electrodes.

3. Results and Discussion

To screen the impact of electrolyte purification on the electrolytes, we performed cyclic voltammograms (CVs) in a three-electrode cell at 50 °C; electrolyte concentration and composition were chosen in accordance with full cell experiments (*i.e.*, mixed electrolyte with 1.0 M $FeCl_2$ and 1.0 M $CrCl_3$ in 3.0 M HCl). The Cr redox reaction is known to be sluggish at room temperatures [38], thus requiring elevated temperatures to proceed at acceptable rates. However, hydrogen (H_2) readily evolves at the Cr redox potential, reducing access to catalyst sites due to bubble formation, and lower efficiencies; these side effects are exacerbated by the elevated temperatures needed to facilitate the Cr reaction.

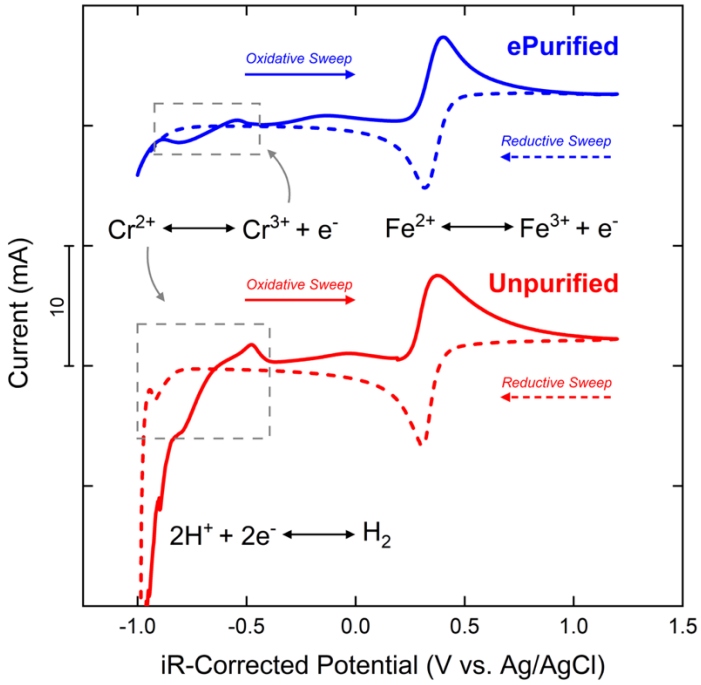

Figure V-2 - Cyclic voltammograms of electrochemically purified (blue) and unpurified (red) electrolytes at a scan rate of 50 mV s^{-1}. The purified electrolyte was harvested from the negative electrolyte after a purification. The electrolyte composition was 1.0 M $FeCl_2$ / 1.0 M $CrCl_3$ in 3.0 M HCl, at a temperature of 50 °C. The working, counter, and reference electrodes used were a glassy carbon disk, a Pt coil, and Ag/AgCl in 3 M NaCl.

Figure V-2 shows CVs for electrochemically purified ("ePurified," blue) and unpurified (red) electrolyte conducted at a scan rate of 50 mV s^{-1}. The solid and dashed lines show the directions of oxidative and reductive sweeps, respectively. The relatively facile and reversible $Fe^{2+/3+}$ redox

couple appears largely unchanged by the purification, with a redox potential of *ca.* 0.45 V vs Ag/AgCl, in accordance with prior literature [226,227]. However, significant changes are observed with the redox events occurring at low potentials. Specifically, the untreated electrolyte demonstrates significant HER and potential contaminant deposition, evinced by the growing reductive current in the range of -0.75 V to -1.0 V vs Ag/AgCl, as compared to the lower reductive currents observed for the purified electrolyte. While, a larger Cr oxidative peak at -0.5 V vs Ag/AgCl is observed for the unpurified electrolyte, direct comparison with the purified electrolyte is obfuscated by the large amount of visually observed H_2 bubbles formed on the preceding reductive sweep, which affects the access of solution-phase actives species to the electrode surface. In contrast, both the reductive and oxidative Cr peaks are visible and discernible for the purified electrolyte, suggesting a balance between mitigating H_2 evolution while also enabling Cr and Fe redox reactions. Further, bubbling was not observed during the CVs in the purified electrolyte. We note that Fe plating and stripping, which occurs at a standard reduction potential at -0.645 V vs Ag/AgCl, could also be a competing reaction at these negative potentials. This reaction is particularly important to mitigate, as its occurrence in the negative half-cell would catalyze HER. Altogether, the CVs suggest that H_2 evolution could be mitigated using the electrolyte purification technique.

We note that the CVs were conducted on a planar glassy carbon surface to avoid complicating the electroanalysis with porous carbon electrodes that would ultimately be used in RFB cells. Accordingly, the results for the CVs are applicable for non-heat-treated materials, enabling qualitative conclusions to be drawn for HER mitigation for only pristine carbon materials, and necessitating full-cell validation with higher-performing heat-treated electrodes that may behave differently. While the CV results are instructive, quantitative agreement between the materials sets is not anticipated, as glassy carbon surfaces are distinct from heat-treated carbon fiber surfaces due to differences in synthesis procedures, carbon allotropes, and relative degrees of surface oxidation.

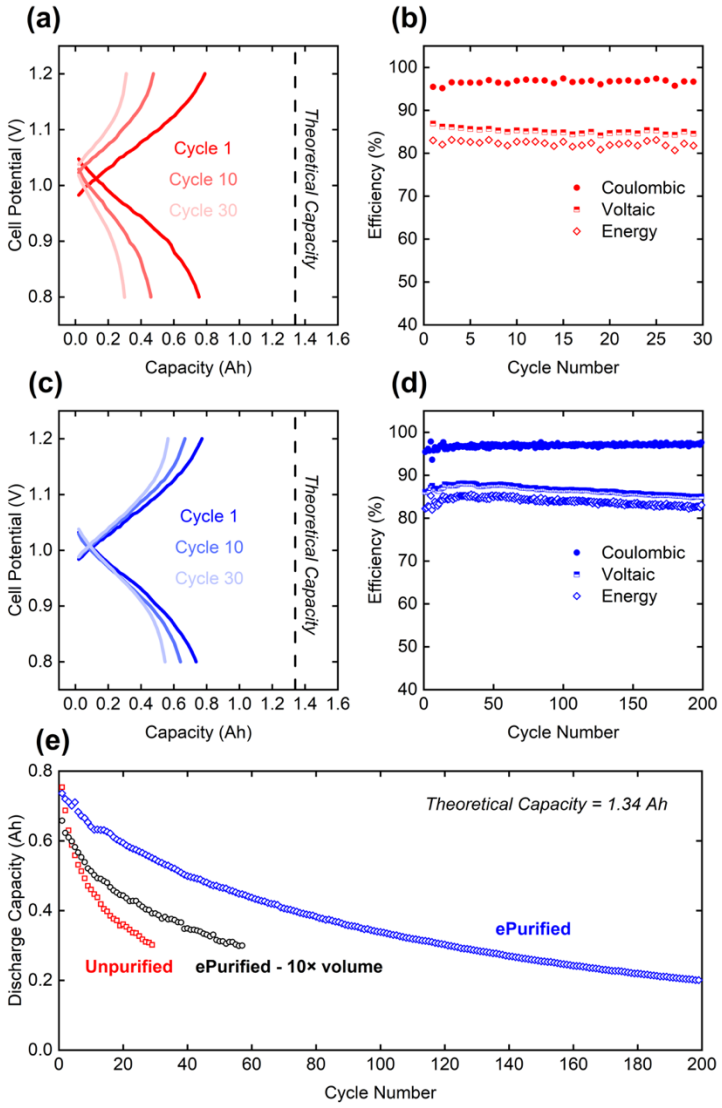

Figure V-3 – Extended single-cell cycling in full Fe-Cr RFBs. (a) Potential vs capacity curves for the 1st, 10th, and 30th cycles for a full Fe-Cr RFB cell with an untreated electrolyte, and (b) corresponding coulombic, voltaic, and energy efficiencies per cycle. (c) Potential vs capacity curves for the 1st, 10th, and 30th cycles for a full Fe-Cr RFB cell with an ePurified electrolyte, and (d) corresponding coulombic, voltaic, and energy efficiencies per cycle. (e) Comparison between the discharge capacity as a function of cycle number for ePurification process on electrolyte with 50 mL volume (blue), ePurification process on electrolyte with 500 mL volume (black), and unpurified electrolyte (red). While the total volumes of electrolyte purified differed, 50 mL of electrolyte was used for cycling in all cases. All cells were cycled at 50 mA cm^{-2} and at an estimated temperature of 50 °C, with an electrolyte composition of 1.0 M $FeCl_2$ / 1.0 M $CrCl_3$ in 3.0 M HCl and an N117 membrane presoaked in 3.0 M HCl for ≥ 24 h. The volumetric flow rate was *ca.* 90 mL min^{-1}.

We evaluate the electrochemical performance of the electrochemically purified and untreated electrolyte in a single-cell Fe-Cr RFB via galvanostatic cycling at 50 mA cm^{-2} at 50 °C. An electrolyte composition of 1.0 M $FeCl_2$ and 1.0 M $CrCl_3$ in 3.0 M HCl was selected to align with the composition used in the CV studies. Figure V-3a shows cycles 1, 10, and 30 for cell with untreated electrolyte and Figure V-3b shows the coulombic, voltaic, and energy efficiencies as a function of cycle number. In comparison, Figure V-3c shows cycles 1, 10, and 30 for the cell with purified electrolyte and Figure V-3d shows the evolution of the efficiencies over 200 cycles. Both purified and pristine electrolyte exhibit an initial discharge of *ca.* 0.74 Ah, demonstrating that negligible capacity is lost to charge imbalances induced by the initial electrochemical purification (*i.e.*, a negligible amount of Fe^{2+} in the positive electrolyte is oxidized against any of the following counter reactions in/at the negative electrolyte/electrode: metal impurity reduction, HER, or Fe cation reduction). For an electrolyte volume of 50 mL, the maximum capacity can be calculated as 1.34 Ah, indicating a 55% electrolyte utilization efficiency. While this is a relatively low accessed capacity, it aligns with prior reports (see Table V-1); as such, understanding and expanding the limits of the Fe-Cr accessed capacity should be the focus of future work. A possible cause is the use of a relatively low upper voltage limit (*e.g.*, 1.2 V) in order to minimize HER. This low initial utilization could also be due in part to only some of the Cr being electrochemically active (*i.e.*, in the correct Cr-speciation) [204,205,228], which is presumably why cells run at lower temperatures have even lower utilizations (see first row in Table V-1). In both conditions, the coulombic, voltaic, and energy efficiencies are comparable. For the purified electrolyte, an average coulombic efficiency of 96.9%, average voltaic efficiency of 86.5%, and an average energy efficiency of 83.9% is achieved, with stable metrics for 200 cycles. For the unpurified electrolyte, an average coulombic efficiency of 96.9%, an average voltaic efficiency of 85.1%, and an average energy efficiency of 82.3% is achieved, though only for 30 cycles. The most notable difference in the cell cycling data across the two electrolytes is the reduced capacity fade rate for the purified electrolyte compared to the untreated electrolyte, as evinced by the slower decay in the discharge capacity as a function of cycle number (Figure V-3e). We posit that the discrepancy in capacity fade despite nearly identical coulombic, voltaic, and energy efficiencies is due to losses from HER during charging from impurities in the unpurified electrolyte, as these efficiencies are relative measures of losses for individual cycles, and are unable to capture behavior across cycles. To quantify the decay rate, we determine the number of cycles at which 50% of the maximum

discharge capacity utilization (*i.e.*, 0.37 Ah) is reached to avoid effects of non-linear fade at later cycles. The steeper initial capacity drop may be a consequence of diminishing activity of the oxygen groups on the electrode formed during oxidative pretreatment that occurs as the electrode undergoes prolonged cycling, whose deactivation is more pronounced towards the Cr redox reaction due to its lower potential [46]. The untreated electrolyte reaches the cutoff within 17 cycles (13.9 h total duration), while the purified electrolyte lasts a prolonged 87 cycles (71.7 h total duration) prior to reaching the same capacity retention. This corresponds to decay rates of 2.94 % / cycle and 0.57 % / cycle for the first 50 cycles for the unpurified and purified electrolytes, respectively. We note that our own efforts to rebalance spent electrolytes by mixing used posolyte and negolyte together, dividing the mixed electrolyte into two equal volumes, and resuming operation did not lead to significant capacity recovery, suggesting that the mechanisms of capacity fade were not solely due to crossover. The same purification protocol was performed with 10× the original electrolyte volume to evaluate its effectiveness as a function of volume to be purified. The same total electrolyte volume of 50 mL was taken from the larger volume of purified electrolyte and cycled. Figure V-3e shows that while capacity fade was mitigated compared to no treatment, it is more rapid than with a smaller volume of purified electrolyte. One possible explanation is that not all the electrolyte impurities are removed with the larger volume of electrolyte if purified using the same electrode size (*i.e.*, there is not enough electrode surface area to plate out all the metal impurities present in the larger electrolyte volume). This hypothesis implies there is, perhaps, a ratio of electrolyte volume to electrode surface area that cannot be exceeded for sufficient purification or operation; quantification and optimization of such a ratio should be the focus of future work.

We seek to contextualize our results within the broader efforts towards alleviating capacity fade in Fe-Cr RFBs. Summaries of performance metrics from a non-exhaustive list of previously reported literature is summarized in Table V-1. Some of the data is adapted in part from the recent review paper by Sun and Zhang [204]. Approximate averages for the coulombic, voltaic, and energy efficiencies of longer-duration galvanostatic cycling tests are shown, along with estimated discharge capacity decay per cycle. Self-reported data were used whenever possible; if the capacity decay rate was not reported, the decay rate to 50% of the original capacity was extracted from published figures. The use of different flow field designs, electrode materials and thicknesses, electrolyte compositions, in-house cell architectures, laboratory practices, and cycle numbers

stymy exact comparison of the approaches used across the literature. Thus, we include operating conditions and parameters used (*i.e.*, electrode materials with geometric dimensions, flow fields, membrane, electrolyte concentrations and volumes). Notably, most strategies to improve the performance in Fe-Cr RFBs rely on materials advances, including membrane design, electrocatalyst development, or electrolyte additives, all designed to suppress HER. To the best of our knowledge, none of these studies refer to specific procedures to activate or purify electrolytes prior to electrochemical evaluation, besides elevating the operating temperature. Furthermore, there is no discussion or consensus on the standard grade of chemicals needed to uphold baseline cell performance. Our approach to electrochemically purify electrolytes results in comparable coulombic efficiency (CE), voltaic efficiency (VE), energy efficiency (EE), and decay rate (DR) to values reported in existing literature.

Table V-1 – Summary of performance metrics from select, recent Fe-Cr RFB literature used to construct Figure V-4. Electrode and flow field combinations, membrane type, and electrolyte compositions are reported, along with the performance metrics consisting of the approximate averages for the coulombic efficiency (CE), voltaic efficiency (VE), and energy efficiency (EE) of longer-duration galvanostatic cycling to estimate discharge capacity decay per cycle. Self-reported data were used whenever possible. If the capacity decay rate was not reported, the decay rate to 50% of the original capacity was extracted from published graphs. Otherwise, the reported decay rate was used, even if it was not to 50% of the original value, as the reported value is expected to be more accurate than the extracted values. We elected to report our decay rate in terms of decay rate to 50% of the original discharge capacity. Chart format and values adapted in part from Sun and Zhang.

Referenced Work	**Electrode / Flow Field / Active Area / Uncompressed Thickness**	**Membrane**	**Electrolyte / Temperature / Volume**	**Current Density (mA cm^{-2})**	**CE (%)**	**VE (%)**	**EE (%)**	**Capacity Decay Rate* (% / cycle)**	**Maximum Discharge Capacity / Theoretical Discharge Capacity (Ah/L)**	**Theoretical Accessible Capacity on Cycle 1 (%)**	**Ref.**
Ahn & Moon *et al.*, 2021	Carbon Felt + Bi-C electrocatalyst / Flow-type / 2.0 × 3.0 cm^2 / 4.3 mm	Nafion 117	1.2 M $FeCl_2$ + 1.5 M $CrCl_3$ in 2.0 M HCl / Room Temperature / 20 mL	40	97.4	88.5	86.2	0.50	9.2 / 32.2	28.6	[215]
	Carbon Felt + KB / Flow-type			40	97.2	82.2	79.9	0.637	9.1 / 32.2	28.3	

	/ 2.0 × 3.0 cm^2 / 4.3 mm										
	Carbon Felt / Flow-type / 2.0 × 3.0 cm^2 / 4.3 mm			40	96	72.8	69.9	0.883	8.08 / 32.2	25.1	
Chen *et al*., 2020	Silicic acid etched 500 °C for 5h Graphite Felt / Flow-through / 3.0 × 3.0 cm^2 / 5 mm	Nafion 115	1.0 M $FeCl_2$ + 1.0 M $CrCl_3$ in 3.0 M HCl / 65 °C / 50 mL	120	92.4	86.3	79.7	0.46	14.60 / 26.8	54.5	[229]
	500 °C for 5h Graphite Felt / Flow-through / 3.0 × 3.0 cm^2 / 5 mm			120	96.4	74.1	71.4	1.16	11.68 / 26.8	43.6	
Sun *et al*., 2019	500 °C for 5h Graphite Felt / Flow-type / 3.0 × 3.0 cm^2 / 5 mm	SPEEK (sulfonated poly(ether ether ketone)	1.0 M $FeCl_2$ + 1.0 M $CrCl_3$ in 3.0 M HCl / 65 °C / 50 mL	80	98.5	80.3	79.1	0.84	-- / 26.8	--	[230]
		Nafion 115		80	96.0	85.7	82.3	1.56	-- / 26.8		
Zhang *et al*., 2019	Graphite Felt / Flow-through / 3.0 × 3.0 cm^2 / 6.25 mm	Nafion 115	1.0 M $FeCl_2$ + 1.0 M $CrCl_3$ in 3.0 M HCl / 65 °C / 50 mL	60	93.1	81.8	76.1	1.19	-- / 26.8	--	[231]
Zhang *et al*., 2020	500 °C for 5 h Graphite Felt / Flow-through / 3.0. × 3.0 cm^2 / 5 mm	Nafion 115	1.0 M $FeCl_2$ + 1.0 M $CrCl_3$ in 3.0 M HCl + 8 mM $BiCl_3$ / 65 °C / 50 mL	60	96.9	89	86.3	1.2	-- / 26.8	--	[232]
	Graphite Felt / Flow-through / 3.0 × 3.0 cm^2 / 5 mm			60	94.3	91.7	86.4	2.9	-- / 26.8	--	
	500 °C for 5 h Carbon Felt / Flow-through / 3.0 × 3.0 cm^2 / 5 mm			60	95.9	83.7	80.3	1.26	-- / 26.8	--	
	Carbon Felt / Flow-through / 3.0 × 3.0 cm^2 / 5 mm			60	84.9	80.6	63.3	2.99	-- / 26.8	--	
Zeng *et al*., 2015	400 °C for 6 h Graphite Felt /	Nafion 212	1.0 M $FeCl_2$ + 1.0 M $CrCl_3$ in	80	96.2	85.8	82.5	1.2	-- / 26.8	--	[25]

	Flow-through / 2.0 × 2.5 cm^2 / 6 mm		3.0 M HCl + 0.01 M Bi^{3+} (Bi_2O_3) / 65 °C / 20 mL								
Zeng *et al*., 2016	Mixed acid-boiled Carbon Paper / Flow-Field Structured / 2.0 × 2.0 cm^2 / 0.8 mm	Nafion 212	1.0 M $FeCl_2$ + 1.0 M $CrCl_3$ in 3.0 M HCl + 0.005 M Bi^{3+} (Bi_2O_3) / 65 °C / 20 mL	160	97.4	85.1	82.9	0.6	-- / 26.8	--	[110]
Zeng *et al*., 2016	500 °C for 5 h Carbon Paper / Interdigitated Flow-Field (IDFF) / 2.0 × 2.0 cm^2 / 0.8 mm	Nafion 212	1.0 M $FeCl_2$ + 1.0 M $CrCl_3$ in 3.0 M HCl + 0.005 M Bi^{3+} (Bi_2O_3) / 65 °C / 20 mL	320	97.8	81.5	79.7	0.5	-- / 26.8	--	[233]
Wang *et al*., 2021	Graphite Felt / Flow-through / 5.0 × 10.0 cm^2 / 5.3 mm	Perfluorosulfonic-acid ion exchange membrane	1.0 M $FeCl_2$ + 1.0 M $CrCl_3$ in 3.0 M HCl + 0.01 M $InCl_3$ / 65 °C / 70 mL	160	98.2	80.1	78.7	0.16	18.7 / 26.8	69.8	[219]
			1.0 M $FeCl_2$ + 1.0 M $CrCl_3$ in 3.0 M HCl / 65 °C / 70 mL	160	97.2	80.1	77.9	0.42	18.6 / 26.8	69.3	
This work: ePurified	500 °C for 5 h Carbon Paper / IDFF / 5.0 × 5.0 cm^2 / 0.84 mm	Nafion 117	1.0 M $FeCl_2$ + 1.0 M $CrCl_3$ in 3.0 M HCl / 50 °C / 50 mL	*50*	*96.9*	*86.5*	*83.9*	*0.57*	*14.8 / 26.8*	*55.0*	--
This work: Unpurified	500 °C for 5 h Carbon Paper / IDFF / 5.0 × 5.0 cm^2 / 0.84 mm	Nafion 117	1.0 M $FeCl_2$ + 1.0 M $CrCl_3$ in 3.0 M HCl / 50 °C / 50 mL	*50*	*96.6*	*85.1*	*82.3*	*2.94*	*15.1 / 26.8*	*56.2*	--

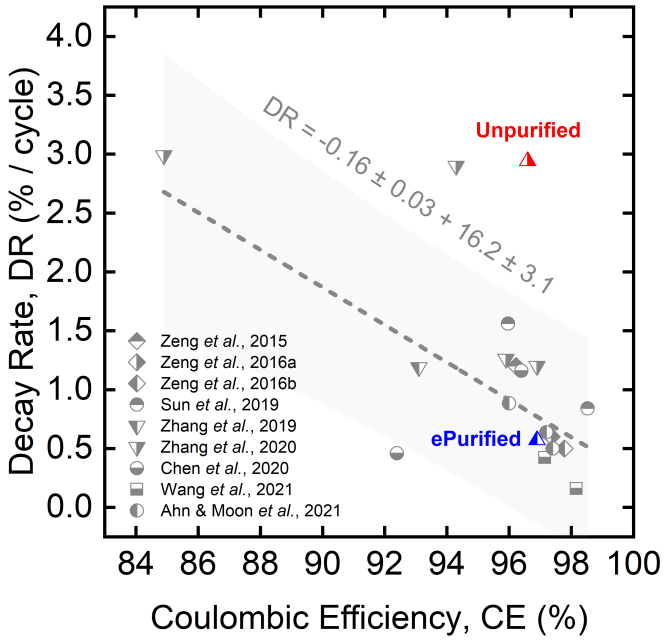

Figure V-4 – Decay rate of initial discharge capacity as a function of average coulombic efficiency. Unpurified electrolyte (red triangle) and purified electrolyte (blue triangle) from this work are shown amid other performance metrics reported in the Fe-Cr RFB literature. The gray dotted trendline is the ordinary least squares fit of the data excluding the unpurified electrolyte and the outlier from Zhang *et al.* (2020) [232].

We hypothesized that DR may be associated with CE, as CE is an indicator of unmatched capacity across subsequent discharge and charge half cycles and we anticipate an important contributor to the DR is HER. The statistical significance of the association between CE and DR was confirmed using the Kendall rank correlation analysis between seven variables (electrode thickness, geometric area, current density rate, CE, VE, EE, and DR); the results are shown in in Figure S1**,** and further details on the statistical basis of the Kendall analysis can be found in the Supporting Information of this work (**Appendix A**). We note that the presence of soluble mediators can also contribute to the H_2 generation in Fe-Cr RFBs (*i.e.*, charge-transfer in solution) [234], although determining the extent and identity of these exchanges is beyond the scope of the present analysis and work. We explore the relationship between DR and CE in Figure V-4 plotting data harvested from the Fe-Cr RFB literature and our own results for the purified and unpurified electrolytes. Despite the range of applied current densities and HER mitigation strategies, we observe a linear negative trend between DR and CE, whereby higher CE is generally correlates to lower DR. We note the existence of two points considered to be outliers; a cell from our own reported unpurified

electrolyte, and a cell using pristine graphite felt from Zhang *et al.* (2020) [232]. These two data points exhibit relatively high DR despite high CE. Excluding these two points, we identify ordinary least squares fit to the DR versus CE data. These values, however, are to be taken semi-quantitatively, as sources of error including ranging current densities, cycle numbers, and self-reported values contribute error; thus, we plot a 95% prediction band to accompany the line-of-best-fit. Further, we note that while the relationship between DR and CE are expected to be negatively correlated, the precise nature of the relationship is likely more nuanced due to convoluting factors such as active species crossover rates and non-linear effects that vary with operating conditions. Nevertheless, our electrochemical purification protocol falls near the fitted trendline towards the higher end of the recorded CEs, suggesting that electrochemical purification strategies can have a similarly beneficial impact on reducing capacity fade as approaches in electrocatalyst design and electrolyte additives.

In order to explain the two outliers in Figure V-4, one may consider the interaction of three key factors: 1) total surface area of the electrodes (especially the negative electrodes), 2) how easily-reducible impurities in the electrolyte can impact the cell performance and the electrolyte composition, and 3) how the addition of Bi can impact both the cell performance and the impact of impurities. The impact on VE and CE of each of these factors, independently, is summarized in Table V-2. Most of the cells summarized in Table V-1 use porous electrodes with high interfacial-to-geometric surface area ratios, as they use thick carbon felts that have been thermally treated. In all of these cases, the impact of impurities on the cell performance should be significantly reduced relative to electrodes with lower interfacial-to-geometric surface ratios since the resulting impurity density on the negative electrode is concomitantly lower. The two outliers identified previously can be explained primarily by their electrode surface areas: our work uses carbon papers that are significantly thinner than felts and have specific surface areas on the order of 5 – 20 $m^2\ g^{-1}$ based on previous reports on the surface areas of heat-treated paper electrodes [235,236], and the felt electrodes used in Zhang 2020 [232] are not thermally activated and these non-treated carbon fibers have surface areas that are *ca.* 6× lower than those that are pre-oxidized (*e.g.*, the reported BET surface areas are < 2 and 9-14 $m^2\ g^{-1}$, respectively). In the other cases that use carbon papers [110,233] or untreated felt electrodes [215,232], Bi cations are added to the electrolyte, which will presumably compete or co-deposit with reducible impurities in the electrolyte. The result is lower amounts of and attenuated effects from reduced impurities deposited on the negative electrodes,

and thus high CEs and low DRs. Unfortunately, the impact of impurities for all of the cases summarized in Table V-1 is limited to qualitative comparisons, as most papers do not report electrolyte chemical purities. Even if these values were reported, it would not be sufficient since the speciation of the impurities would also need to be known for a quantitative assessment of the impact.

Table V-2. The expected impact on VE and CE of three key factors.

	Higher total electrode surface area	**Impurities that can readily be reduced at the negative electrode**	**Addition of Bi catalysts**
Impact on VE	Higher, due to lower reaction turnover rates per actual area at given operating geometric current density	None expected	Higher, due to reduced overpotential on negative electrode
Impact on CE	Indirectly higher*, due to reduced overpotentials	Lower, if these reduced impurities act as HER catalysts	Indirectly higher*, due to reduced overpotentials on negative electrode
Interactions	Lower density of reduced impurities (and Bi, if present) per actual area	Less impact with higher surface area electrodes or with the addition of Bi	Lower density and attenuated HER from reduced impurities since Bi counteracts effects of impurities on negative electrodes

* The relation is indirect under the assumption that the reduced overpotential enabled by the factor encourages operation at higher current density, and thus higher CE.

To investigate the origin of the deposited species during electrochemical purification, we performed scanning electron microscopy (SEM) and energy dispersive x-ray spectroscopy (EDS) on the negative electrodes used in the purification step comparing the results to those of an unexposed heat-treated SGL 39AA electrode (see Figure S2 in the Supporting Information of this work, found in **Appendix A**). While the SEM / EDS revealed that the negative electrode used in the purification process additionally exhibited Fe, Cr, and chlorine signals in addition to carbon and oxygen species and trace silicon from the electrode, it remains difficult to pinpoint the precise phases of the plated contaminants without a more detailed spectroscopic analysis. Although we posit that the effect of high concentrations of active species and impurities from various sources

are mitigated when first subjected to the electrochemical purification step, we also hypothesize that the impurity concentrations are relatively low and thus difficult to detect, but non-negligible, as discharge capacity decay rate is dependent on the amount of purified electrolyte volume as a function of electrode volume (Figure V-3e). If these impurities act as HER catalysts, only a small amount is required to have a significant impact as shown in the CVs in Figure V-2. Further studies leveraging more precise *in situ* or *ex situ* spectroscopy will prove valuable to ascertain the chemical identities of the deposited impurities.

4. Conclusions

Hydrogen-evolution mitigation strategies in Fe-Cr RFB systems have largely focused on materials and reactor design innovation. These techniques can add cost and complexity, particularly approaches that utilizes expensive metals (*e.g.*, Bi, In) as catalysts on the electrode or additives in the electrolyte. Here, we demonstrate an alternative, potentially low-cost approach to mitigate HER: electrochemical electrolyte purification. We demonstrate that this strategy leads to significant reduction in capacity fade at appreciable current density over extended cycling experiments and produces results that are on-par with literature that teach materials-centric strategies. We hypothesize that the purification process reduced and filtered out metal impurities that can catalyze deleterious hydrogen generation on the negative electrode lowering accessible capacity over time. Importantly, this purification process does not appear to induce a significant charge imbalance that would, in itself, reduce the accessible capacity. We show that a clear association between discharge capacity decay rate and coulombic efficiency exists based on durational cycling data obtained from literature, and that our electrochemically purified data falls within that trend, while the cell with unpurified electrolyte demonstrates abnormally high decay rate with moderate coulombic efficiency. The connection between coulombic efficiency and decay rate semi-quantitatively elucidates the importance of attenuating HER attempted through numerous strategies for more resilient Fe-Cr RFBs.

Future work should focus on exploring the universality of the strategy across materials sets (*i.e.*, electrolytes of varying purity levels, electrodes of different formats), operating conditions (*i.e.*, temperatures, flow rates), and related electrochemical purification approaches (*i.e.*, potential holds, different potential cutoffs), in tandem with precise methods for impurity detection. Finally, despite

the improvements realized through electrolyte purification, the cell performance remains poor: total accessed capacity, even during the first cycle, is limited (~60%) and discharge capacity decay rate is rapid (*e.g.*, ≈ 50% in approximately 100 cycles), indicating high rates of irreversible capacity loss persist (as the discharge capacity was not recoverable via electrolyte rebalancing). Concerted research efforts are needed to understand and control the fundamental processes that govern the performance and longevity of Fe-Cr RFBs.

VI. Conclusions & future work

There is a need to decarbonize the power sector, and RFBs present a wide design space for addressing its long-duration applications. The need is pressing, so we must navigate the design space efficiently to advance promising solutions that will be economically viable. To this end, my thesis has sought to develop new techno-economic models and studies to evaluate, compare, and design RFB chemistries. I have used these tools to develop tangible, quantitative targets for economic viability for various classes of chemistries (*e.g.*, fade rates, servicing fees, electrolyte and materials costs, etc.), as well as identified important qualitative considerations for scalable chemistries, such as the diversification of the supply chain of critical materials. The ultimate goal is to use these models to drive actual research, development, and deployment of promising RFB chemistries. I have provided a brief example of this process in **Chapters III and V**, where the former identified a promising chemistry via TEA (*i.e.*, Fe-Cr) and the latter demonstrated how one might address the technical challenges of its commercialization in a laboratory setting (*i.e.*, electrolyte purification to reduce hydrogen evolution and promote long-term operation of the system). Much more of this translation between techno-economic modeling and demonstration or deployment is needed, as there are still no clear front-running RFB chemistries outside of the canonical VRFB. With decarbonization deadlines nearing, I feel it is crucial that the RFB community starts choosing – via utilization of the types of models and analyses presented in this work – promising candidates from the vast range of alternative chemistries being explored in the academic community and accelerating their development for commercialization and deployment.

While lower-cost and higher-abundance RFB chemistries are likely needed for more significant, long-term deployment of RFBs, my studies have shown me that we ought to deploy the solutions that are ready now (*i.e.*, VRFBs), dealing with the consequences of these more expensive and hard-to-scale chemistries in the near-term, while simultaneously preparing the next generation of battery chemistries. As shown in **Chapter IV**, deployment of VRFBs in the near-term would significantly help adoption of new RFB chemistries down the line by driving down the costs of chemistry-unspecific stack components and de-risking the technology. This is crucial, as the small existing production scale of RFB systems, as well as many of their critical components, remains an impediment to their broader-scale deployment. Further, a benefit to the simple and open

architecture of RFBs is that we could feasibly consider switching out chemistries in the long-term, especially if the electrolyte is leased (as is becoming increasingly popular for vanadium systems). Electrolyte leasing is an example of a larger takeaway from my thesis, which is that other disciplines (*e.g.*, policy, investment strategies, etc.) are crucial for overcoming the hurdles RFBs face for broadscale deployment. Thus, my recommendation for follow-up work is to start integrating the findings from this thesis with considerations in other disciplines to more holistically find solutions that will drive investment and deployment.

For example, government efforts could help de-risk RFBs and simultaneously drive down stack costs. Newer technologies like the RFB that are technically ready for deployment (*i.e.*, the VRFB) are struggling to compete with Li-ion at such low production volumes, as the only real demand for them is long-duration grid applications, which are very nascent markets. This "chicken and the egg" problem may not be solved in the private sector alone, but rather may require government intervention to support technology de-risking and cost reductions of these nascent storage solutions. Generally, there is a need for someone to test and support (via direct procurement) large-scale demonstrations. One avenue to execute this could be through government funding of extramural, commercial demonstration projects, as was previously done via the American Recovery and Reinvestment Act (ARRA). Presently, a lot of funding for demonstration projects out of the DOE is coming from the Office of Electricity's Energy Storage (OE-ES) program. However, this funding has mostly gone to national labs and has not been offered via open solicitations, which would involve the private sector and may accelerate progress. Further, the government could develop a dedicated program for downstream grid storage demonstrations that have shown promise in many of their earlier, development-phase programs (*e.g.*, ARPA-E). The recent SCALEUP (Seeding Critical Advances for Leading Energy technologies with Untapped Potential) program at ARPA-E partly addresses this need [237].

Thankfully, the cost curve relative to production scale looks steep for RFBs. Utilizing an open, "sandwich" type architecture, each individual stack component is fairly simple in design, and all together are easily assembled. Currently, RFB companies remain small and seem to be reinventing the wheel each time, sourcing their own stack parts at small volumes. Centralization of these efforts would significantly increase production volumes and reduce cost. The hesitancy around such an approach likely lies in companies' desire to keep IP and a competitive advantage. For some stack parts, such reservations can be more easily overcame due to their ubiquity and simplicity (*e.g.*, end

plates, gaskets, frames, bolts, pipes and manifolds, and overall assembly). For other, more performance-affecting parts (*e.g.*, membranes, electrodes, and flow fields), this may be more challenging. With an abundance of private capital, it is hard to imagine how government mandates (*e.g.*, demanding IP remain public on certain projects that it may fund) could be implemented successfully. Rather, such collaborative agreements involving IP-sharing usually play out in the private sector through mergers and acquisitions. Alternatively, the government (maybe the DOE, Department of Defense, or other government operations) could incentivize such practices by negotiating a large-scale purchase agreement with one or more RFB manufacturers under the conditions of centralized sourcing of certain components. Most examples of this kind of large-scale government procurement of a particular technology lie in military operations motivated by war: for example, the F-35 (a strike fighter aircraft) procurement program [238]. Thus, it may unfortunately take more drastic effects from climate change to catalyze such actions. In general, the stack is a good subsystem to target for cost reduction via TEA, policy, etc., as it is largely independent of chemistry and thus can be advanced in the interim where new canonical chemistries are still being developed.

To this end, while my thesis focused primarily on RFB chemistries, the stack itself could also benefit from more TEA. Very few studies have exhaustively probed stack materials design (*e.g.*, electrodes, membranes, and flow fields) from a full techno-economic perspective that considers short- and long- term cost tradeoffs and chemistry-specificity. With the stack controlling important and operationally-dependent parameters such as current, efficiencies, etc., this may require combining the techno-economic models discussed in this thesis – which have thus far utilized simplified representations of the physical performance of the battery – with physics-based models that capture more of these parameters. Indeed, incorporation of physics-based models would allow one to explore many interesting topics, including: chemistry-informed membrane design (*e.g.*, inherent tradeoffs between cost, conductivity, and permeability, see **Appendix B** for a brief demonstration of this), cycling profile (*e.g.*, comparing the performance and decay under conventionally modeled/demonstrated galvanostatic profiles versus more realistic power-based profiles), crossover under different chemistry configurations, simulation of electrolyte maintenance methods, etc.

Another example of questions my research has raised that are outside of the scope of chemical engineering pertain to the "investability" of RFB technologies. For example, as a battery architecture that can house nearly infinite chemistries – an aspect of RFBs that is relatively unique and generally attractive for the versatility it allows – there can be a difficulty differentiating between the many similar choices of next generation low-cost chemistries. This actually complicates and, perhaps, ultimately deters investment decisions. Further, there may be a fear that a better, lower-cost and/or higher-performing chemistry could be always developed. Thus, it is important not only to develop an economically competitive RFB chemistry that can be practically operated in the long term from materials that are low cost, accessible, and scalable, but we must also consider the intellectual property (IP) and competitive advantage a chemistry could utilize to actually commercialize it at all. Indeed, I have seen these questions prevent investments in start-ups for RFBs utilizing alternative chemistries. This may necessitate alternate approaches to actualize investments in this space; for example, a utility or group of utilities (*i.e.*, large enterprises with capital and deployment opportunities) could "pick a winner" (or a group of winners) by investing in a particular start-up/chemistry (or a group of start-ups/chemistries, of which they would later determine the most viable through further research and development efforts). The utility could then install a significant volume of demonstration projects to give the chemistry/start-up the competitive, first-player advantage needed to beat out other prospects.

This is a short list of recommended next steps and considerations, and the ideas presented here could comprise multiple more PhDs across various disciplines. I hope people read this thesis and are inspired to take on some of these challenges at their research labs or companies. As I enter the venture capital investment space for energy storage, I will certainly bring these considerations and ideas with me to potentially promote investment and deployment of RFBs.

VII. Appendix A – Supporting information for Chapter V

1. Correlation plot of relevant variables for Fe-Cr RFB cell operation

To assess the correlation between parameters relevant for RFB cell operation, an analysis using the Kendall tau (τ) coefficient [239] was performed for the set of variables including the electrode thickness (Thick), electrode geometric area (Area), geometric current density (Rate), coulombic efficiency (CE), voltaic efficiency (VE), energy efficiency (EE), and decay rate (DR). The Kendall rank correlation was chosen for this analysis, as it is a non-parametric measure that determines the strength of association based on concordance and discordance in the data and does not assume a relationship between the variables being assessed. For any pair of indices $1 \leq i < j \leq n$ where n is the total number of observations for variables x and y, a pair of observation is concordant if ($x_i - x_j$) and ($y_i - y_j$) have the same sign, discordant if they have opposite signs, and neither if either $x_i = x_j$ or $y_i = y_j$. Kendall's τ is defined as the difference between the number of concordant and discordant pairs divided by the number of ways to select two data points from n. Mathematically, τ can be defined by EquationVII-1 [239]:

$$\tau = \frac{2K}{n(n-1)}; \quad K = \sum_{i=1}^{n-1} \sum_{j=i+1}^{n} \xi\left(x_{a,i}, x_{a,j}, y_{b,i}, y_{b,j}\right) \tag{VII-1}$$

Where ξ is the conditional given by Equation VII-2:

$$\xi\left(x_{a,i}, x_{a,j}, y_{b,i}, y_{b,j}\right) = \begin{cases} 1 & \text{if} \quad \left(x_{a,i} - x_{a,j}\right)\left(y_{b,i} - y_{b,j}\right) > 0 \\ 0 & \text{if} \quad \left(x_{a,i} - x_{a,j}\right)\left(y_{b,i} - y_{b,j}\right) = 0 \\ -1 & \text{if} \quad \left(x_{a,i} - x_{a,j}\right)\left(y_{b,i} - y_{b,j}\right) < 0 \end{cases} \tag{VII-2}$$

Figure VII-1 shows the correlation plot of all seven variables. The number in each subplot corresponds to τ, while the magenta line is the best linear fit to the data. The numbers highlighted in red font are determined to be statistically significant based on a *p*-value of less than 0.05. The electrode geometric area and thickness, voltaic efficiency, energy efficiency, coulombic efficiency, and decay rate are all shown to be statistically significant. All computation and plotting were performed using the MATLAB® function *corrplot*.

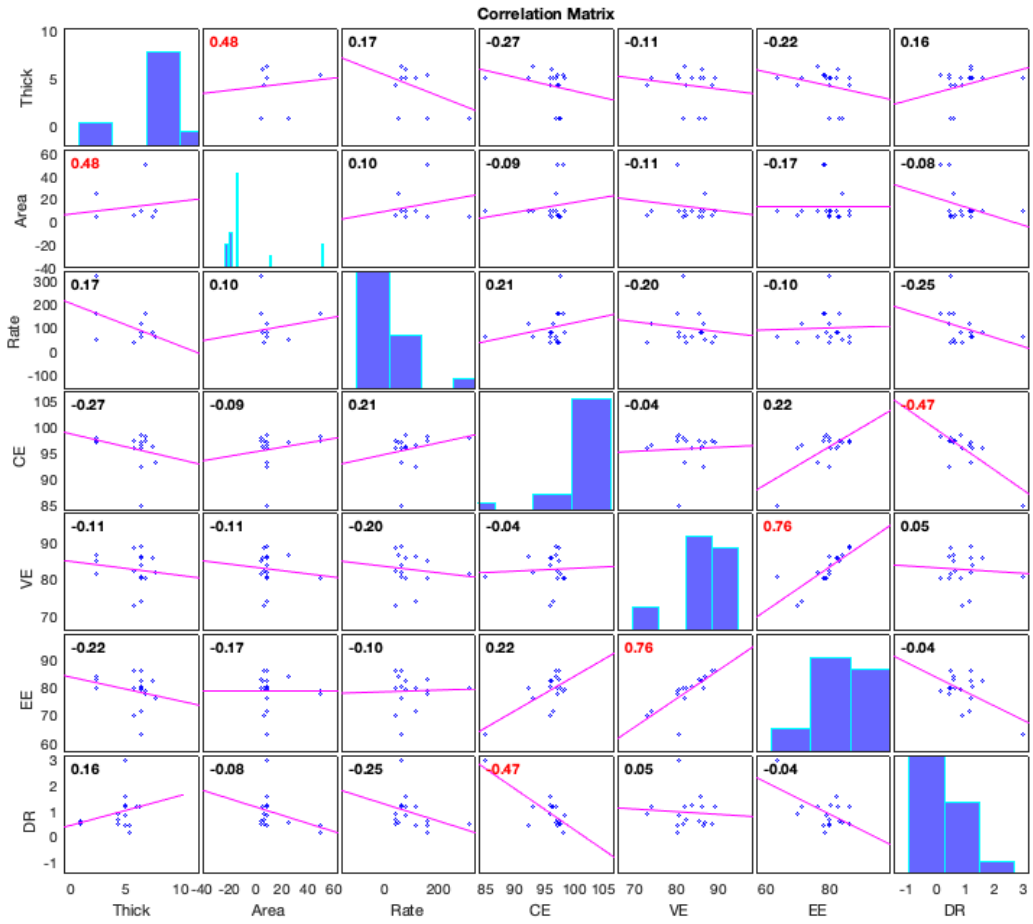

Figure VII-1 – Kendall rank correlation matrix of seven variables relevant to Fe-Cr redox flow battery (RFB) cell operation. The variables examined are the electrode thickness in mm (Thick), the geometric active area in cm^2 (Area), the geometric current density in mA cm^{-2} (Rate), the Coulombic Efficiency in % (CE), the Voltaic Efficiency in % (VE), the Energy Efficiency in % (EE), and the Decay Rate in % (DR). The correlation plot and test for significant correlations was generated using MATLAB's *corrplot* function. Statistically important relations are highlighted in red, showing that the relationship between DR and CE is statistically significant.

2. Post-mortem spectroscopy of electrodes

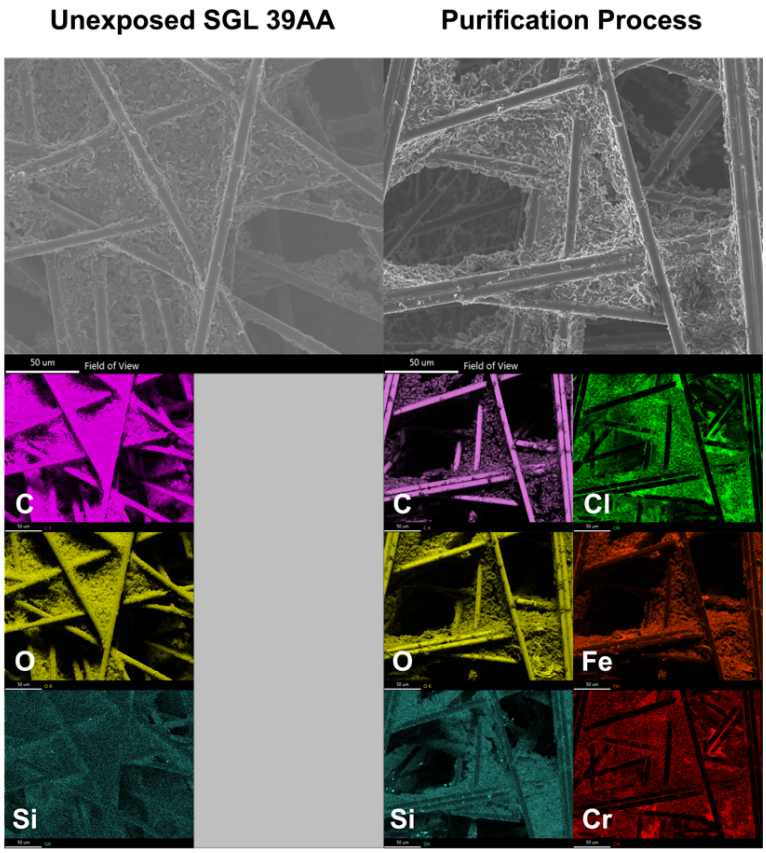

Figure VII-2. Scanning electron microscopy (SEM) and energy dispersive X-ray spectroscopy (EDS) of heat-treated SGL 39AA electrode (500 °C, 5 h), electrode reduced in Fe-Cr RFB negative electrolyte, and electrode soaked in unpurified Fe-Cr RFB electrolyte overnight. SEM / EDS was performed using a Zeiss Merlin High-Resolution SEM, with a 10 keV electron energy and 9.2-mm working distance and an in-lens secondary electron detector. The negative electrode used in the purification process exhibits additional Fe, Cr, and chlorine signals in addition to carbon and oxygen species and trace silicon from the electrode.

VIII. Appendix B – Example of techno-economic- and chemistry-informed design of membranes for RFBs, enabled by incorporation of physics-based models

As the reactor component with the highest cost as well as very consequential performance outcomes from a levelized cost standpoint (*i.e.*, prevention of crossover), there is a lot of on-going redox flow battery (RFB) membrane development exploring a vast range of materials as well as cost and performance criteria (*e.g.*, permeability and selectivity, conductivity, cost, etc.). However, these design criteria are often obscured and uninformed by the RFB chemistry or techno-economic analyses (TEAs). Many researchers are trying to create better membranes to minimize crossover, such as the next generation of ion-exchange membranes or through development of size-discretionary membranes like polymers of intrinsic microporosity (PIMs). However, the key design criteria are often variable across studies (*e.g.*, high conductivity, high selectivity, or low cost) [69,240], as there has been little consideration of what properties are most ideal for the long-term economic outlook for a given chemistry [17]. For example, symmetric chemistries like vanadium have been shown to be highly unaffected, in terms of their levelized cost, by the crossover rate, because crossover remediation (*i.e.*, rebalancing) can be performed very frequently and inexpensively [60]. In these cases, it is likely much more desirable to have a low-cost membrane than a more expensive, highly selective membrane. Size-exclusion separators are one potentially low-cost alternative [241] that may also be more selective in some systems where, in tandem, the molecular size of the active species can be tuned such that they are larger than the membrane's pores (*e.g.*, large organic molecules) [105]. In the most extreme case, single ion-conducting (SIC) membranes (likely ceramic-containing materials) can be designed for perfect selectivity, though this comes at the cost of relatively extreme resistances that increase power costs

and reactor sizes dramatically [115,120]. Overall, the field of RFB membrane development could benefit from more explicit consideration of long-term performance and cost tradeoffs, via chemistry-specific TEAs, to better inform the design goals. To this end, my colleague Bertrand Neyhouse and I are working on a study that fundamentally explores the basic design principles of RFB membranes, how they affect the battery performance and techno-economics, and how such analyses can be used to inform membrane development and selection for a particular chemistry or class of chemistries.

In addition to representing a new area of RFB-related techno-economic study for me, this project is distinct from my previous TEA work (represented throughout this thesis) in that it is utilizing a 0D, physics-based, cell-level RFB model to inform the performance inputs needed for the TEAs. My previous studies have used high-level, fixed metrics that are generally uninformed by the battery's operating conditions (*e.g.*, fade rates, capacity accessed, efficiencies, etc.). While using a physics-based model allows us to explore how operation affects these performance metrics and, thus, the techno-economics, it also adds complexity computationally (affecting analysis time) and conceptually. The latter of these complexities has been the focus of the initial work performed so far: how do we create generalizable case studies? What assumptions do we have to make, and how do those assumptions affect or determine the range of situations (*e.g.*, chemistries, membranes, practical operation or design scenarios, etc.) our analyses can apply to? These questions have been difficult to navigate but are important foundational steps that simultaneously force us to intimately understand the 0D model itself (thus helping the development of this work). While our efforts exploring these questions do not lend themselves to presentable data, I will attempt to show some initial conceptualizations of the types of avenues we are thinking of exploring with this membrane study (which will continue in my absence).

One example of the simplifying assumptions made in my previous studies, due to the lack of physics-informed modeling, lies in the "mixed electrolyte" studies. As a brief recap, RFBs with asymmetric chemistries must find a way to deal with crossover that leads to cross-contamination of the electrolyte and capacity decay. If the various active species are stable in the opposing cell environments, an efficient approach to dealing with the crossover issue is to use the "spectator strategy," where both active species are dissolved in each half-cell electrolyte (considered in depth in **Chapter III**). In more detail, each electrolyte is mixed with equal concentrations of the active species of interest and the spectator species, which is simply the active species in the other half-cell. This transforms asymmetric chemistries into pseudo-symmetric chemistries and allows for utilization of the same VRFB rebalancing methods [12,42–45,60] to remediate losses due to crossover. Further, crossover is actually mitigated by the spectator methodology itself [16,25], as diffusive fluxes that drive crossover between the two electrolytes are significantly decreased [127]. The tradeoff is that the strategy decreases energy density and increases electrolyte cost via the addition of the spectator species. In the analysis previously performed (see Figure III-3), we assumed the electrolyte cost of an RFB using the spectator strategy would be exactly double the cost of a non-mixed electrolyte configuration and simply compared the electrolyte costs to other incumbents (*e.g.*, vanadium) for determining viability, as it is assumed maintenance costs for these systems would be virtually zero due to the near elimination of crossover, as described above.

However, the equilibrium of mixed electrolytes may not always be equal concentrations of each active species in each half-cell due to the other crossover driving forces (in particular, electro-migration). Figure VIII-1 below demonstrates this using the 0D model: depending on the diffusivity of the active species and the conductivity of the membrane (here, assuming positively charged active species), the equilibrium point can range between 40-60% of theoretical capacity

(*i.e.*, not necessarily perfectly mixed electrolytes, which would represent 50% of capacity retained at equilibrium). This affects our assumptions of the electrolyte cost per kWh of rated storage capacity (*e.g.*, 40% and 60% capacity retention equilibrium points would mean costs are greater or lower, respectively, than those shown in Figure III-3).

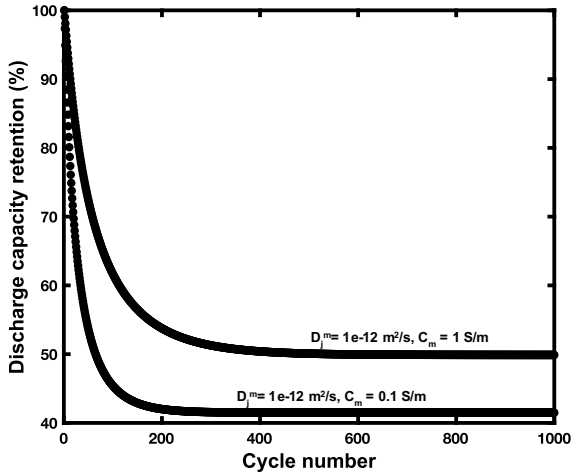

Figure VIII-1 – Discharge capacity retention over 1000 cycles for a generic, 1 V RFB chemistry utilizing positivity charged redox active species. Two cases are shown utilizing different values for the average diffusivity of all active species through the membrane (D_j^m) and the membrane conductivity (C_m).

With the use of a 0D model, we can thus explore the effect of membrane choice on this sort of analysis. Further, we can start to add more practical complexities: for example, the conductivity value affects the area-specific-resistance (ASR) of the cell, which affects the power density and thus power costs (Figure VIII-2). Each diffusivity and conductivity scenario alters the voltaic and coulombic efficiencies, which affect the power and electrolyte costs as well. Finally, we can make assumptions about the effect of membrane performance on membrane cost: as a first pass, say conventional membrane options used in aqueous environments (*e.g.*, separators or ion-exchange membranes) may have conductivities ranging from 0.1 to 1 S/m that could correspond (linearly,

perhaps) to areal costs between 50 and 300 $/m^2, as higher-performing membranes would be more expensive to produce (Figure VIII-2). These membranes will possess varying active species diffusivities, say between 1e-11 and 1e-13 m^2/s.

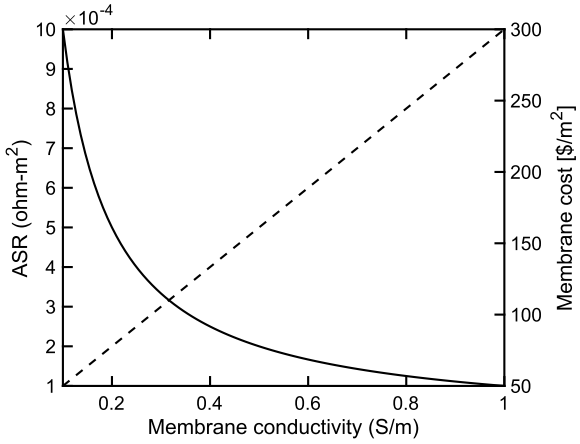

Figure VIII-2 - Area-specific-resistance (ASR) of the cell (left y-axis, solid line) and estimated membrane cost (right y-axis, dashed line) as a function of membrane conductivity (at a fixed membrane thickness of 100 microns.

So, we vary diffusivity and conductivity separately and derive ASR and membrane cost as a function of conductivity as shown in Figure VIII-2 above. These variables affect the battery's energy capacity at the equilibrium level (which we then size the system to), as well as the electrolyte and power costs. This gives us a map of capital costs as a function of these variables, shown below as Figure VIII-3. We see the consideration of these effects have important consequences on the capital cost, which ranges from 250 – 800 $/kWh (at a 5.25 h duration).

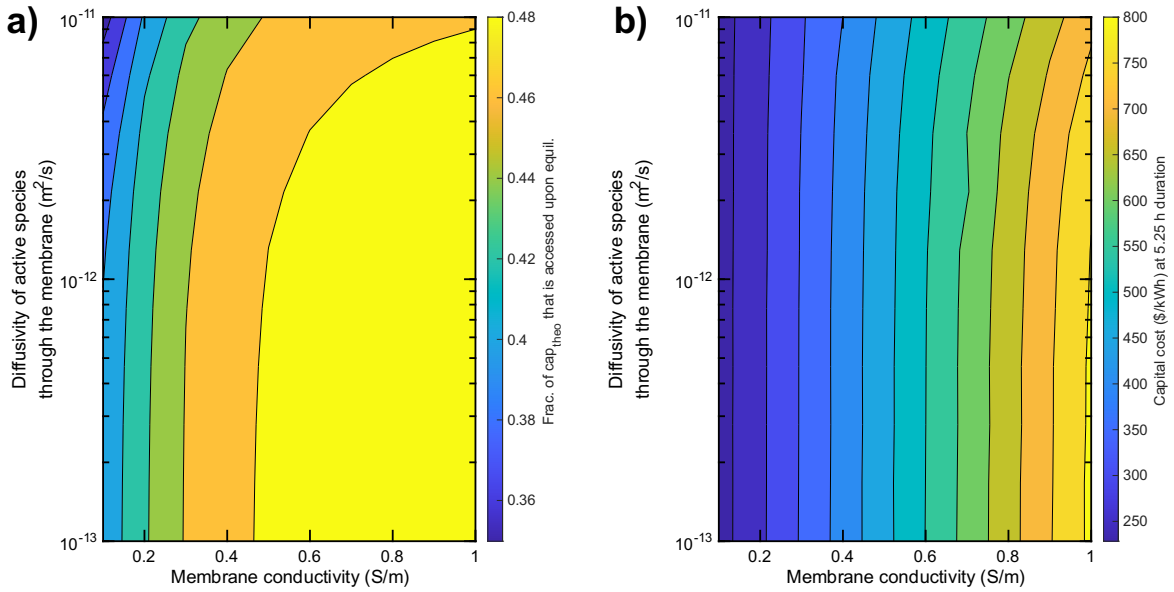

Figure VIII-3 – Color maps showing the fraction of theoretical capacity accessed upon equilibrium (a) and the system capital cost (at a 5.25 hour duration) when the system is sized to this equilibrated capacity (b) as a function of membrane conductivity (x-axis) and diffusivity of the active species through the membrane (y-axis).

This is just one example of many analyses we are considering exploring with the combination of the TEA and 0D models. In addition to exploring more parameters (*e.g.*, current density) and looking at more specific case studies (*e.g.*, large organics with PIMs, membrane design for asymmetric chemistries, etc.), we also plan to explore different computational methods (*e.g.*, machine learning) to facilitate more complex analyses.

References

[1] Intergovernmental Panel on Climate Change, Global Warming of 1.5 C, 2018. https://www.ipcc.ch/sr15/.

[2] H. Zsiboracs, N. Hegedusne Baranyai, A. Vincze, L. Zentko, Z. Birkner, K. Mate, G. Pinter, Intermittent Renewable Energy Sources: The Role of Energy Storage in the European Power System of 2040, Electronics. 8 (2019) 729. https://doi.org/10.3390/electronics8070729.

[3] J.P. Barton, D.G. Infield, Energy storage and its use with intermittent renewable energy, IEEE Trans. Energy Convers. 19 (2004) 441–448. https://doi.org/10.1109/TEC.2003.822305.

[4] P. Denholm, Y. Sun, T. Mai, An Introduction to Grid Services: Concepts, Technical Requirements, and Provision from Wind, Denver, CO, 2019. https://www.nrel.gov/docs/fy19osti/72578.pdf.

[5] D. Larcher, J.M. Tarascon, Towards greener and more sustainable batteries for electrical energy storage, Nat. Chem. 7 (2015) 19–29. https://doi.org/10.1038/nchem.2085.

[6] V. Viswanathan, A. Crawford, D. Stephenson, S. Kim, W. Wang, B. Li, G. Coffey, E. Thomsen, G. Graff, P. Balducci, M. Kintner-Meyer, V. Sprenkle, Cost and performance model for redox flow batteries, J. Power Sources. 247 (2014) 1040–1051. https://doi.org/10.1016/j.jpowsour.2012.12.023.

[7] B. Dunn, H. Kamath, J. Tarascon, Electrical energy storage for the grid: A battery of choices, Sci. Mag. 334 (2011) 928–936. https://doi.org/10.1126/science.1212741.

[8] X.-Z. Yuan, C. Song, A. Platt, N. Zhao, H. Wang, H. Li, K. Fatih, D. Jang, A review of all-vanadium redox flow battery durability: Degradation mechanisms and mitigation strategies, Int. J. Energy Res. (2019) 1–40. https://doi.org/10.1002/er.4607.

[9] US Department of Energy, Grid Energy Storage, 2013. https://www.energy.gov/sites/prod/files/2014/09/f18/Grid Energy Storage December 2013.pdf.

[10] ARPA-E, ARPA-E: The First Seven Years, 2016. https://arpa-e.energy.gov/sites/default/files/documents/files/Volume 1_ARPA-E_ImpactSheetCompilation_FINAL.pdf.

[11] US Department of Energy, DOE OE Global Energy Storage Database, (2020). https://www.sandia.gov/ess-ssl/global-energy-storage-database-home/ (accessed January 10, 2020).

[12] Y. Zhang, L. Liu, J. Xi, Z. Wu, X. Qiu, The benefits and limitations of electrolyte mixing in vanadium flow batteries, Appl. Energy. 204 (2017) 373–381. https://doi.org/10.1016/j.apenergy.2017.07.049.

[13] M. Ulaganathan, V. Aravindan, Q. Yan, S. Madhavi, M. Skyllas-Kazacos, T.M. Lim, Recent Advancements in All-Vanadium Redox Flow Batteries, Adv. Mater. Interfaces. 3 (2016) 1–22. https://doi.org/10.1002/admi.201500309.

[14] R.A. Potash, J.R. McKone, S. Conte, H.D. Abruña, On the Benefits of a Symmetric Redox

Flow Battery, J. Electrochem. Soc. 163 (2016) A338–A344. https://doi.org/10.1149/2.0971602jes.

[15] M. Skyllas-Kazacos, M. Kazacos, State of charge monitoring methods for vanadium redox flow battery control, J. Power Sources. 196 (2011) 8822–8827. https://doi.org/10.1016/j.jpowsour.2011.06.080.

[16] M.L. Perry, J.D. Saraidaridis, R.M. Darling, Crossover Mitigation Strategies for Redox-Flow Batteries, Curr. Opin. Electrochem. 21 (2020) 311–318. https://doi.org/10.1016/j.coelec.2020.03.024.

[17] C. Minke, T. Turek, Economics of vanadium redox flow battery membranes, J. Power Sources. 286 (2015) 247–257. https://doi.org/10.1016/j.jpowsour.2015.03.144.

[18] G. Kear, A.A. Shah, F.C. Walsh, Development of the all-vanadium redox flow battery for energy storage: a review of technological, financial and policy aspects, Int. J. Energy Res. 36 (2012) 1105–1120. https://doi.org/10.1002/er.1863.

[19] M. Zheng, J. Sun, C. Meinrenken, T. Wang, Pathways towards enhanced techno-economic performance of flow battery systems in energy system applications, J. Electrochem. Energy Convers. Storage. 16 (2019) 021001-1-021001–11. https://doi.org/10.1115/1.4040921.

[20] M. Zhang, M. Moore, J.S. Watson, T.A. Zawodzinski, R.M. Counce, Capital Cost Sensitivity Analysis of an All-Vanadium Redox-Flow Battery, J. Electrochem. Soc. 159 (2012) A1183–A1188. https://doi.org/10.1149/2.041208jes.

[21] J. Noack, L. Wietschel, N. Roznyatovskaya, K. Pinkwart, J. Tübke, Techno-economic modeling and analysis of redox flow battery systems, Energies. 9 (2016). https://doi.org/10.3390/en9080627.

[22] T. Lüth, S. König, M. Suriyah, T. Leibfried, Passive components limit the cost reduction of conventionally designed vanadium redox flow batteries, Energy Procedia. 155 (2018) 379–389. https://doi.org/10.1016/j.egypro.2018.11.040.

[23] A. Crawford, V. Viswanathan, D. Stephenson, W. Wang, E. Thomsen, D. Reed, B. Li, P. Balducci, M. Kintner-Meyer, V. Sprenkle, Comparative analysis for various redox flow batteries chemistries using a cost performance model, J. Power Sources. 293 (2015) 388–399. https://doi.org/10.1016/j.jpowsour.2015.05.066.

[24] M.-A. Goulet, M.J. Aziz, Flow Battery Molecular Reactant Stability Determined by Symmetric Cell Cycling Methods, J. Electrochem. Soc. 165 (2018) A1466–A1477. https://doi.org/10.1149/2.0891807jes.

[25] Y.K. Zeng, T.S. Zhao, L. An, X.L. Zhou, L. Wei, A comparative study of all-vanadium and iron-chromium redox flow batteries for large-scale energy storage, J. Power Sources. 300 (2015) 438–443. https://doi.org/10.1016/j.jpowsour.2015.09.100.

[26] M.L. Perry, A.Z. Weber, Advanced Redox-Flow Batteries: A Perspective, J. Electrochem. Soc. 163 (2016) A5064–A5067. https://doi.org/10.1149/2.0101601jes.

[27] D.G. Kwabi, Y. Ji, M.J. Aziz, Electrolyte Lifetime in Aqueous Organic Redox Flow Batteries: A Critical Review, Chem. Rev. 120 (2020) 6467–6489. https://doi.org/10.1021/acs.chemrev.9b00599.

[28] L. Wei, M.C. Wu, T.S. Zhao, Y.K. Zeng, Y.X. Ren, An aqueous alkaline battery consisting of inexpensive all-iron redox chemistries for large-scale energy storage, Appl. Energy. 215 (2018) 98–105. https://doi.org/10.1016/j.apenergy.2018.01.080.

[29] E.A. Olivetti, G. Ceder, G.G. Gaustad, X. Fu, Lithium-Ion Battery Supply Chain Considerations: Analysis of Potential Bottlenecks in Critical Metals, Joule. 1 (2017) 229–243. https://doi.org/10.1016/j.joule.2017.08.019.

[30] W. Dai, Y. Shen, Z. Li, L. Yu, J. Xi, X. Qiu, SPEEK/Graphene oxide nanocomposite membranes with superior cyclability for highly efficient vanadium redox flow battery, J. Mater. Chem. A. 2 (2014) 12423–12432. https://doi.org/10.1039/c4ta02124j.

[31] S. Kim, J. Yan, B. Schwenzer, J. Zhang, L. Li, J. Liu, Z. Yang, M.A. Hickner, Cycling performance and efficiency of sulfonated poly(sulfone) membranes in vanadium redox flow batteries, Electrochem. Commun. 12 (2010) 1650–1653. https://doi.org/10.1016/j.elecom.2010.09.018.

[32] B. Jiang, L. Wu, L. Yu, X. Qiu, J. Xi, A comparative study of Nafion series membranes for vanadium redox flow batteries, J. Memb. Sci. 510 (2016) 18–26. https://doi.org/10.1016/j.memsci.2016.03.007.

[33] Y. Ashraf Gandomi, D.S. Aaron, M.M. Mench, Influence of membrane equivalentweight and reinforcement on ionic species crossover in all-vanadium redox flow batteries, Membranes (Basel). 7 (2017) 7–10. https://doi.org/10.3390/membranes7020029.

[34] L. Cao, A. Kronander, A. Tang, D.W. Wang, M. Skyllas-Kazacos, Membrane permeability rates of vanadium ions and their effects on temperature variation in vanadium redox batteries, Energies. 9 (2016). https://doi.org/10.3390/en9121058.

[35] K.W. Knehr, E. Agar, C.R. Dennison, A.R. Kalidindi, E.C. Kumbur, A Transient Vanadium Flow Battery Model Incorporating Vanadium Crossover and Water Transport through the Membrane, J. Electrochem. Soc. 159 (2012) A1446–A1459. https://doi.org/10.1149/2.017209jes.

[36] V.P. Nemani, K.C. Smith, Analysis of Crossover-Induced Capacity Fade in Redox Flow Batteries with Non-Selective Separators, J. Electrochem. Soc. 165 (2018) A3144–A3155. https://doi.org/10.1149/2.0701813jes.

[37] P.A. Boettcher, E. Agar, C.R. Dennison, E.C. Kumbur, Modeling of Ion Crossover in Vanadium Redox Flow Batteries: A Computationally-Efficient Lumped Parameter Approach for Extended Cycling, J. Electrochem. Soc. 163 (2016) A5244–A5252. https://doi.org/10.1149/2.0311601jes.

[38] M. Skyllas-Kazacos, Performance Improvements and Cost Considerations of the Vanadium Redox Flow Battery, ECS Trans. 89 (2019) 29–45. https://doi.org/10.1149/08901.0029ecst.

[39] Vanadium Price, (2021). https://www.vanadiumprice.com/ (accessed November 8, 2021).

[40] X.G. Yang, Q. Ye, P. Cheng, T.S. Zhao, Effects of the electric field on ion crossover in vanadium redox flow batteries, Appl. Energy. 145 (2015) 306–319. https://doi.org/10.1016/j.apenergy.2015.02.038.

[41] R.M. Darling, A.Z. Weber, M.C. Tucker, M.L. Perry, The Influence of Electric Field on Crossover in Redox-Flow Batteries, J. Electrochem. Soc. 163 (2015) A5014–A5022.

https://doi.org/10.1149/2.0031601jes.

[42] S. Corcuera, M. Skyllas-Kazacos, State-of-Charge Monitoring and Electrolyte Rebalancing Methods for the Vanadium Redox Flow Battery, Eur. Chem. Bull. 1 (2012) 511–519. https://doi.org/10.17628/ECB.2012.1.511.

[43] S. Roe, C. Menictas, M. Skyllas-Kazacos, A High Energy Density Vanadium Redox Flow Battery with 3 M Vanadium Electrolyte, J. Electrochem. Soc. 163 (2016) A5023–A5028. https://doi.org/10.1149/2.0041601jes.

[44] Q. Luo, L. Li, W. Wang, Z. Nie, X. Wei, B. Li, B. Chen, Z. Yang, V. Sprenkle, Capacity decay and remediation of nafion-based all-vanadium redox flow batteries, ChemSusChem. 6 (2013) 268–274. https://doi.org/10.1002/cssc.201200730.

[45] S. Rudolph, U. Schröder, I.M. Bayanov, On-line controlled state of charge rebalancing in vanadium redox flow battery, J. Electroanal. Chem. 703 (2013) 29–37. https://doi.org/10.1016/j.jelechem.2013.05.011.

[46] N. Roznyatovskaya, J. Noack, M. Fühl, K. Pinkwart, J. Tübke, Towards an all-vanadium redox-flow battery electrolyte: electrooxidation of V(III) in V(IV)/V(III) redox couple, Electrochim. Acta. 211 (2016) 926–932. https://doi.org/10.1016/j.electacta.2016.06.073.

[47] R.M. Darling, A. Smeltz, S.T. Junker, M.L. Perry, Distribution of electrolytes in a flow battery, 9,853,310, 2013. http://patft.uspto.gov/netacgi/nph-Parser?Sect1=PTO1&Sect2=HITOFF&d=PALL&p=1&u=%2Fnetahtml%2FPTO%2Fsrchnum.htm&r=1&f=G&l=50&s1=9853310.PN.&OS=PN/9853310&RS=PN/9853310.

[48] K. Wang, L. Liu, J. Xi, Z. Wu, X. Qiu, Reduction of capacity decay in vanadium flow batteries by an electrolyte-reflow method, J. Power Sources. 338 (2017) 17–25. https://doi.org/10.1016/j.jpowsour.2016.11.031.

[49] A. Bhattarai, N. Wai, R. Schweiss, A. Whitehead, G.G. Scherer, P.C. Ghimire, T.M. Lim, H.H. Hng, Vanadium redox flow battery with slotted porous electrodes and automatic rebalancing demonstrated on a 1 kW system level, Appl. Energy. 236 (2019) 437–443. https://doi.org/10.1016/j.apenergy.2018.12.001.

[50] A. Bhattarai, P. Ghimire, A. Whitehead, R. Schweiss, G. Scherer, N. Wai, H. Hng, Novel Approaches for Solving the Capacity Fade Problem during Operation of a Vanadium Redox Flow Battery, Batteries. 4 (2018) 48. https://doi.org/10.3390/batteries4040048.

[51] K. Schafner, M. Becker, T. Turek, Capacity balancing for vanadium redox flow batteries through electrolyte overflow, J. Appl. Electrochem. 48 (2018) 639–649. https://doi.org/10.1007/s10800-018-1187-1.

[52] B. Li, Q. Luo, X. Wei, Z. Nie, E. Thomsen, B. Chen, V. Sprenkle, W. Wang, Capacity decay mechanism of microporous separator-based all-vanadium redox flow batteries and its recovery, ChemSusChem. 7 (2014) 577–584. https://doi.org/10.1002/cssc.201300706.

[53] H.C. Hesse, M. Schimpe, D. Kucevic, A. Jossen, Lithium-Ion Battery Storage for the Grid — A Review of Stationary Battery Storage System Design Tailored for Applications in Modern Power Grids, Energies. 10 (2017). https://doi.org/10.3390/en10122107.

[54] Department of Energy, Levelized Cost of Energy (LCOE), (2015). https://www.energy.gov/sites/prod/files/2015/08/f25/LCOE.pdf (accessed February 7,

2019).

[55] Lazard, Lazard's Levelized Cost of Storage Analysis - Version 4.0, 2018.

[56] C.S. Lai, M.D. McCulloch, Levelized cost of electricity for solar photovoltaic and electrical energy storage, Appl. Energy. 190 (2017) 191–203. https://doi.org/10.1016/j.apenergy.2016.12.153.

[57] National Renewable Energy Laboratory, Simple Levelied Cost of Energy (LCOE) Calculator Documentation, (n.d.). https://www.nrel.gov/analysis/tech-lcoe-documentation.html (accessed October 9, 2019).

[58] O. Schmidt, S. Melchior, A. Hawkes, I. Staffell, Projecting the Future Levelized Cost of Electricity Storage Technologies, Joule. 3 (2019) 81–100. https://doi.org/10.1016/j.joule.2018.12.008.

[59] Lazard, Lazard's Levelized Cost of Storage Analysis - Version 3.0, 2017.

[60] K.E. Rodby, T.J. Carney, Y. Ashraf Gandomi, J.L. Barton, R.M. Darling, F.R. Brushett, Assessing the levelized cost of vanadium redox flow batteries with capacity fade and rebalancing., J. Power Sources. 460 (2020) 227958. https://doi.org/10.1016/j.jpowsour.2020.227958.

[61] R.M. Darling, K.G. Gallagher, J.A. Kowalski, H. Seungbum, F.R. Brushett, Pathways to low-cost electrochemical energy storage: a comparison of aqueous and nonaqueous flow batteries, Energy Environ. Sci. 7 (2014) 3459–3477. https://doi.org/10.1039/C4EE02158D.

[62] U.S. Energy Information Administration, Electric Power Monthly: with data for July 2018, 2018.

[63] US Department of Labor, Consumer Price Index - August 2018, 2018.

[64] Chemicals: Oxalic Acid, Alibaba. (2019).

[65] S.N. Bizzari, M. Blagoev, Oxalic Acid - Chemical Economics Handbook, 2010.

[66] S. Kumar, S. Jayanti, High Energy Efficiency With Low-Pressure Drop Configuration for an All-Vanadium Redox Flow Battery, J. Electrochem. Energy Convers. Storage. 13 (2017) 041005. https://doi.org/10.1115/1.4035847.

[67] J. Xi, B. Jiang, L. Yu, L. Liu, Membrane evaluation for vanadium flow batteries in a temperature range of −20–50 °C, J. Memb. Sci. 522 (2017) 45–55. https://doi.org/10.1016/j.memsci.2016.09.012.

[68] A. Rohatgi, WebPlotDigitizer v4.1, (2018). https://automeris.io/WebPlotDigitizer.

[69] S.W. Choi, T.H. Kim, S.W. Jo, J.Y. Lee, S.H. Cha, Y.T. Hong, Hydrocarbon membranes with high selectivity and enhanced stability for vanadium redox flow battery applications: Comparative study with sulfonated poly(ether sulfone)s and sulfonated poly(thioether ether sulfone)s, Electrochim. Acta. 259 (2018) 427–439. https://doi.org/10.1016/j.electacta.2017.10.121.

[70] S. Kim, T.B. Tighe, B. Schwenzer, J. Yan, J. Zhang, J. Liu, Z. Yang, M.A. Hickner, Chemical and mechanical degradation of sulfonated poly(sulfone) membranes in vanadium redox flow batteries, J. Appl. Electrochem. 41 (2011) 1201–1213. https://doi.org/10.1007/s10800-011-0313-0.

[71] R. Basosi, M. Cellura, Life Cycle Assessment of Energy Systems and Sustainable Energy Technologies, 2019. https://doi.org/10.1007/978-3-319-93740-3.

[72] redT, Technology, (2018). https://redtenergy.com/about/technology/ (accessed March 31, 2019).

[73] Vionx Energy, Vanadium Redox Flow Battery: A Better Solution, (2018). https://www.vionxenergy.com/products/ (accessed March 31, 2019).

[74] VRB Energy, VRB Energy, (2019).

[75] M. Skyllas-Kazacos, L. Cao, M. Kazacos, N. Kausar, A. Mousa, Vanadium Electrolyte Studies for the Vanadium Redox Battery—A Review, ChemSusChem. 9 (2016) 1521–1543. https://doi.org/10.1002/cssc.201600102.

[76] L. Cao, M. Skyllas-Kazacos, C. Menictas, J. Noack, A review of electrolyte additives and impurities in vanadium redox flow batteries, J. Energy Chem. 27 (2018) 1269–1291. https://doi.org/10.1016/j.jechem.2018.04.007.

[77] E. Agar, A. Benjamin, C.R. Dennison, D. Chen, M.A. Hickner, E.C. Kumbur, Reducing capacity fade in vanadium redox flow batteries by altering charging and discharging currents, J. Power Sources. 246 (2014) 767–774. https://doi.org/10.1016/j.jpowsour.2013.08.023.

[78] I. Derr, A. Fetyan, K. Schutjajew, C. Roth, Electrochemical analysis of the performance loss in all vanadium redox flow batteries using different cut-off voltages, Electrochim. Acta. 224 (2017) 9–16. https://doi.org/10.1016/j.electacta.2016.12.043.

[79] M. Nourani, C.R. Dennison, X. Jin, F. Liu, E. Agar, Elucidating Effects of Faradaic Imbalance on Vanadium Redox Flow Battery Performance : Experimental Characterization, 166 (2019) 3844–3851. https://doi.org/10.1149/2.0851915jes.

[80] I. Pawel, The cost of storage - How to calculate the levelized cost of stored energy (LCOE) and applications to renewable energy generation, Energy Procedia. 46 (2014) 68–77. https://doi.org/10.1016/j.egypro.2014.01.159.

[81] C. Minke, T. Turek, Materials, system designs and modelling approaches in techno-economic assessment of all-vanadium redox flow batteries – A review, J. Power Sources. 376 (2018) 66–81. https://doi.org/10.1016/j.jpowsour.2017.11.058.

[82] Tri-Service Electrical Working Group, Stationary Battery and Charger Sizing: Battery Sizing for Applications with a Duty Cycle, 2008. https://www.wbdg.org/FFC/DOD/STC/twewg_tp4.pdf.

[83] J. Spector, A New Path to Market for Flow Batteries: Rent an Electrolyte, Greentech Media. (2019). https://www.greentechmedia.com/articles/read/new-path-to-market-for-flow-batteries-rent-an-electrolyte#gs.e1qdww.

[84] VRB Energy, A renewable energy future driven by vanadium, World Mater. Forum. (2018). https://worldmaterialsforum.com/files/Presentations2018/PS1/WMF-2018-Ivanhoe-Robert Friedland.pdf (accessed March 29, 2019).

[85] D. Stringer, One Battery Material Sector Is Cheering For Lower Prices, Bloomberg. (2019). https://www.bloomberg.com/news/articles/2019-09-19/one-battery-material-sector-is-

cheering-for-lower-prices.

[86] G. Williams, Vanadium Outlook 2019: After the "Year of Vanadium," What's Next?, Invest. News. (2018). https://investingnews.com/daily/resource-investing/battery-metals-investing/vanadium-investing/vanadium-outlook/ (accessed March 29, 2019).

[87] A.P. Monaghan, I. Strydom, A.G. Dormehl, Process for Producing Vanadyl/Vanadous Sulphate, US6764663B2, 2004.

[88] J. Bedder, Z. Cripps, Roskill: What lies ahead for a vanadium market in deficit?, Globe Newswire. (2019). https://www.globenewswire.com/news-release/2019/05/07/1818067/0/en/Roskill-What-lies-ahead-for-a-vanadium-market-in-deficit.html.

[89] M. Marr-Johnson, No Title, London Bullion Assoc. (n.d.) 20–22. http://www.lbma.org.uk/assets/blog/alchemist_articles/Alch29Marr-Johnson.pdf (accessed November 7, 2019).

[90] I. Derr, M. Bruns, J. Langner, A. Fetyan, J. Melke, C. Roth, Degradation of all-vanadium redox flow batteries (VRFB) investigated by electrochemical impedance and X-ray photoelectron spectroscopy: Part 2 electrochemical degradation, J. Power Sources. 325 (2016) 351–359. https://doi.org/10.1016/j.jpowsour.2016.06.040.

[91] D.N. Buckley, D. Oboroceanu, N. Quill, C. Lenihan, D. Ní Eidhin, R.P. Lynch, Electrolyte Stability in Vanadium Flow Batteries, MRS Adv. (2018) 1–12. https://doi.org/10.1557/adv.2018.496.

[92] P. Trogadas, O.O. Taiwo, B. Tjaden, T.P. Neville, S. Yun, J. Parrondo, V. Ramani, M.O. Coppens, D.J.L. Brett, P.R. Shearing, X-ray micro-tomography as a diagnostic tool for the electrode degradation in vanadium redox flow batteries, Electrochem. Commun. 48 (2014) 155–159. https://doi.org/10.1016/j.elecom.2014.09.010.

[93] Y. Wen, Y. Xu, J. Cheng, G. Cao, Y. Yang, Investigation on the stability of electrolyte in vanadium flow batteries, Electrochim. Acta. 96 (2013) 268–273. https://doi.org/10.1016/j.electacta.2013.02.091.

[94] P. Alotto, M. Guarnieri, F. Moro, Redox flow batteries for the storage of renewable energy: A review, Renew. Sustain. Energy Rev. 29 (2014) 325–335. https://doi.org/10.1016/j.rser.2013.08.001.

[95] H. Prifti, A. Parasuraman, S. Winardi, T.M. Lim, M. Skyllas-Kazacos, Membranes for redox flow battery applications, Membranes (Basel). 2 (2012) 275–306. https://doi.org/10.3390/membranes2020275.

[96] J. Winsberg, C. Stolze, S. Muench, F. Liedl, M.D. Hager, U.S. Schubert, TEMPO/Phenazine Combi-Molecule: A Redox- Active Material for Symmetric Aqueous Redox- Flow Batteries, ACS Energy Lett. 1 (2016) 976–980. https://doi.org/10.1021/acsenergylett.6b00413.

[97] L. Tong, Y. Jing, R.G. Gordon, M.J. Aziz, Symmetric All-Quinone Aqueous Battery, ACS Appl. Energy Mater. 2 (2019) 4016–4021. https://doi.org/10.1021/acsaem.9b00691.

[98] G.D. Charlton, S.M. Barbon, J.B. Gilroy, C.A. Dyker, G.D. Charlton, S.M. Barbon, J.B. Gilroy, C.A. Dyker, A bipolar verdazyl radical for a symmetric all-organic redox flow-type

battery, J. Energy Chem. 34 (2019) 52–56. https://doi.org/10.1016/j.jechem.2018.09.020.

[99] W. Duan, R.S. Vemuri, J.D. Milshtein, S. Laramie, R.D. Dmello, J. Huang, L. Zhang, D. Hu, M. Vijayakumar, W. Wang, J. Liu, R.M. Darling, L. Thompson, K. Smith, S. Moore, R. Brushett, X. Wei, A symmetric organic-based nonaqueous redox flow battery and its state of charge diagnostics by FTIR, J. Mater. Chem. A. 4 (2016) 5448–5456. https://doi.org/10.1039/c6ta01177b.

[100] Q. Liu, A.E.S. Sleightholme, A.A. Shinkle, Y. Li, L.T. Thompson, Non-aqueous vanadium acetylacetonate electrolyte for redox flow batteries, Electrochem. Commun. 11 (2009) 2312–2315. https://doi.org/10.1016/j.elecom.2009.10.006.

[101] M.H. Chakrabarti, R.A.W. Dryfe, E.P.L. Roberts, Evaluation of electrolytes for redox flow battery applications, 52 (2007) 2189–2195. https://doi.org/10.1016/j.electacta.2006.08.052.

[102] H. Kim, T. Yoon, J. Jang, J. Mun, H. Park, J. Heon, S.M. Oh, A tetradentate Ni (II) complex cation as a single redox couple for non-aqueous flow batteries, J. Power Sources. 283 (2015) 300–304. https://doi.org/10.1016/j.jpowsour.2015.02.083.

[103] US Geological Survey, Mineral Commodity Summaries 2020, 2020.

[104] V. Dieterich, J.D. Milshtein, J.L. Barton, T.J. Carney, R.M. Darling, Estimating the cost of organic battery active materials : a case study on anthraquinone disulfonic acid Estimating the cost of organic battery active materials : a case study on anthraquinone disulfonic acid, Transl. Mater. Res. (n.d.) aacb0e. https://doi.org/10.1088/2053-1613/aacb0e.

[105] Y.Y. Lai, X. Li, Y. Zhu, Polymeric Active Materials for Redox Flow Battery Application, ACS Appl. Polym. Mater. 2 (2020) 113–128. https://doi.org/10.1021/acsapm.9b00864.

[106] F.R. Brushett, M.J. Aziz, K.E. Rodby, On Lifetime and Cost of Redox-Active Organics for Aqueous Flow Batteries, ACS Energy Lett. 5 (2020) 879–884. https://doi.org/10.1021/acsenergylett.0c00140.

[107] M.A. Goulet, L. Tong, D.A. Pollack, D.P. Tabor, S.A. Odom, A. Aspuru-Guzik, E.E. Kwan, R.G. Gordon, M.J. Aziz, Extending the lifetime of organic flow batteries via redox state management, J. Am. Chem. Soc. 141 (2020) 8014–8019. https://doi.org/10.1021/jacs.8b13295.

[108] S. Jin, E.M. Fell, L. Vina-Lopez, Y. Jing, P.W. Michalak, R.G. Gordon, M.J. Aziz, Near Neutral pH Redox Flow Battery with Low Permeability and Long-Lifetime Phosphonated Viologen Active Species, Adv. Energy Mater. 2000100 (2020) 1–10. https://doi.org/10.1002/aenm.202000100.

[109] M. Wu, Y. Jing, A.A. Wong, E.M. Fell, S. Jin, Z. Tang, R.G. Gordon, M.J. Aziz, Extremely Stable Anthraquinone Negolytes Synthesized from Common Precursors, Chem. (2020) 1–11. https://doi.org/10.1016/j.chempr.2020.03.021.

[110] Y.K. Zeng, X.L. Zhou, L. An, L. Wei, T.S. Zhao, A high-performance flow-field structured iron-chromium redox flow battery, J. Power Sources. 324 (2016) 738–744. https://doi.org/10.1016/j.jpowsour.2016.05.138.

[111] A. Dinesh, S. Olivera, K. Venkatesh, M.S. Santosh, M.G. Priya, Inamuddin, A.M. Asiri, H.B. Muralidhara, Iron-based flow batteries to store renewable energies, Environ. Chem. Lett. 16 (2018) 683–694. https://doi.org/10.1007/s10311-018-0709-8.

[112] L. Su, A.F. Badel, C. Cao, J.J. Hinricher, F.R. Brushett, Toward an Inexpensive Aqueous Polysulfide−Polyiodide Redox Flow Battery, Ind. Eng. Chem. Res. (2017) 9783–9792. https://doi.org/10.1021/acs.iecr.7b01476.

[113] X. Wei, G. Xia, B. Kirby, E. Thomsen, B. Li, Z. Nie, G.G. Graff, J. Liu, V. Sprenkle, W. Wang, An Aqueous Redox Flow Battery Based on Neutral Alkali Metal Ferri / ferrocyanide and Polysulfide Electrolytes, J. Electrochem. Soc. 163 (2016) 5150–5153. https://doi.org/10.1149/2.0221601jes.

[114] M.C. Wu, T.S. Zhao, H.R. Jiang, Y.K. Zeng, Y.X. Ren, High-performance zinc bromine flow battery via improved design of electrolyte and electrode, J. Power Sources. 355 (2017) 62–68. https://doi.org/10.1016/j.jpowsour.2017.04.058.

[115] E. Allcorn, G. Nagasubramanian, H.D.P. Iii, E. Spoerke, D. Ingersoll, Elimination of active species crossover in a room temperature, neutral pH, aqueous flow battery using a ceramic NaSICON membrane, J. Power Sources. 378 (2018) 353–361. https://doi.org/10.1016/j.jpowsour.2017.12.041.

[116] Y. Wang, Y. Wang, H. Zhou, A Li – Liquid Cathode Battery Based on a Hybrid Electrolyte, ChemSusChem. 4 (2011) 1087–1090. https://doi.org/10.1002/cssc.201100201.

[117] N. Xu, X. Li, X. Zhao, J.B. Goodenough, K. Huang, A novel solid oxide redox flow battery for grid energy storage, Energy Environ. Sci. 4 (2011) 4942–4946. https://doi.org/10.1039/c1ee02489b.

[118] C. Stolze, C. Schmerbauch, C. Friebe, U.S. Schubert, A Tubular Polymer Redox Flow Battery with a Ceramic Membrane, Energy Technol. (2017) 225–227. https://doi.org/10.1002/ente.201600304.

[119] Q. Huang, Q. Wang, Next-Generation, High-Energy-Density Redox Flow Batteries, Chempluschem. 80 (2015) 312–322. https://doi.org/10.1002/cplu.201402099.

[120] K.E. Rodby, M.L. Perry, F.R. Brushett, Assessing capacity loss remediation methods for asymmetric redox flow battery chemistries using levelized cost of storage, J. Power Sources. 506 (2021) 230085. https://doi.org/10.1016/j.jpowsour.2021.230085.

[121] R.F. Gahn, N.H. Hagedorn, J.A. Johnson, Cycling Performace of the Iron- Chromium Redox Energy Storage System Conservation and Renewable Energy, Nasa Tm-87034. (1985).

[122] S. Wang, Z. Xu, X. Wu, H. Zhao, J. Zhao, J. Liu, C. Yan, X. Fan, Analyses and optimization of electrolyte concentration on the electrochemical performance of iron-chromium flow battery, Appl. Energy. 271 (2020) 115252. https://doi.org/10.1016/j.apenergy.2020.115252.

[123] R.F. Schulte, B.N. Bryden, Mineral Industry Surveys: Chromium December 2020, 2020. https://prd-wret.s3.us-west-2.amazonaws.com/assets/palladium/production/atoms/files/mis-202012-chrom.pdf.

[124] Z. Li, M.S. Pan, L. Su, P.C. Tsai, A.F. Badel, J.M. Valle, S.L. Eiler, K. Xiang, F.R. Brushett, Y.M. Chiang, Air-Breathing Aqueous Sulfur Flow Battery for Ultralow-Cost Long-Duration Electrical Storage, Joule. 1 (2017) 306–327. https://doi.org/10.1016/j.joule.2017.08.007.

[125] T.D. Gregory, M.L. Perry, P. Albertus, Cost and price projections of synthetic active materials for redox flow batteries, J. Power Sources. 499 (2021) 229965. https://doi.org/10.1016/j.jpowsour.2021.229965.

[126] J. Mellentine, Performance Characterization and Cost Assessment of an Iron Hybrid Flow Battery, Univ. Icel. (2011) 139. http://skemman.is/en/stream/get/1946/7698/20100/1/RES_Mellentine_Thesis_Paper_FINAL.pdf.

[127] R. Darling, K. Gallagher, W. Xie, L. Su, F. Brushett, Transport Property Requirements for Flow Battery Separators, J. Electrochem. Soc. 163 (2016) A5029–A5040. https://doi.org/10.1149/2.0051601jes.

[128] KEMIWATT, (n.d.). https://kemiwatt.com/.

[129] Green Energy Storage, (n.d.). http://www.greenenergystorage.eu/en/battery/.

[130] CMBlu, (n.d.). https://www.cmblu.de/.

[131] XL Batteries, (n.d.). https://www.xl-batteries.com/.

[132] JenaBatteries, (n.d.). https://jenabatteries.de/en/.

[133] B. Huskinson, M.P. Marshak, C. Suh, S. Er, M.R. Gerhardt, C.J. Galvin, X. Chen, A. Aspuru-Guzik, R.G. Gordon, M.J. Aziz, A metal-free organic-inorganic aqueous flow battery, Nature. 505 (2014) 195–198. https://doi.org/10.1038/nature12909.

[134] Y. Ji, M. Goulet, D.A. Pollack, D.G. Kwabi, S. Jin, D. De Porcellinis, E.F. Kerr, R.G. Gordon, M.J. Aziz, A Phosphonate-Functionalized Quinone Redox Flow Battery at Near-Neutral pH with Record Capacity Retention Rate, Adv. Energy Mater. 9 (2019). https://doi.org/10.1002/aenm.201900039.

[135] D.G. Kwabi, K. Lin, Y. Ji, E.F. Kerr, M. Goulet, D. De Porcellinis, D.P. Tabor, D.A. Pollack, R.G. Gordon, Alkaline Quinone Flow Battery with Long Lifetime at pH 12, Joule. 2 (2018) 1907–1908. https://doi.org/10.1016/j.joule.2018.08.013.

[136] C.S. Sevov, R.E.M. Brooner, E. Chenard, R.S. Assary, J.S. Moore, J. Rodriguez-Lopez, M.S. Sanford, Evolutionary Design of Low Molecular Weight Organic Anolyte Materials for Applications in Nonaqueous Redox Flow Batteries, J. Am. Chem. Soc. 137 (2015) 14465–14472. https://doi.org/10.1021/jacs.5b09572.

[137] Z. Yang, L. Tong, D.P. Tabor, E.S. Beh, M. Goulet, D. De Porcellinis, A. Aspuru-guzik, R.G. Gordon, M.J. Aziz, Alkaline Benzoquinone Aqueous Flow Battery for Large-Scale Storage of Electrical Energy, Adv. Energy Mater. 8 (2018). https://doi.org/10.1002/aenm.201702056.

[138] J.D. Robert, M.C. Caserio, Separation, Purification, & Identification of Organic Compounds, in: Basic Princ. Org. Chem., W.A. Benjamin, Inc., 1977.

[139] Y. Ren, X. Mao, T.A. Hatton, An Asymmetric Electrochemical System with Complementary Tunability in Hydrophobicity for Selective Separations of Organics, (2019). https://doi.org/10.1021/acscentsci.9b00379.

[140] A.M. Grumezescu, ed., Water Purification, Academic Press, 2017.

[141] Y.R. Dong, H. Kaku, K. Hanafusa, K. Moriuchi, T. Shigematsu, A Novel

Titanium/Manganese Redox Flow Battery, ECS Trans. 69 (2015) 59–67. https://doi.org/10.1149/06918.0059ecst.

[142] B. Yang, A. Murali, A. Nirmalchandar, B. Jayathilake, G.K.S. Prakash, S.R. Narayanan, A Durable, Inexpensive and Scalable Redox Flow Battery Based on Iron Sulfate and Anthraquinone Disulfonic Acid, J. Electrochem. Soc. 167 (2020) 060520. https://doi.org/10.1149/1945-7111/ab84f8.

[143] R. Gahn, N. Hagedorn, J. Ling, Single Cell Performance Studies on the Fe / Cr Redox Energy Storage System Using Mixed Reactant Solutions at Elevated Temperature Conservation and Renewable Energy Division of Energy Storage Systems, Proc. Eighteenth Intersoc. Energy Convers. Eng. Conf. Orlando, FL, August 21-26, 1983. Vol. 4. (1983) 1647–1652.

[144] Y.S. Kim, S.H. Oh, E. Kim, D. Kim, S. Kim, C.H. Chu, K. Park, Iron-chrome crossover through nafion membrane in iron-chrome redox flow battery, Korean Chem. Eng. Res. 56 (2018) 24–28. https://doi.org/10.9713/kcer.2018.56.1.24.

[145] L. Su, J.A. Kowalski, K.J. Carroll, F.R. Brushett, Recent Developments and Trends in Redox Flow Batteries, in: Z. Zhang, S.S. Zhang (Eds.), Recharg. Batter. Mater. Technol. New Trends, Springer International Publishing, Cham, 2015: pp. 673–712. https://doi.org/10.1007/978-3-319-15458-9_24.

[146] B. Hu, J. Luo, C. DeBruler, M. Hu, W. Wu, T.L. Liu, Redox-Active Inorganic Materials for Redox Flow Batteries, in: H. Wang, B.P.T. Fokwa (Eds.), Inorg. Batter. Mater., Wiley, 2019: pp. 211–236.

[147] L. Zhang, Y. Qian, R. Feng, Y. Ding, X. Zu, C. Zhang, X. Guo, W. Wang, G. Yu, Reversible redox chemistry in azobenzene-based organic molecules for high-capacity and long-life nonaqueous redox flow batteries, Nat. Commun. 11 (2020) 3843. https://doi.org/10.1038/s41467-020-17662-y.

[148] D. Ghosh, M.K. Sinha, M.K. Purkait, A comparative analysis of low-cost ceramic membrane preparation for effective fl uoride removal using hybrid technique, Desalination. 327 (2013) 2–13. https://doi.org/10.1016/j.desal.2013.08.003.

[149] B.K. Nandi, R. Uppaluri, M.K. Purkait, Treatment of Oily Waste Water Using Low-Cost Ceramic Membrane : Flux Decline Mechanism and Economic Feasibility, Sep. Sci. Technol. 44 (2009) 2840–2869. https://doi.org/10.1080/01496390903136004.

[150] B.K. Nandi, A. Moparthi, R. Uppaluri, M.K. Purkait, Treatment of oily wastewater using low cost ceramic membrane : Comparative assessment of pore blocking and artificial neural network models, Chem. Eng. Res. Des. 88 (2009) 881–892. https://doi.org/10.1016/j.cherd.2009.12.005.

[151] S.K. Hubadillah, Z. Harun, M.H.D. Othman, A.F. Ismail, W.N.W. Salleh, H. Basri, M.Z. Yunos, P. Gani, Preparation and characterization of low cost porous ceramic membrane support from kaolin using phase inversion / sintering technique for gas separation : Effect of kaolin content and non-solvent coagulant bath, Chem. Eng. Res. Des. 112 (2016) 24–35. https://doi.org/10.1016/j.cherd.2016.06.007.

[152] R.V. Kumar, L. Goswami, K. Pakshirajan, G. Pugazhenthi, Dairy wastewater treatment using a novel low cost tubular ceramic membrane and membrane fouling mechanism using

pore blocking models, J. Water Process Eng. 13 (2016) 168–175. https://doi.org/http://dx.doi.org/10.1016/j.jwpe.2016.08.012.

[153] Y. Yan, S.G. Robinson, M.S. Sigman, M.S. Sanford, Mechanism-Based Design of a High-Potential Catholyte Enables a 3.2 v All-Organic Nonaqueous Redox Flow Battery, J. Am. Chem. Soc. 141 (2019) 15301–15306. https://doi.org/10.1021/jacs.9b07345.

[154] V. Henze, Battery Pack Prices Cited Below $100/kWh for the First Time in 2020, While Market Average Sits at $137/kWh, BloombergNEF. (2020). https://about.bnef.com/blog/battery-pack-prices-cited-below-100-kwh-for-the-first-time-in-2020-while-market-average-sits-at-137-kwh/.

[155] J. Winsberg, T. Hagemann, T. Janoschka, M.D. Hager, U.S. Schubert, Redox-Flow Batteries: From Metals to Organic Redox-Active Materials, Angew. Chemie - Int. Ed. 56 (2017) 686–711. https://doi.org/10.1002/anie.201604925.

[156] A. Khor, P. Leung, M.R. Mohamed, C. Flox, Q. Xu, L. An, R.G.A. Wills, J.R. Morante, A.A. Shah, Review of zinc-based hybrid flow batteries: From fundamentals to applications, Mater. Today Energy. 8 (2018) 80–108. https://doi.org/10.1016/j.mtener.2017.12.012.

[157] S.Y. Chung, J.T. Bloking, Y.M. Chiang, Electronically conductive phospho-olivines as lithium storage electrodes, Nat. Mater. 1 (2002) 123–128. https://doi.org/10.1038/nmat732.

[158] D.A. Santos, M.K. Dixit, P.P. Kumar, S. Banerjee, Assessing the Role of Vanadium Technologies in Decarbonizing Hard-to-Abate Sectors and Enabling the Energy Transition, IScience. (2021) 103277. https://doi.org/10.1016/j.isci.2021.103277.

[159] S. Weber, J. Peters, M. Baumann, M.R. Weil, Life cycle assessment of a Vanadium Redox Flow Battery, Environ. Sci. Technol. (2018) acs.est.8b02073. https://doi.org/10.1021/acs.est.8b02073.

[160] D.J. White, L.S. Levy, Vanadium: Environmental hazard or environmental opportunity? A perspective on some key research needs, Environ. Sci. Process. Impacts. 23 (2021) 527–534. https://doi.org/10.1039/d0em00470g.

[161] Ashley-Oyewole, Endangered Element Vanadium: Can the Texas Oil and Gas Sector provide it a Sustainable Future?, Int. J. Appl. Sci. Technol. 11 (2021) 1–8. https://doi.org/10.30845/ijast.v11n1p1.

[162] A. Ciotola, M. Fuss, S. Colombo, W.R. Poganietz, The potential supply risk of vanadium for the renewable energy transition in Germany, J. Energy Storage. 33 (2021) 102094. https://doi.org/10.1016/j.est.2020.102094.

[163] F. Gao, A.U. Olayiwola, B. Liu, S. Wang, H. Du, J. Li, X. Wang, D. Chen, Y. Zhang, Review of Vanadium Production Part I: Primary Resources, Miner. Process. Extr. Metall. Rev. 00 (2021) 1–23. https://doi.org/10.1080/08827508.2021.1883013.

[164] U.S. Geological Survey, Mineral Commodity Summaries, 2021. https://pubs.usgs.gov/periodicals/mcs2021/mcs2021.pdf.

[165] W.F. Cannon, B.E. Kimball, L.A. Corathers, Manganese, Chapter L, Reston, VA, 2017. https://pubs.usgs.gov/pp/1802/o/pp1802o.pdf.

[166] Z. Li, M.S. Pan, L. Su, P.C. Tsai, A.F. Badel, J.M. Valle, S.L. Eiler, K. Xiang, F.R. Brushett,

Y.M. Chiang, Air-Breathing Aqueous Sulfur Flow Battery for Ultralow-Cost Long-Duration Electrical Storage, Joule. 1 (2017) 306–327. https://doi.org/10.1016/j.joule.2017.08.007.

[167] U. S. Department of the Interior, Final List of Critical Minerals 2018, Fed. Regist. 83 (2018) 23295–23296. https://www.govinfo.gov/content/pkg/FR-2018-05-18/pdf/2018-10667.pdf.

[168] Bushveld Minerals, Acquisition of brownfield production assets from Vanchem Vanadium Products Limited, 2019. http://www.bushveldminerals.com/wp-content/uploads/2019/05/Acquisition-of-the-Vanchem-Plant-SAJV-Business-and-Ivanti-Shares_.pdf.

[169] Bushveld Minerals, About Vanadium, (2021). https://www.bushveldminerals.com/about-vanadium/ (accessed August 11, 2021).

[170] Largo Resources, Investor Presentation, 2021. https://s27.q4cdn.com/288457300/files/doc_presentations/2021/May/LGO_Corporate-Presentation_May.pdf.

[171] K.D. Kelley, C.T. Scott, D.E. Polyak, B.E. Kimball, Critical Mineral Resources of the United States — Economic and Environmental Geology and Prospects for Future Supply: Vanadium, 2017. https://doi.org/https://doi.org/ 10.3133/pp1802U.

[172] M.A. Al-Ghouti, Y.S. Al-Degs, A. Ghrair, H. Khoury, M. Ziedan, Extraction and separation of vanadium and nickel from fly ash produced in heavy fuel power plants, Chem. Eng. J. 173 (2011) 191–197. https://doi.org/10.1016/j.cej.2011.07.080.

[173] MIT Energy Initiative, Future of Storage (in preparation), Cambridge, MA, 2022.

[174] M. Attah, F. Hildor, D. Yilmaz, H. Leion, Vanadium recovery from steel converter slag utilised as an oxygen carrier in oxygen carrier aided combustion (OCAC), J. Clean. Prod. 293 (2021) 126159. https://doi.org/10.1016/j.jclepro.2021.126159.

[175] K. Muthukumar, K.M. Patel, D. Mohapatra, B. Padh, B.R. Reddy, Selective recovery of vanadium as AMV from calcium vanadate sludge by direct AS leaching process: An industrial approach, Waste Manag. 102 (2020) 815–822. https://doi.org/10.1016/j.wasman.2019.11.040.

[176] X.S. Li, B. Xie, Extraction of vanadium from high calcium vanadium slag using direct roasting and soda leaching, Int. J. Miner. Metall. Mater. 19 (2012) 595–601. https://doi.org/10.1007/s12613-012-0600-8.

[177] Staff Reporter, Highveld Steel ticks over, gearing up to rise once again, Mail Guard. (2018). https://mg.co.za/article/2018-02-09-00-highveld-steel-ticks-over-gearing-up-to-rise-once-again/ (accessed November 8, 2021).

[178] M. Lindvall, Selective oxidation of Vanadium prior to Iron and Phosphorus, Lulea University of Technology, 2006. https://www.diva-portal.org/smash/get/diva2:1017882/FULLTEXT01.pdf.

[179] D.E. Polyak, 2018 Minerals Yearbook - Vanadium, 2018. https://www.usgs.gov.

[180] Technology Metals Australia, Mine closure and stricter China regulations are doing wonders for vanadium, Stockhead. (2018). https://stockhead.com.au/resources/mine-

closure-and-stricter-china-regulations-are-doing-wonders-for-vanadium/.

[181] Y. Li, Implementation of Chinese Rebar Standard Has Resulted in 89% of Surveyed Rebar Producers Adopting Vanadium in Rebar Production, Vanitec. (2019). http://vanitec.org/latest-from-vanitec/article/implementation-of-chinese-rebar-standard-has-resulted-in-89-of-surveyed-reb.

[182] G. Kavlak, J. McNerney, R.L. Jaffe, J.E. Trancik, Metal production requirements for rapid photovoltaics deployment, Energy Environ. Sci. 8 (2015) 1651–1659. https://doi.org/10.1039/c5ee00585j.

[183] T.G. Gutowski, S. Sahni, J.M. Allwood, M.F. Ashby, E. Worrell, The energy required to produce materials: constraints on energy-intensity improvements, parameters of demand, Philos. Trans. R. Soc. A Math. Phys. Eng. Sci. 371 (2013) 20120003. https://doi.org/10.1098/rsta.2012.0003.

[184] B.H.E. Hilliard, 1994 Minerals Yearbook - Vanadium, 1994. https://s3-us-west-2.amazonaws.com/prd-wret/assets/palladium/production/mineral-pubs/vanadium/700494.pdf.

[185] D.E. Polyak, Mineral Commodity Summaries - Vanadium, 2022. https://pubs.usgs.gov/periodicals/mcs2022/mcs2022-vanadium.pdf.

[186] VRB Energy, VRB Energy signs Strategic Cooperation Framework Agreement with Pangang Group Vanadium and Titanium Resources, the world's largest vanadium oxide producer; Agreement includes long-term supply and leasing of vanadium electrolyte, and joint development of t, GloveNewswire. (2018). https://www.globenewswire.com/news-release/2018/06/27/1530483/0/en/VRB-Energy-signs-Strategic-Cooperation-Framework-Agreement-with-Pangang-Group-Vanadium-and-Titanium-Resources-the-world-s-largest-vanadium-oxide-producer-Agreement-includes-long-te.html (accessed March 29, 2019).

[187] USGS, Cobalt Statistics and Information, 2021.

[188] M. Frenzel, C. Mikolajczak, M.A. Reuter, J. Gutzmer, Quantifying the relative availability of high-tech by-product metals – The cases of gallium, germanium and indium, Resour. Policy. 52 (2017) 327–335. https://doi.org/10.1016/j.resourpol.2017.04.008.

[189] P.R. Taylor, S.A. Shuey, E.E. Vidal, J.C. Gomez, Extractive metallurgy of vanadium-containing titaniferous magnetite ores: a review, Miner. Metall. Process. 23 (2006) 80–86. https://doi.org/https://doi.org/10.1007/BF03403340.

[190] M.P. Bailey, Vanadium Recovery from Steel Slag Scales Up, Chem. Eng. Essentials CPI Prof. (2021). https://www.chemengonline.com/vanadium-recovery/#:~:text=Vanadium recovery from steel slag scales up By,byproduct of steelmaking%2C has been significantly scaled up. (accessed September 12, 2021).

[191] T.G. Goonan, Vanadium Recycling in the United States in 2004, 2011.

[192] M. Imtiaz, M.S. Rizwan, S. Xiong, H. Li, M. Ashraf, S.M. Shahzad, M. Shahzad, M. Rizwan, S. Tu, Vanadium, recent advancements and research prospects: A review, Environ. Int. 80 (2015) 79–88. https://doi.org/10.1016/j.envint.2015.03.018.

[193] D. Schuler, M. Buchert, R. Liu, S. Dittrich, C. Merz, Study on Rare Earths and Their Recycling, 2011. https://reinhardbuetikofer.eu/wp-content/uploads/2011/01/Rare-earths-

study_Oeko-Institut_Jan-2011.pdf.

[194] Australian Vanadium Limited, The Australian Vanadium Project, (n.d.). https://www.australianvanadium.com.au/announcements/technical-and-financial-pfs-update/.

[195] TNG Limited, Mount Peake Project Fact Sheet, (n.d.). https://www.tngltd.com.au/wp-content/uploads/2021/03/TNG-Fact-Sheet-28-Feb-2021.pdf.

[196] Multicom Resources Limited, Saint Elmo Vanadium Project, (2021). https://saintelmoproject.com.au (accessed September 11, 2021).

[197] Silver Elephant Mining Corp., GIBELLINI (VANADIUM), (2021). https://www.silverelef.com/projects/gibellini-vanadium/ (accessed September 11, 2021).

[198] US Vanadium, U.S. Vanadium Successfully Recycles Electrolyte From Vanadium Redox Flow Batteries At A 97% Recovery Rate, (2021). https://usvanadium.com/u-s-vanadium-successfully-recycles-electrolyte-from-vanadium-redox-flow-batteries-at-a-97-recovery-rate/ (accessed February 6, 2021).

[199] Largo Resources, Largo Resources Launches Largo Clean Energy; Creating a Leading, Vertically Integrated and Sustainable Renewable Energy Storage Provider, Cision. (2020). https://www.prnewswire.com/news-releases/largo-resources-launches-largo-clean-energy-creating-a-leading-vertically-integrated-and-sustainable-renewable-energy-storage-provider-301188398.html (accessed August 9, 2021).

[200] G. Spilker, Why the Cobalt Market Is Changing Rapidly, Str. (2021). https://www.thestreet.com/investing/why-the-cobalt-market-is-changing-rapidly.

[201] A. Guthrie, Largo Announces Proposed Qualifying Transaction for New Physical Vanadium Holding Company, Largo Physical Vanadium Corporation, Largo Inc. (2022). https://s27.q4cdn.com/288457300/files/doc_news/Largo-Announces-Proposed-Qualifying-Transaction-for-New-Physical-Vanadium-Holding-Company-Largo-Physical-Vanadium-Corp-2022.pdf.

[202] Stryten Energy Enters The Long-Duration Energy Storage Market With Acquisition Of Storion Energy's Vanadium Redox Flow Battery Technology, Vanadium Price. (2022). https://www.vanadiumprice.com/stryten-energy-enters-the-long-duration-energy-storage-market-with-acquisition-of-storion-energys-vanadium-redox-flow-battery-technology/.

[203] M.L. Perry, K.E. Rodby, F.R. Brushett, Untapped Potential: The Need and Opportunity for High-Voltage Aqueous Redox Flow Batteries, ACS Energy Lett. (2022) 659–667. https://doi.org/10.1021/acsenergylett.1c02225.

[204] C. Sun, H. Zhang, Review of the Development of First-Generation Redox Flow Batteries: Iron-Chromium System, ChemSusChem. (2021). https://doi.org/10.1002/cssc.202101798.

[205] D.A. Johnson, M.A. Reid, Chemical and Electrochemical Behavior of the Cr(III)/Cr(II) Half-Cell in the Iron-Chromium Redox Energy Storage System, J. Electrochem. Soc. 132 (1985) 1058–1062. https://doi.org/10.1149/1.2114015.

[206] O.K. Chang, A.Q. Pham, Rebalancing electrolytes in redox flow battery systems, 8,916,281 B2, 2014. https://patentimages.storage.googleapis.com/d2/5e/1a/b28d7c61f426b0/US8916281.pdf.

[207] K. Wei, L. Li, Fe-Cr redox flow battery systems including a balance arrangement and methods of manufacture and operation, 10,777,836 B1, 2020. https://patentimages.storage.googleapis.com/6f/7f/ab/b0a5ed8b9b1b76/US10777836.pdf.

[208] R.M. Darling, M.L. Perry, Method of maintaining health of flow battery, 20160056487 A1, 2013.

[209] L. LI, Q. Luo, Near Neutral Aqueous Fe-Cr Complex Flow Battery: Reducing Electricity Storage Cost to < $100/kWh, ECS Meet. Abstr. MA2021-02 (2021) 120–120. https://doi.org/10.1149/MA2021-021120mtgabs.

[210] Y.K. Zeng, T.S. Zhao, X.L. Zhou, J. Zou, Y.X. Ren, A hydrogen-ferric ion rebalance cell operating at low hydrogen concentrations for capacity restoration of iron-chromium redox flow batteries, J. Power Sources. 352 (2017) 77–82. https://doi.org/10.1016/j.jpowsour.2017.03.125.

[211] R.F. Gahn, Method and apparatus for rebalancing a redox flow cell system, 4,576,878, 1986. https://patentimages.storage.googleapis.com/48/f3/fa/16f7760ad6b677/US4576878.pdf.

[212] Y. Song, C.E. Evans, Method and system for rebalancing electrolytes in a redox flow battery system, 10,923,753, 2021. https://www.osti.gov/biblio/1805523.

[213] E. Wesoff, Flow Battery Startup EnerVault Files for Assignment Before Creditors, Greentech Media. (2015). https://www.greentechmedia.com/articles/read/Flow-Battery-Startup-EnerVault-Files-For-Assignment-Before-Creditors.

[214] E. Wesoff, Flow Battery Aspirant Imergy Has Let Go Its Staff and Is Selling Its Assets, Greentech Media. (2016). https://www.greentechmedia.com/articles/read/flow-battery-aspirant-imergy-has-let-go-its-staff-and-is-selling-its-assets.

[215] Y. Ahn, J. Moon, S.E. Park, J. Shin, J. Wook Choi, K.J. Kim, High-performance bifunctional electrocatalyst for iron-chromium redox flow batteries, Chem. Eng. J. 421 (2021) 127855. https://doi.org/10.1016/j.cej.2020.127855.

[216] Y.K. Zeng, T.S. Zhao, X.L. Zhou, L. Zeng, L. Wei, The effects of design parameters on the charge-discharge performance of iron-chromium redox flow batteries, Appl. Energy. 182 (2016) 204–209. https://doi.org/10.1016/j.apenergy.2016.08.135.

[217] H. Zhang, Y. Tan, J. Li, B. Xue, Studies on properties of rayon- and polyacrylonitrile-based graphite felt electrodes affecting Fe/Cr redox flow battery performance, Electrochim. Acta. 248 (2017) 603–613. https://doi.org/10.1016/j.electacta.2017.08.016.

[218] S.R. Tirukkovalluri, R.K. Hanuman Gorthi, Synthesis, characterization and evaluation of Pb electroplated carbon felts for achieving maximum efficiency of Fe-Cr redox flow cell, J. New Mater. Electrochem. Syst. 16 (2013) 287–292. https://doi.org/10.14447/jnmes.v16i4.155.

[219] S. Wang, Z. Xu, X. Wu, H. Zhao, J. Zhao, J. Liu, C. Yan, X. Fan, Excellent stability and electrochemical performance of the electrolyte with indium ion for iron–chromium flow battery, Elsevier Ltd, 2021. https://doi.org/10.1016/j.electacta.2020.137524.

[220] M. Lopez-Atalaya, G. Codina, J.R. Perez, J.L. Vazquez, A. Aldaz, Optimization studies on a Fe/Cr redox flow battery, J. Power Sources. 39 (1992) 147–154. https://doi.org/10.1016/0378-7753(92)80133-V.

[221] B.H. Robb, S.E. Waters, M.P. Marshak, Evaluating aqueous flow battery electrolytes: a coordinated approach, Dalt. Trans. 49 (2020) 16047–16053. https://doi.org/10.1039/d0dt02462g.

[222] S.E. Waters, B.H. Robb, M.P. Marshak, M.P. Marshak, Effect of Chelation on Iron-Chromium Redox Flow Batteries, ACS Energy Lett. 5 (2020) 1758–1762. https://doi.org/10.1021/acsenergylett.0c00761.

[223] M. Keshavarz, A. Varadarajan, Preparation of flow cell battery electrolytes from raw materials, US 8,394,529 B2, 2013.

[224] J.T. Sullivan, Electrochemical-based purification of electrolyte solutions, and related systems and methods, US 10333164, 2019. https://patents.justia.com/patent/10333164.

[225] Z.M. Norman, A.B. Papandrew, R.C. Klet, M. Millard, Methods and devices for removing impurities from electrolytes, WO 2020/086645 A1, 2020.

[226] J. Friedl, U. Stimming, Determining Electron Transfer Kinetics at Porous Electrodes, Electrochim. Acta. 227 (2017) 235–245. https://doi.org/10.1016/j.electacta.2017.01.010.

[227] M. Heydari Gharahcheshmeh, C.T.C. Wan, Y. Ashraf Gandomi, K. V. Greco, A. Forner-Cuenca, Y.M. Chiang, F.R. Brushett, K.K. Gleason, Ultrathin Conformal oCVD PEDOT Coatings on Carbon Electrodes Enable Improved Performance of Redox Flow Batteries, Adv. Mater. Interfaces. 7 (2020) 1–11. https://doi.org/10.1002/admi.202000855.

[228] D.S. Cheng, A. Reiner, E. Hollax, Activation of hydrochloric acid-CrCl3 · 6H2 solutions with N-alkyfamines, J. Appl. Electrochem. 15 (1985) 63–70. https://doi.org/10.1007/BF00617741.

[229] N. Chen, H. Zhang, X.D. Luo, C.Y. Sun, SiO2-decorated graphite felt electrode by silicic acid etching for iron-chromium redox flow battery, Electrochim. Acta. 336 (2020) 135646. https://doi.org/10.1016/j.electacta.2020.135646.

[230] C.Y. Sun, H. Zhang, X.D. Luo, N. Chen, A comparative study of Nafion and sulfonated poly(ether ether ketone) membrane performance for iron-chromium redox flow battery, Ionics (Kiel). 25 (2019) 4219–4229. https://doi.org/10.1007/s11581-019-02971-0.

[231] H. Zhang, Y. Tan, X.D. Luo, C.Y. Sun, N. Chen, Polarization Effects of a Rayon and Polyacrylonitrile Based Graphite Felt for Iron-Chromium Redox Flow Batteries, ChemElectroChem. 6 (2019) 3175–3188. https://doi.org/10.1002/celc.201900518.

[232] H. Zhang, N. Chen, C. Sun, X. Luo, Investigations on physicochemical properties and electrochemical performance of graphite felt and carbon felt for iron-chromium redox flow battery, Int. J. Energy Res. 44 (2020) 3839–3853. https://doi.org/10.1002/er.5179.

[233] Y.K. Zeng, X.L. Zhou, L. Zeng, X.H. Yan, T.S. Zhao, Performance enhancement of iron-chromium redox flow batteries by employing interdigitated flow fields, J. Power Sources. 327 (2016) 258–264. https://doi.org/10.1016/j.jpowsour.2016.07.066.

[234] Z.P. Ifkovits, J.M. Evans, M.C. Meier, K.M. Papadantonakis, N.S. Lewis, Decoupled electrochemical water-splitting systems: A review and perspective, Energy Environ. Sci. 14 (2021) 4740–4759. https://doi.org/10.1039/d1ee01226f.

[235] K. V. Greco, A. Forner-Cuenca, A. Mularczyk, J. Eller, F.R. Brushett, Elucidating the

Nuanced Effects of Thermal Pretreatment on Carbon Paper Electrodes for Vanadium Redox Flow Batteries, ACS Appl. Mater. Interfaces. 10 (2018) 44430–44442. https://doi.org/10.1021/acsami.8b15793.

[236] K. V. Greco, J.K. Bonesteel, N. Chanut, C. Tai-Chieh Wan, Y.M. Chiang, F.R. Brushett, Limited Accessibility to Surface Area Generated by Thermal Pretreatment of Electrodes Reduces Its Impact on Redox Flow Battery Performance, ACS Appl. Energy Mater. 4 (2021) 13516–13527. https://doi.org/10.1021/acsaem.1c01980.

[237] A. Goldstein, Federal Policy to Accelerate Innovation in Long-Duration Energy Storage : The Case for Flow Batteries, 2021.

[238] Congressional Research Service, F-35 Joint Strike Fighter (JSF) Program, 2020. https://sgp.fas.org/crs/weapons/RL30563.pdf.

[239] M.G. Kendall, Rank Correlation Methods, Griffin, London, 1948.

[240] F.J. Oldenburg, T.J. Schmidt, L. Gubler, Tackling capacity fading in vanadium flow batteries with amphoteric membranes, J. Power Sources. 368 (2017) 68–72. https://doi.org/10.1016/j.jpowsour.2017.09.051.

[241] X. Wei, B. Li, W. Wang, X. Wei, B.I.N. Li, W.E.I. Wang, Porous Polymeric Composite Separators for Redox Flow Batteries Porous Polymeric Composite Separators for Redox Flow Batteries, 3724 (2015). https://doi.org/10.1080/15583724.2015.1011276.

Permissions

Chapter II was reproduced from work previously published in the Journal of Power Sources:

K.E. Rodby, T.J. Carney, Y. Ashraf Gandomi, J.L. Barton, R.M. Darling, F.R. Brushett, Assessing the levelized cost of vanadium redox flow batteries with capacity fade and rebalancing., J. Power Sources. 460 (2020) 227958. https://doi.org/10.1016/j.jpowsour.2020.227958.

Chapter III was reproduced from work previously published in the Journal of Power Sources:

K.E. Rodby, M.L. Perry, F.R. Brushett, Assessing capacity loss remediation methods for asymmetric redox flow battery chemistries using levelized cost of storage, J. Power Sources. 506 (2021) 230085. https://doi.org/10.1016/j.jpowsour.2021.230085.

Chapter IV represents work that is, at the time of writing, being prepared for submission to the International Materials Review.

Chapter V and it's Supporting Information (**Chapter VII**) represent work that is, at the time of writing, being prepared for submission to an undetermined journal.